University of Minho
School of Engineering

Pedro Domingos Moreira da Rocha Campos do Vale

Aircraft Wing Structure Benchmark: Cantilever vs. Braced Wing Configurations

october 2023

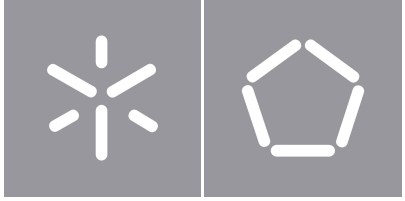

University of Minho
School of Engineering

Pedro Domingos Moreira da Rocha Campos do Vale

Aircraft Wing Structure Benchmark: Cantilever vs. Braced Wing Configurations

Masters Dissertation
Integrated Master's Degree in Mechanical Engineering

Dissertation supervised by
Nuno Miguel Magalhães Dourado

october 2023

Copyright and Terms of Use for Third Party Work

License granted to users of this work:

Acknowledgements

First and foremost, I would like to thank **Pedro Albuquerque**, my company supervisor at CEiiA, for his guidance during the preparation of this thesis, which became essential for the results presented here, for his dedication, effort and enthusiasm, which motivated me to give my best during the elaboration of this work and always pushed me to go further.

To my colleague and friend from CEiiA **Vladislav Frunza**, my thanks, who was always present to provide an helping hand, whenever the need arised, to his curiosity and interest about my work.

I am also thankful to my academic supervisor at the University of Minho, **Nuno Dourado**, who, not only during the time I was writing this thesis, but also throughout my whole academic time at the University of Minho, supported me in several situations, being always there to provide me guidance and advice.

I am grateful to my friend and colleague, **Leonardo Mazzitelli**, who accompanied me during the preparation of this thesis, with whom I was able to share ideas, receive some late-night feedback sessions and moral support.

I would like to express my gratitude to **André Pereira**, who, by sharing his developed work, helped and facilitated the completion of this thesis.

To everyone at CEiiA who have shared their time, knowledge and work to help me throughout my thesis journey, my thanks.

Last but not least, I would like to mention my family, especially my parents, who have always supported me and kept my spirits and motivation high during this process.

Statement of Integrity

I hereby declare having conducted this academic work with integrity.

I confirm that I have not used plagiarism or any form of undue use of information or falsification of results along the process leading to its elaboration.

I further declare that I have fully acknowledged the Code of Ethical Conduct of the University of Minho.

University of Minho, Braga, january 2024

Pedro Domingos Moreira da Rocha Campos do Vale

Abstract

This thesis presents a comprehensive analysis of aircraft wing structures, specifically comparing cantilever and braced wing configurations across a range of aspect ratios. The study employs Hypermesh, a powerful finite element analysis tool, which is a standard software in the aeronautical industry, to investigate the structural performance of these two wing designs. The objective is to provide recommendations for the use of wing braces in different aspect ratio scenarios, using the Cessna 408 Skycourier as a reference aircraft model for the finite element model (FEM).

This work encompasses five different aspect ratios, ranging from 9.8 to 13.8, with incremental steps of one unit. Two critical analyses, SOL101 static analysis and SOL105 buckling analysis, are conducted to assess the structural integrity and stability of both cantilever and braced wing configurations. Through these analyses, the study examines factors such as stress distribution, maximum stress, and critical buckling loads. Also, it includes a connection angle study, to define the angle range for a sized brace.

By comparing the performance of cantilevered and braced wing configurations with different aspect ratios, it was shown that the braced wing configuration is more advantageous for the class of aircraft CS-23, particularly in terms of structural weight. This represents a weight saving of around 35%, corroborating previous studies, which translate into greater range, greater payload capacity and lower operating costs.

Keywords Wing Braces, Cantilever Wing, Static Analysis, Buckling Analysis

Resumo

Esta tese apresenta uma análise exaustiva das estruturas das asas de aeronaves, comparando especificamente as configurações de asas em *cantilever* e com tirantes numa série de razão de aspecto de asa. O estudo utiliza o *Hypermesh*, uma poderosa ferramenta de análise de elementos finitos, que é um *software* padrão na indústria aeronáutica, para investigar o desempenho estrutural destas duas configurações de asa. O objetivo é fornecer recomendações para a utilização de tirantes de asa em diferentes cenários de razão de aspeto, utilizando o Cessna 408 Skycourier como modelo de aeronave de referência para o modelo de elementos finitos (FEM).

Este trabalho abrange cinco razões de aspeto diferentes, variando de 9,8 a 13,8, com passos incrementais de uma unidade. São efectuadas duas análises críticas, a análise estática SOL101 e a análise de encurvadura SOL105, para avaliar a integridade estrutural e a estabilidade das configurações de asa em cantilever e com tirantes. Através destas análises, o estudo examina factores como a distribuição de tensões, a tensão máxima e as cargas de encurvadura críticas. Inclui também um estudo do ângulo de ligação, para definir a gama de ângulos para um tirante dimensionado.

Ao comparar o desempenho das asas em cantilever e com tirantes com diferentes rácios de aspeto, foi demonstrado que a configuração com tirantes é mais vantajosa para a categoria de aeronaves da classe CS-23, designadamente em termos de peso estrutural. Isto representa uma poupança de peso na ordem dos 35%, corroborando os estudos anteriormente realizados, que se traduzem num maior alcance, maior capacidade de carga útil e menores custos operacionais.

Palavras-chave Asas com Tirantes, Asa Cantilever, Análise Estática, Análise à Encurvadura

Contents

List of Figures

List of Tables

List of Acronyms

BW Braced Wing

CAR Civil Aviation Regulations

CEiiA Centre of Engineering & Product Development

CFD Computer Fluid Dynamics

CS Certification Specifications

CS-23 EASA Certification Specifications (CSs) for Normal, Utility, Aerobatic and Commuter Aeroplanes

CW Cantilevered Wing

C408 Cessna 408 Sky Courier

EASA European Aviation Safety Agency

FAA Federal Aviation Administration

FAR Federal Aviation Regulations

FEM Finite Element Analysis

GA General Aviation

HQ Headquarters

JAR Joint Aviation Regulations

L Landing

MLG Main Landing Gear

MTOM Maximum Take-Off Mass

MTOW Maximum Take-Off Weight

NACA National Advisory Committee for Aeronautics

OEM Original Equipment Manufacturer

PACT Parque do Alentejo de Ciência e Tecnologia

SPC Single Point Constrain

STOL Short Take-off and Landing

TO Take-Off

Part I

Introductory material

Chapter 1

Introduction

In this chapter the motives behind the development of this thesis is presented, followed by a short description of the company where this work was developed, its working fields as well as the integration of this work on their projects, the defined objectives as well as the respective organization of this thesis along with an historical background focusing on the evolution of the wing structures is done.

1.1 Motivation and Framework

Based on an initial study conducted by CEiiA (Centre of Engineering & Product Development), in which comparative analyses between aircraft in the Light Transport Category (which fit under the "Normal, Utility, Aerobatic, and Commuter Category Aeroplanes" EASA CS-23), it was found that these aircraft fall into two different configurations as seen in Fig.(1.1): Continuous Cantilever Wing Configuration and Braced Wing Configuration.

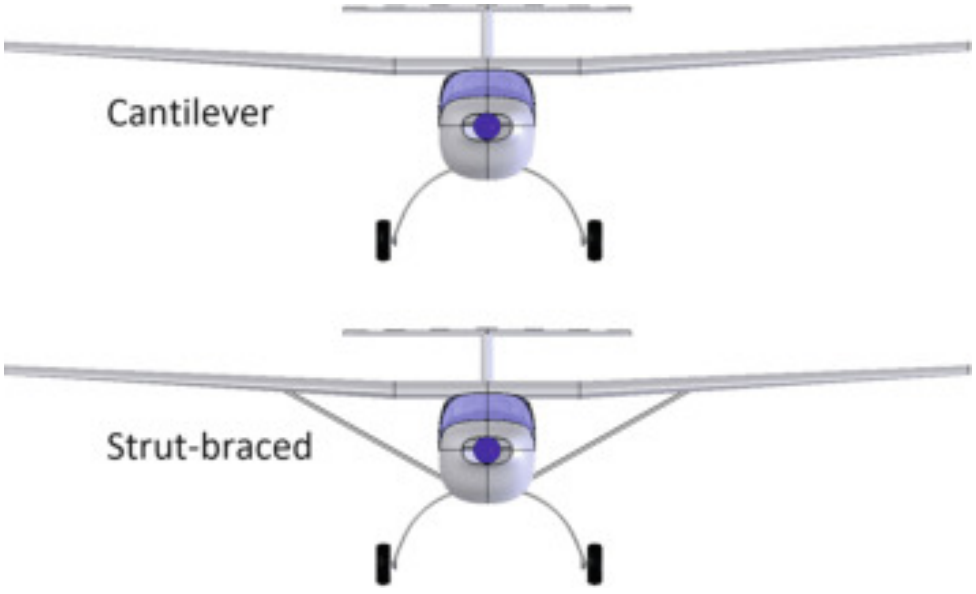

Figure 1.1: Continuous Cantilever Wing vs Braced Wing Configuration (1)(p.104)

Through literature consultations (2), it was observed that the Braced Wing Configuration allows to obtain a 30% reduction in wing weight when compared to the Continuous Cantilever Wing.

It is intended to address several aspects:

- Although both wing configurations have been structurally pre-designed by CEiiA, they have not been structurally optimized (in terms of skeleton, thickness, position of ribs, stiffeners ribs, stiffeners and stringers), and further studies should include these aspects to provide a better comparison;

- The likely impacts of the fuselage structural mass due to the different wing arrangements in order to deepen the current study;

- A further optimization study regarding the wing brace, wing brace fairing and interaction with the engines.

1.2 CEiiA

CEiiA was created in 1999 with the goal of supporting the competitiveness of the Portuguese automotive industry. Since then, CEiiA diversified the activity, and is now focused on aeronautics, urban mobility, automotive, ocean and space.They are currently one of the 10 largest R&D investors in Portugal, being an international reference in the sustainable mobility area and recognized in the aeronautical world for their skills in structural engineering. (3)

From the several locations where it operates, both in Portugal and in other countries, their HQ is located in Matosinhos Fig.(1.2). The content of this thesis was developed in their most recent facility located in Évora, being part of PACT (Parque do Alentejo de Ciência e Tecnologia), in collaboration with their aeronautical team, more precisely the structures team.

Figure 1.2: CeiiA HQ in Matosinhos (4)

Regarding the aeronautical field, CEiiA, achieved a remarkable feat, by participating in the development of Embraer KC-390 Fig.(1.4), having as primary structures, its elevator and fuselage, while as secondary structure the sponson, employing more than 500.000 hours of engineering in this project Fig.(1.3). Throughout this project their engineering teams were able to acquire valuable knowledge, that is of huge aid for their current project, the development of a lightweight aircraft. If this project comes to fruition, it's possible to say that this thesis had the aim to provide a comprehensive study which can be used for the development of the 1st fully Portuguese made aircraft.

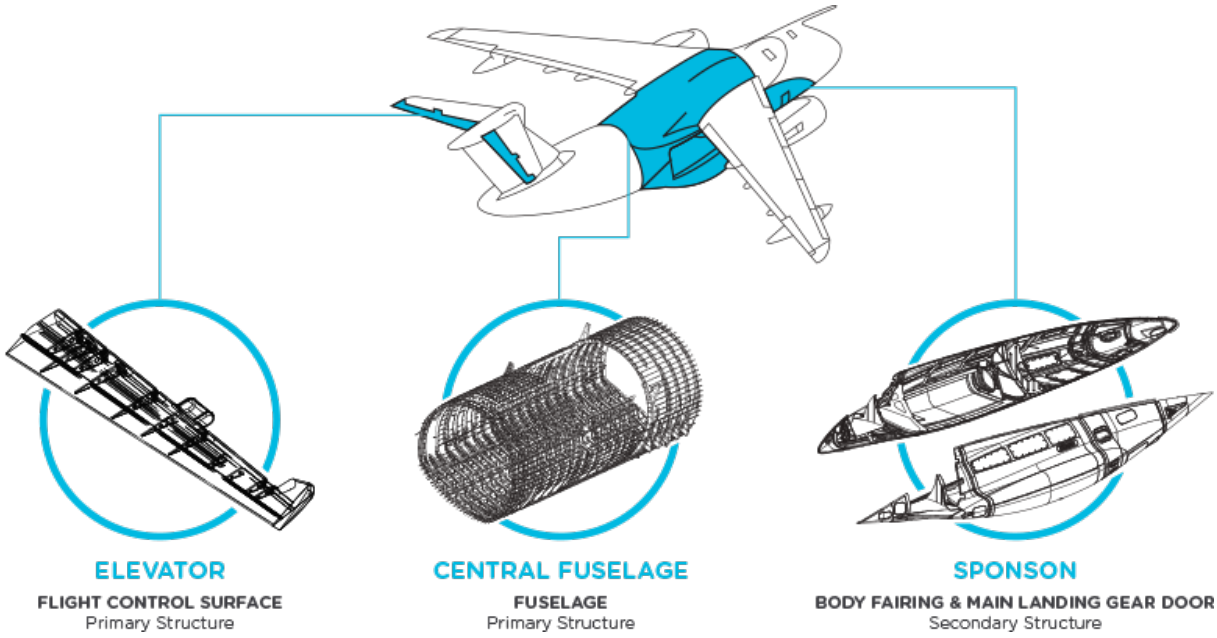

Figure 1.3: Embraer KC-390 - CEiiA developed components (5)

Figure 1.4: Embraer KC-390 - Inflight (6)

It is in this context and with the author curiosity and willingness to learn more about the aeronautical field that this thesis was developed, joining their structural team in Évora.

1.3 Objectives

The main objective is to develop a simplified typical light aircraft EASA CS-23 (close to its maximum take-off mass) global finite element model.

Create two versions of the FEM, one with and another without wing braces.

Minimizing both models' structural mass, in order to perform a structural strength (SOL 101 (Nastran Solver Code)) and buckling (SOL 105) analyzes.

Benchmarking the relative structural performance between a continuous cantilever wing (such as Indonesian Aerospace N-219, Dornier 228, Let L-410 Turbolet) and a braced wing (Cessna Sky Courier, De Havilland DHC-6 Twin Otter, PZL M28 Skytruck), taking into consideration the following points:

- Wing brace, brace to wing and brace to fuselage structural mass;
- Wing brace aerodynamic penalty;
- Overall aircraft mass;
- Structural synergy between Main Landing Gear and brace structure.

Optimizing the Wing braces regarding the following design variables:

- Wing brace fairing;
- Brace inclination angle;
- Brace to Wing mounted Engines wake interaction (wing and engine performance).

Discuss the advantages/disadvantages and providing recommendations to the use of wing braces, depending on:

- Aircraft Operation (altitude and velocities);
- Aircraft Dimensions (Maximum Take-off Mass and Wingspan);
- Engine location (either spanwise or fuselage mounted).

For the purpose of this structural efficiency comparative study, the following wing configurations were considered:

- Cantilevered wing with no reinforcements and an independent MLG (Main Landing Gear);
- Two half-wings with wing reinforcements and MLG.

The studies were done on a relative basis, following static predimensioning.

Some aspects considered in the developed study:

- The Wing Tank Volume will be significantly decreased by having two half-wings instead of a cantilevered wing;
- The Aerodynamic Drag due to the addition of the brace structure should be evaluated, including the

additional weight due to the fairing;

- The brace beams should be sized considering their failure to compression (buckling/crippling).

It is intended with the improvement of the past studies, to increase the degree of accuracy of the percentage savings, which is obtained in terms of structural weight in the Braced Wings configuration compared to the Cantilever Wing configuration.

1.4 Dissertation Organization

In chapter two, referring to the **State of the Art**, an introduction of several different concepts are made to help unfamiliarized readers interpret and understand the process and results obtained during the simulations made. In this chapter, different competitors are adressed, where brief summaries of the corresponding main characteristics and distinguishable features of state of the art airplanes will both be compared, with braced and cantilever wing configurations.

In chapter three, a brief explanation on the main issue and the challenges this problem possess, to the development of the comparison is made. While in the following chapter, the fourth one, which is the core of this work, an extensive and detailed description of all the process done since the motivation behind the reference aircraft chosen for the simulations, its issues and procedure, as well as the development of the wing brace components will be explained. Several estimates will be made with different load cases and an inertia relief study is conducted.

In chapter five, there is the result analysis of the different studies conducted, an explanation about the limitations and considerations that must be done to make this a viable comparison, while the main variables studied are explained. All of this is done in order to conduct a sensitivity analysis that will determine the most meaningful variables and their corresponding effect when studying the use or not of braced wings on aeroplanes.

In the sixth chapter some conclusions are drawn and possible future work that could be further exploited is shown.

Regarding the final chapter, the original activities planned are compared with the actual development of the project.

1.5 Historical Background

1.5.1 The Past

The history of aviation extends back for several thousand years, but regarding the early years of aviation after Wilbur and Orville Wright's famous flight on December 17, 1903, wing structures were predominantly composed of wood and fabric materials. Biplanes and triplanes were common designs during this period between the 1900 and 1920 Fig.(1.5). These wings usually featured multiple sets of wings stacked on top of each other, connected by struts and wires to provide stability and strength. (7)

Figure 1.5: Duigan Biplane, built at Mia Mia, Victoria in 1910 (8)

By the 1930s, the world witnessed a transition to metal structures, as aircraft manufacturers started utilizing aluminum alloys for wing construction. It was this shift, that allowed for stronger and more streamlined wings as known today. Metal ribs, spars, and stringers were incorporated to provide rigidity and support, while metal sheets formed the wing skin. In this era several advancements in monoplane designs were made, where monoplane wings started replacing the multiple-wing configurations.

With the advent of jet-powered aircraft in the 1940's, wing design underwent significant changes. Swept wings with backward sweep angles became popular due to their ability to handle high speeds more efficiently, since they reduce the drag and increase the critical Mach number Fig.(1.6). It was also during this era that new insights were made in the aerodynamics field and the use of new materials led to the use of advanced aluminum alloys. (9)

Figure 1.6: The de Havilland Comet, first commercial jet airliner which began service on 9 January, 1951 (10)

From the 1970s onwards, the use of composite materials greatly increased, due to their significant enhanced properties/specific strength compared to common materials used until then. A good example would be carbon fiber-reinforced polymers, which gained prominence in wing design, since they offer high strength-to-weight ratios, increased structural integrity, and improved resistance to fatigue (11; 12).For the above mentioned reasons composites allowed the development of lighter, more fuel-efficient aircraft with enhanced maneuverability. Being aware of this advantages, composite wings, consisting of carbon fiber skins, with honeycomb structures, and integrated ribs and spars, became increasingly common in modern aircraft design. (13; 14)

Essentially, it can be concluded that each era brought innovations in materials, construction techniques, and aerodynamic design, resulting in wings that are stronger, lighter, and more efficient.

1.5.2 The Present and Future

With the expectable computing power increase over the next decades, computational analysis techniques, such as finite element analysis (FEM) and computer fluid dynamics (CFD) , will play an increasingly important role in wing structure development, since these tools will allow for more detailed simulations of structural performance, aerodynamic behavior and optimization algorithms, at a larger scale, which will help in decision making while reducing the need for extensive physical prototyping.

It is easy to conclude that present and future developments in wing structure will involve the integration of several different fields which have the potential to enhance the performance, efficiency, and safety of future aircraft wings.

Chapter 2

State of the Art

In this chapter the main components of a conventional wing will be explained, including their function and working principles behind it. Then the different wing loads, a wing is subject during flight along with his measurement methods will be shown. Several aircraft will be compared regarding their wing structure, three examples with a continuous cantilever wing and another three with braced wings. At the end of this chapter some certification requirements and limitations imposed by this regulations will be explained.

2.1 Aircraft Wing Structure

In this section an aircraft wing structure will be analysed. Its constitution as well as each element function and their basic working principles will be explained. This section will allow to understand the modelling choices taken in the development of this study as well as the several constraints that exist during the development of a wing.

2.1.1 Main Components

An aircraft wing structure is composed by several elements. In Fig.(2.1) it is possible to identify some of the basic terms used.

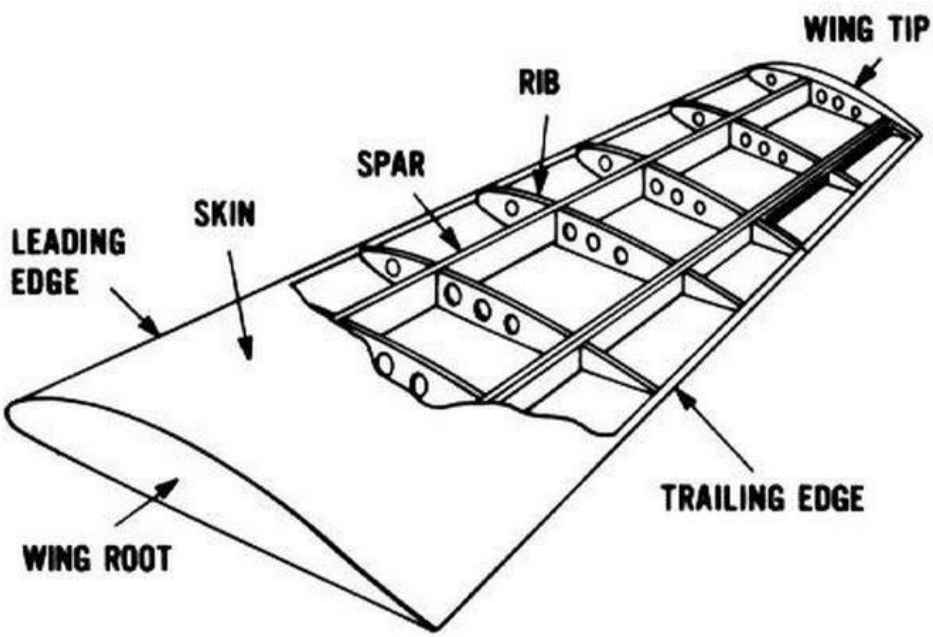

Figure 2.1: Wing Structure Main Components (15)

In Fig.(2.1) it is possible to identify:

- The Spars: The spars act as the backbone of an aircraft wing. It's a strong, sturdy beam that runs from one wingtip to the other, giving the wing its shape and providing the main support for the entire structure. Just like our backbone supports our body, the spar carries most of the bending loads and helps keep the wing rigid and stable during flight. It's an essential component that ensures that the wing can withstand the forces and stresses encountered while the aircraft is in the air.

- The Ribs: The ribs on an untapered and unswept aircraft wing are typically perpendicular to the spars. They serve as the internal foundation for the wing, giving its shape and support. Along with the spars, they form the wing's aerodynamic shape and support the outer wing skin, just like the human ribs do in our bodies and thus their name. The strength and durability of the wing during flight is ensured by these structures, which transfer forces between the skin and spar.

- The Wing Skin: The wing skin of an aircraft provides the aerodynamic shape, helping in the generation of lift, since its smooth surface allows the air to flow smoothly over the wing, creating the necessary forces for the flight, while distributes the loads and forces evenly to ensure the wing remains strong and stable during flight. It also works similarly as a shield or armor that covers the framework of the wing. It's the outer layer that protects the important components inside the wing. Just like our skin keeps our body protected, the wing skin acts as a protective barrier for its internal parts.

- The Wing Root: Corresponds to the attached part of the wing to the fuselage. It is thus the inboard

portion of the wing, which ensures a secure connection between the wing and the rest of the aircraft, enabling the transfer of aerodynamic forces and moments during flight.

- Wing Tip: The wing tip, as the name suggests, is the outboard portion of the wing. It is located at the far end or the tip of each wing. If well designed, the wing tip helps managing the airflow over the wing, reducing the formation of wingtip vortices. There are several devices such as winglets that can help minimize drag and improve the overall aerodynamic efficiency of the aircraft, which alter the airflow patterns, reducing the energy loss, and contributing to an improved fuel efficiency and lift-to-drag ratio.

- Leading Edge: It is the foremost part of the wing, and thus is exposed to the oncoming airflow during flight. Its primary function is to maintain the wing's aerodynamic efficiency and structural integrity. To achieve this, it is meticulously designed with a smooth and rounded shape, aimed at ensuring an even distribution of aerodynamic forces and reducing drag-induced stresses on the wing's structure.

- Trailing Edge: The trailing edge is the rearmost structural element of the wing, situated at the opposite end of the leading edge, and it interacts with the airflow behind the aircraft during flight. Structurally, the trailing edge is vital for maintaining control and maneuverability of the aircraft. It often incorporates movable control surfaces, such as flaps and ailerons, which serve to adjust the wing's camber and surface area during various flight phases, such as takeoff and landing, to precisely control the corresponding lift coefficient required at different speeds.

- Wing Box: Although not represented in Fig.(2.1), the wing box refers to the enclosed structure formed by the spars, ribs, and skin of the wing, which besides providing the main structural strength of the structure it houses various internal components such as fuel tanks, control mechanisms, and landing gear attachment points. (15)

It's important to note that the skin mainly works in shear, but ribs work in bending. So, these have bending and shear stresses. The same happens with the spars. The spars and skin together form the wing box to work in torsion.

2.1.2 Working Principles

An aircraft wing has several working principles. To understand them, first it is necessary to learn their main purpose. The main and primary function of an aircraft wing is to generate lift, and thus counteract the force of gravity and keep the aircraft flying Fig.(2.2). Lift is the upward force that opposes the aircraft's weight and enables it to stay airborne.

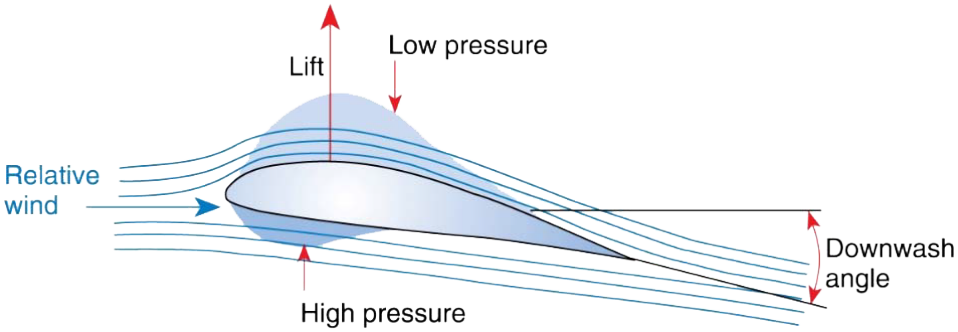

Figure 2.2: Lift Generation Schematic (16)

The generation of lift is primarily achieved through the aerodynamic properties of the wing's shape, known as the airfoil. The crucial factor in lift generation is the production of circulation, which induces a curvature in the airflow around the wing. This curvature, in turn, affects the pressure and inertia forces of the air, resulting in lift that is normal to the incoming airflow. It is this pressure difference between both surfaces that creates an upward force called lift.

Adjusting the angle at which the wing meets the oncoming airflow (angle of attack), and using control surfaces like flaps and ailerons, pilots can manipulate the amount of lift generated during the different phases of an aircraft's flight.

However the lift generated is not the same all across the wing, since many different factors such as wind vortices, turbulence, different surface roughness, or other components like the fuselage, engines or wingtip devices affect the distribution of lift generated across the different sections of the airplane, as shown in Fig.(2.3), this lift distribution ideally should approach an elliptical distribution, however that is not the case in most real situations.

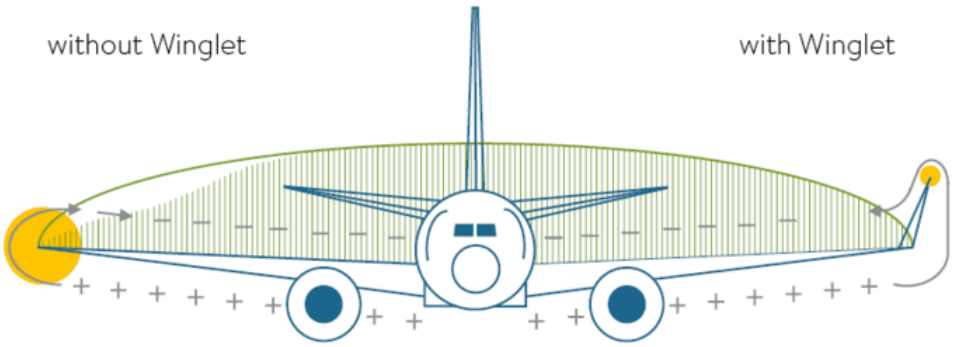

Figure 2.3: Comparison between the lift distribution across the airplane wing section with and without winglets, affected by the wingtip vortices airflow area represented in the yellow circles (17)

It is also commonly used for engines stowage and to bear fuel and include control surfaces. They

are also designed to be able to withstand the forces and stresses encountered during flight, such as aerodynamic loads, gusts and maneuvers.

Furthermore, the wings also house various systems and components essential for flight operations. These may include fuel tanks, landing gear mechanisms, control surfaces (such as flaps and ailerons), and instrumentation for navigation and communication. The wings provide a dedicated space to accommodate these systems, ensuring proper functionality and integration into the overall aircraft structure.

2.2 Aircraft Loads

From a load perspective it is possible to understand that lift, will generate a corresponding lift force that counteracts the weight force of the aircraft, but besides this two counteracting forces, there are two forces which play an important role in an airplane wing, those are drag and thrust, assuming the engines are mounted on the wings. A schematic with the actuating forces on a wing in shown below on Fig.(2.4):

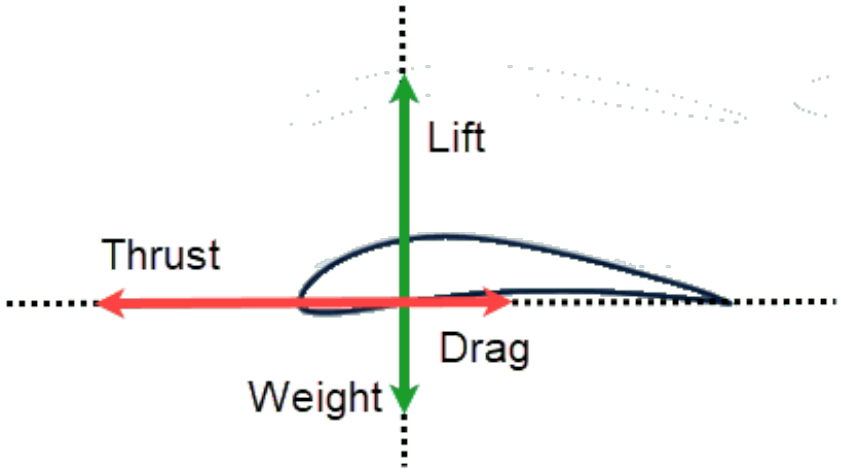

Figure 2.4: Wing load schematic of actuating forces on an airfoil (18)

While lift is essential, it will generate an unwanted byproduct, known as drag, which is the result of two main factors, namely profile/parasitic drag and induced drag as seen in Fig.(2.5).

Profile/parasitic drag, which is the result of the aerodynamic resistance to motion due to the shape of the aircraft as it moves through the air. It will be bigger with an increase of speed. Also the geometry and shape of the aircraft determines how much air resistance is experienced, that's why by creating streamlined shapes and smooth surfaces help reducing the drag produced, since this shape tend to have lower drag coefficients.

Regarding induced drag, it refers to the lift-producing aspects of the wing's design, particularly its

angle of attack and the distribution of lift along the wing's span. As the wing passes through the air, an area of lower air pressure is formed on the top of the wing. Higher-pressure air below the wing seeks equilibrium with the lower pressure area above, resulting in a vortex flow from the bottom of the wing to the top. The airflow behind the trailing edge of the wing is altered by these vortices in both direction and speed. Downwash is the term for the downward deflection of the airflow. Lift is always perpendicular to the relative wind, so downwash shifts the relative wind downward, which is a crucial point. The lift vector tilts backward as the amount of downwash rises, causing induced drag.

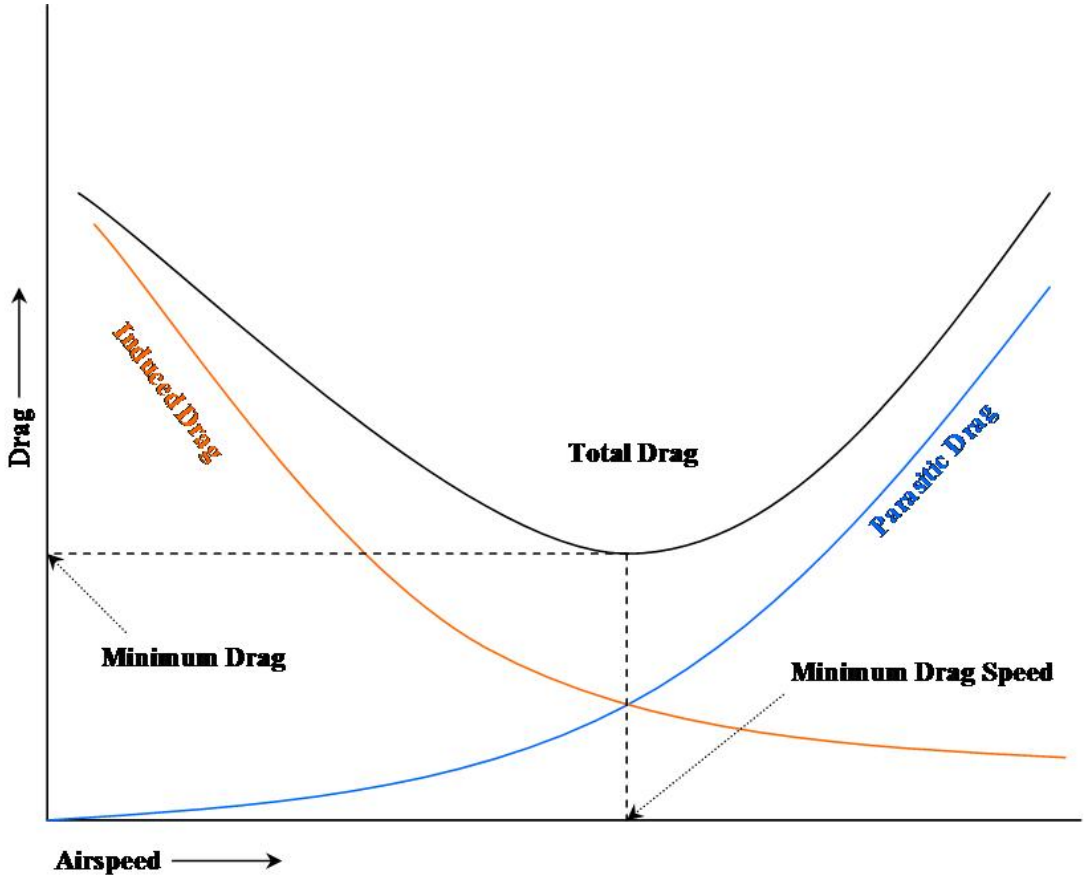

Figure 2.5: Drag components and respective total drag graph according to airspeed (19)

Since wind is far from being constant, as the air flows over the wing, it is pretty common to become turbulent, causing disruptions in the smooth airflow. Turbulence will therefore increase drag by creating swirling air pockets that create resistance against the aircraft's motion. There are various design features, such as winglets, that are incorporated to manage airflow and reduce turbulence-induced drag. Winglets, though, do not directly affect turbulence. They take advantage of the tip vortex lateral induced velocity to produce a force that, at a given design wing lift coefficient, points forward. These were some of the reasons why during design it is important to minimize drag, since it directly affects fuel efficiency and

performance, allowing the aircraft to fly more efficiently and achieve higher speeds.

Thrust can be considered as the opposing force to drag. The primary responsibility of generating thrust, lies with the engines which through a powerful jet of exhaust gases or other propulsive mechanisms, such as propellers, create a thrust force pushing the aircraft forward. When an aircraft is in flight, it requires a forward propulsion force to counteract the drag that acts in the opposite direction of its motion through the air, if thrust is higher than drag, then the aeroplane is accelerating, which is the case shown in Fig.(2.4), this increase in speed, will make the air resistance gradually increase, which as mentioned before is a component of drag, up to the point that thrust and drag will have equal absolute value but opposing signs, entering constant speed flight.

Before moving to the definition and measurement of each respective force it is relevant to take into consideration that this forces balance can be altered due to a change in the relative direction of the air passing through the airfoil. This can happen due a change of the altitude of the aircraft, creating, what's called, an angle of attack, which would be different from 0° as seen in Fig.(2.6):

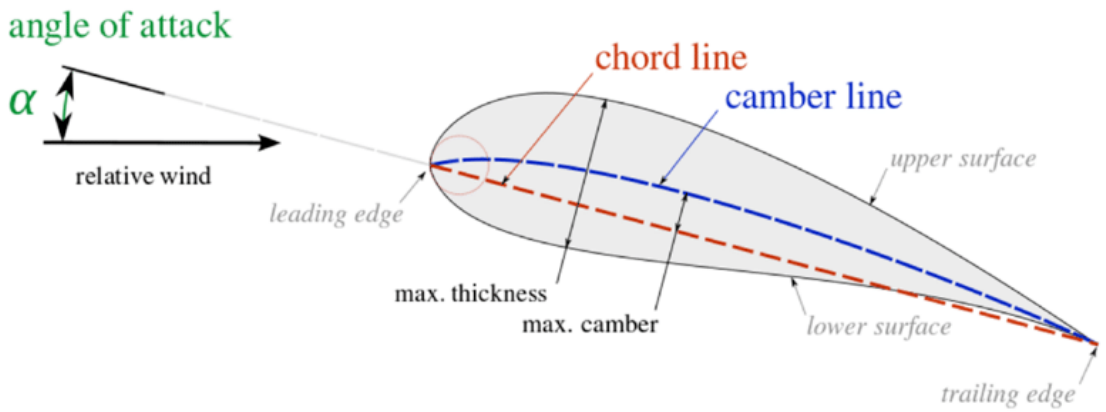

Figure 2.6: Airfoil schematic, representing an angle of attack (20)

The mean camber line (represented in blue in Fig.(2.6) is the imaginary line which is located at the same distance from the two surfaces of the airfoil, being usually used to indicate the average curvature of it. With respect to the chord line, which connects the leading edge to the trailing edge in a straight line, it works as a baseline from which other measurements, such as the angle of attack are measured.

The angle of attack is thus defined as the angle between the wing's chord line and the oncoming airflow. By varying the angle of attack of an airfoil it's possible to produce more or less lift and corresponding drag generated by the wing, as needed for the different flight phases. In case of a symmetric airfoil the lift generated when the angle of attack is at 0° in relation to the relative incoming air, is 0, since the air is

gonna flow at same speed in both surfaces and thus no pressure difference is generated, however most of the wings used on airplanes have a camber.

For simplicity, in the studies considered in this thesis, all of them will be at constant altitude with no relative direction from the wind and the airfoil. The introduction of this concepts are only necessary for an understanding of the choice procedure and existing codes for an airfoil in later chapters.

2.2.1 Definition and Measurement

In order to measure each wing load, several methods and instruments are used. Starting with the lift force, it is usually inferred through other measurements, being one of the most common methods using load cells or strain gauges, installed at critical points in the wing structure, which will detect the deformation or strain caused by the lift force applied on the wing. By calibrating and making the respective readings it is possible to estimate the lift force based on the measured strain.

From a theoretical point of view lift can be calculated using a simple formula (21):

$$L = \frac{1}{2}\rho V^2 C_L S \tag{2.1}$$

Where:

$L \longrightarrow Lift\ Force$

$\rho \longrightarrow Air\ Density$

$V \longrightarrow Airspeed$

$C_L \longrightarrow Lift\ Coefficient$

$S \longrightarrow Wing\ Area$

It is relevant to note that C_L is a dimensionless value that quantifies the lift characteristics of an airfoil or wing at a specific angle of attack, Reynolds number and Mach number, being usually determined experimentally or through computational methods, although lift coefficient can also be calculated as $C_L = \frac{L}{qS}$ which is the lift force (L) divided by the wing area (S) multiplied by the dynamic air pressure (q), which is given by $q = \frac{\rho V^2}{2}$ which is the air density (ρ), airspeed squared (V). Similarly drag coefficient is written as $C_D = \frac{D}{qS}$, where the only difference is the drag force (D), where the other variables have the same meaning. (22)

Equation (2.1) can be used for an approximation of the lift measurement which is close to reality, however this formula follows certain assumptions, such as inviscid, incompressible flow and considers an ideal airfoil shape, which are all far from the reality. Also the relationship between lift and other parameters

like the angle of attack, airspeed, and airfoil shape are nonlinear, and that's why lift coefficient (C_L) is introduced in the equation to represent that nonlinearity. In order to determine the precise coefficient of lift for a given airfoil, requires extensive wind tunnel testing or computational fluid dynamics (CFD) simulations to capture the detailed flow characteristics and pressure distributions. It's through the collection of this data, that manufacturers can validate the predicted lift characteristics and ensure they comply with regulatory standards, since experimental data provides a reliable basis for these evaluations.

The weight of an aircraft is typically known and determined based on the design and equipment installed on the aircraft. It can be measured during the manufacturing process or calculated based on the known weights of the individual components. To measure the actual weight of an airplane, there are specialized weighing scales or load cells that can be used. The weight measurements can be made by either weighing the entire aircraft or measuring the force exerted by the weight at specific points. (23)

From a mathematical point of view it can be determined through Newton's second law:

$$W = mg \tag{2.2}$$

Where:

$W \longrightarrow Weight$

$m \longrightarrow Mass$

$g \longrightarrow Gravity$

Although it's important to note that this simple approach doesn't take into account factors such as the weight not being evenly distributed throughout the structure of the aircraft, or the fact that the mass of an aircraft is not constant during the whole flight operations due to fuel consumption, payload changes and eventual equipment additions or removals, these are the motives that lead to the need to monitor this changes in real-time during flight. Weight can also be determined, at same level flight, according to the lift equation since $W = L = \frac{1}{2}\rho V^2 C_L S$.

Consider the following situation, if the speed of an aircraft is reduced, and therefore the lift generated decreases, but it is required to stay at a straight level flight, in order to increase the lift produced with a lower speed, the angle of attack needs to be changed, this means that the lift force vector will not be totally vertical, which results in a rearward vector that contributes to the drag component, this situation is shown in the following schematic in Fig.(2.7):

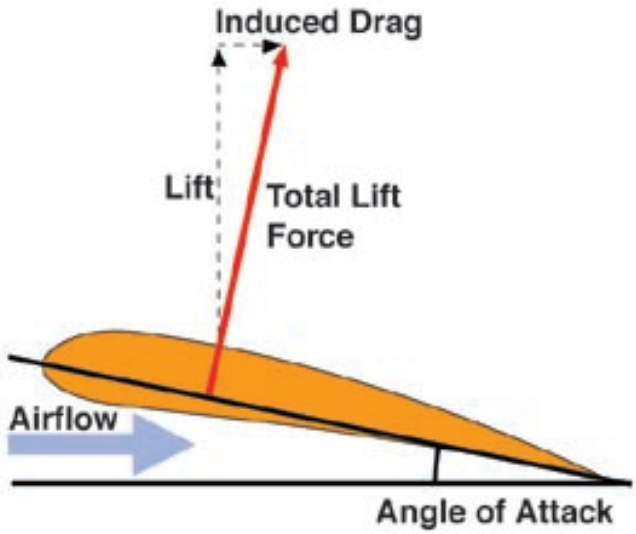

Figure 2.7: Example of induced drag generated by the lift force, when the angle of attack is different from 0° (24)

Drag can be also calculated with a similar formula shown for lift, but that it considers a drag coefficient instead of a lift one, which for the same motives described above poses some disadvantages in comparison to experimental data.

$$D = \frac{1}{2}\rho V^2 C_D S \tag{2.3}$$

Where:

$D \longrightarrow Drag\ Force$

$C_D \longrightarrow Drag\ Coefficient$

2.3 Braced Wing Concept

In this section the concept of braced wings is introduced, while exploring its main advantages and disadvantages.

Typically, one quarter to one third of an airline costs are related to fuel consumption of the aircraft (25), so it is no surprise that one of the biggest selling points of the next upcoming airplane to invest is the one that can be more fuel efficient, which means it needs to have less drag.

It is hard to change parasitic wing drag since design constraints and certification requirements play a

huge role in shaping the aircraft, so the easiest way to reduce drag would be by changing the lift-induced drag. This is exactly what a braced wing also known as trussed wing can improve.

The concept of braced wings is not new, as seen in the historical background provided in cahpter 1.5. (26)

Thin wings, with high aspect ratio, would provide lift with low drag during cruise, making the aircraft more efficient during that flight phase. Considering modern airplanes spend most of their time when they are flying at cruise altitude, being this flight phase the one that spends the vast majority of the energy required for flight (27), it will theoretically maximize the overall advantage of using braces, and thus it's being currently studied by OEM's such as *Boeing*, as a possible way to improve fuel consumption. (28)

Firstly, and more importantly a braced wing can significantly enhance the structural stiffness of the wing, this means that by incorporating braces, it becomes possible to have higher aspect ratio wings which are more efficient due to their ability to reduce induced drag and improved L/D ratio. In other words, braces allow to maintain the necessary wing strength and deflection, without penalizing their structural mass, while they can withstand its increased wingspan, which is one of the conditions required for drag reduction.

However, it is important to note that the implementation of wing braces also presents some challenges, for example, the increased wing span of the aircraft, specially if this concept is applied to commercial aeroplanes is that a significant portion of the outboard wing could possibly need to be folded to comply with the airport restrictions or to facilitate storage in hangars. This is especially relevant in airports that don't possess long runways, that may also have tall obstructions like buildings or natural obstacles near the runways.

Also, it can be argued that higher aspect ratio wings, may limit the possibility of fuel storage, due to the smaller wing box, this added to the fact that the use of the folding part of the wing for that purpose becomes unfeasible, as is the case with B777-X (29). This change can result in the necessity for alternative fuel storage solutions such as utilizing other areas within the aircraft, such as beneath the cargo floor along the length of the fuselage.

The placement of wing braces needs careful consideration, as it can affect and be affected by the wing span-wise location. In the case of wing-mounted engines, the interaction between the airflow around the engine and the braces could potentially disrupt the airflow over the top of the wing, where the majority of lift is generated. This aspect requires thorough analysis and design considerations to minimize any adverse effects on aerodynamic performance. One possible solution would be mounting the engines higher on the wing, although this may pose challenges in terms of maintenance and servicing.

To summarize, while wing braces offer advantages such as increased structural stiffness and reduced induced drag, there are associated challenges to address, including fuel storage considerations, careful engine placement and added drag by the structure. Careful engineering and design choices are crucial to mitigate these challenges and optimize the overall performance and efficiency of next-generation aircraft. (30)

2.4 Braced Wing Competitors

In the next subsections several braced wing aircraft competitors examples, following this concept, will be studied along with their main characteristics for later comparison with continuous cantilever wing aeroplanes of the same class.

2.4.1 Textron CESSNA 408 Sky Courier

In order to understand the CESSNA 408 Sky Courier aircraft, being the newer model built by Textron, it is important to understand a bit of the background of the previous developed models.

Textron Cessna 408 SkyCourier, comes following the needs of FedEx Federal Express, which has placed an initial order for 100 of this model.

Being one of the largest aircraft manufacturers by number of aircraft produced, this company is known for their utility aircraft as well as the thousands of pilots trained worldwide and for its business jets. This new twin-engine propeller-driven aircraft is the first after almost 30 years. The previous twin-engine built is known as the Cessna 441 Conquest II Fig.(2.8), produced in Kansas. (31)

Figure 2.8: Cessna 441 Conquest II during flight (32)

The C208 Caravan Fig.(2.9) is a single-engine turboprop made also at the request of FedEx by Cessna in the 1980s, focusing on operation in small airports with few infrastructures.

This aircraft's reputation has grown since then, making it the only single-engine aircraft authorized to carry the US president if needed, given its reliability and robustness. Later on, Cessna decided to create the twin-engine version, and again members of the FedEx Express design and engineering teams participated in the Textron Aviation Customer Council to help shape the aircraft's design, features and aid with maintenance.

Figure 2.9: Cessna 208 Caravan (33)

With this new aircraft, Cessna 408 Sky Courier Fig.(2.10), Cessna and FedEx renewed their collaboration. With the new C408, Fedex now has nearly twice the payload capacity (2.72 tons versus 1.67 ton for the C208), while being able to have containers on board, something unthinkable on the smaller single-engine plane.

The aircraft is powered by two wing-mounted Pratt & Whitney PT6A-65SC turboprop engines and uses four-bladed McCauley Propeller C779, 110-inch aluminum propellers, which is fully feathered with reversible pitch, designed to enhance the aircraft's performance when carrying large loads.

It has a maximum cruise speed of over 200 knots (370 km/h) and a maximum range of 920 nautical miles (1704 km).

The aircraft features two braces with a large door with a flat-floor cabin, and the freighter version can hold up to three LD3 containers with an impressive payload capacity of approximately 2268 kg. (34)

Figure 2.10: Cessna 408 Sky Courier in an airport runway runway (35)

In Fig.A.1 present in Appendix A, relevant information regarding the passenger plane dimensions and characteristics is shown. (36)

2.4.2 De Havilland Canada DHC-6 Twin Otter

The de Havilland Canada created the Canada DHC-6 Twin Otter Fig.(2.11), a Canadian STOL (Short Take-off and Landing) utility aircraft, which displays two braced wings and manufactured it from 1965 to 1988. Viking Air obtained the aircraft type certificate and resumed its production in 2008 before resuming the use of the DHC in its name in 2022. The aircraft is a successful passenger transport aircraft, normally with 18–20 seats, but it works as well as a freight and medical evacuation aircraft. Due to its fixed tricycle landing gear, STOL capabilities, twin turboprop engines, and high rate of ascent, it is capable of carrying passengers and cargo into remote semi-prepared locations, including ski and water-based operations. The Twin Otter aircraft have been sold around the world to customers operating in the harshest environments, including sub-zero temperatures in Antarctica, the hottest deserts of North Africa, the mountainous regions of the Himalayas, and the open water of the Indian Ocean archipelagos. It became the best-selling 19 passenger aircraft of all time, still unequalled for its durability and adaptability, as a testament to its tough build and remarkable STOL performance. The United States Army Parachute Team and the 98th Flight Training Squadron of the United States Air Force both operate the Twin Otter, which has also gained popularity in commercial skydiving operations. (37; 38)

Figure 2.11: De Havilland Canada DHC-6 Twin Otter (37)

A table with relevant characteristics of this aircraft is present in Annex B.

2.4.3 PZL M28 Skytruck

The M28 Skytruck Fig.(2.12) was created by PZL Mielec, a division of the aerospace manufacturer Lockheed Martin, to accommodate a variety of uses, including aerial surveillance, marine patrol, search and rescue missions and para-dropping, besides carrying freight and passengers. Its tough design, includes two braces, a high-wing and reinforced landing gear, which allows it to take-off and land on small airstrips, which makes it useful for carrying missions in hard-to-reach places.

Its interior is modular, enabling an easy reconfiguration to meet various mission needs, and therefore increases its versatility.

With a range of up to 932 nautical miles (1500 km) and a maximum cruising speed of roughly 192 knots (355 km/h), the aircraft can travel long distances without sacrificing its payload capacity. (39; 40)

Figure 2.12: PZL M28 Skytruck (41)

Annex C has some relevant dimensions regarding this aircraft and extra information can be found on the respective website cited.

2.5 Continuous Cantilever Wing Competitors

The continuous cantilever wing structure is an efficient wing design used in aircraft, since it provides several advantages from a structural perspective.

One of the primary benefits of a continuous cantilever wing in comparison with its braced competitors is its enhanced aerodynamic efficiency. Without external struts or supports, there is less interference with the airflow over the wing's surface, reducing drag and improving its overall performance.

This design allows for higher speeds and increased fuel efficiency, which are both crucial factors in modern day aviation, particularly in commercial airliners and long-range aircraft.

Furthermore, the absence of external supports also reduces the complexity of the wing assembly, simplifying maintenance and reducing potential failure points. With fewer components to maintain and inspect, the continuous cantilever wing design enhances the aircraft's overall reliability and decreases maintenance costs over its operational life.

Another advantage is the increased usable space within the aircraft's wingspan. The lack of external bracing allows for a more spacious wing interior, which can be utilized for additional fuel storage, auxiliary systems, or payload capacity, since braces can penetrate on the internal aircraft wing space. This extra

space enhances the aircraft's versatility and adaptability for various mission profiles, making it suitable for both passenger and cargo applications.

However, since in this configuration, the wing extends outward from the fuselage without any external supports or braces, it relies on the wing's internal structure to support the entire aerodynamic and operational loads experienced during flight, this leads to a more robust wing in comparison with its braced wing competitors since it must be capable of withstanding alone the various loads experienced during flight. These loads aren't so evenly distributed as in the braced wing configurations. This leads to the fact that the overall thickness needed to provide the necessary strength and stiffness to bear the bending and torsional moments encountered in flight is larger, and thus it accounts for an increased wing weight in comparison with the braced wing concept. Changing materials to new composites or titanium alloys may be able to achieve the required strength-to-weight ratio, ensuring the wing remains lightweight yet durable. (42)

2.5.1 Indonesian Aerospace N-219

The Indonesian Aerospace N-219 Fig.(2.13) is an aircraft developed by PT Dirgantara Indonesia (PTDI), a state-owned aerospace company based in Indonesia. This aircraft aligns with Indonesia's vision to improve regional air connectivity, addressing the unique aviation needs of remote areas and fostering socio-economic development in the country. This aircraft aims to reduce dependency on foreign aircraft imports and to promote self-reliance in the aviation sector. By offering a cost-effective and reliable solution for regional air transportation, this indigenous aircraft plays a crucial role in expanding access to essential services, promoting tourism, and facilitating the movement of goods and people across the country.

The N-219 features a rugged high-wing design and sturdy landing gear, enabling it to operate from short and semi-prepared airstrips, which are common in Indonesia's remote and island-dotted regions. This capability opens up access to previously underserved areas, facilitating the transportation of passengers, cargo and essential supplies.

Designed with versatility in mind, the N-219 can be easily adapted for various roles. Its spacious and configurable interior allows for different seating arrangements, accommodating up to 19 passengers or carrying a combination of passengers and cargo, depending on the mission requirements.

Powered by two Pratt & Whitney Canada PT6A-42 turboprop engines, the N-219 exhibits a maximum speed of approximately 240 knots (390 km/h) and a range of up to 550 miles (890km) with full payload, making it well-suited for short to medium-range flights within Indonesia's vast archipelago.(43; 44)

Figure 2.13: Indonesian Aerospace N-219 (45)

For performance information of this aircraft consult Annex D.

2.5.2 Dornier 228

The Dornier 228 Fig.(2.14), crafted by Dornier GmbH is a twin-turboprop aircraft which displays a cantilever wing, that is used for a broad array of missions, from regional connections to specialized tasks.

The Dornier 228 impressive performance is attributed to its two high-performance turboprop engines Garrett TPE331, providing a high maximum speed of 223kn (413km/h) and an impressive range of 690mi (1111km). This ensures efficiency and reliability for short to medium-range flights. The aircraft's cost-effective operational features have made it an attractive option for regional airlines and governmental entities, enhancing connectivity and supporting economic growth in remote areas. (46)

Throughout its extensive history, the Dornier 228 has earned the trust of operators worldwide. Its consistent performance and ability to operate in diverse conditions have solidified its position as a reliable and sought-after aircraft. As it continues to serve a multitude of missions across the globe, the Dornier 228 remains a testament to German engineering and innovation, embodying the core values of dependability, versatility, and operational excellence. (47)

Figure 2.14: Dornier 228 (48)

The respective measurements and main characteristics are found in Annex E.

2.5.3 Let L-410 Turbolet

The Let L-410 Turbolet Fig.(2.15), manufactured by Let Kunovice, its another adaptable twin-turboprop aircraft with a cantilever wing, suited for remote missions. It's a reliable choice for accessing challenging terrains and remote areas.

Powered by two Walter M601 turboprop engines, the Let L-410 Turbolet features a maximum speed of 219 kn (405km/h) and range for short to medium-distance flights around 930 mi (1500km).

As a testament to Let Kunovice's engineering prowess, the Let L-410 Turbolet continues to demonstrate its dependability and resilience in diverse environments. A go-to aircraft for critical missions worldwide, it embodies the core values of reliability, versatility, and operational efficiency, making it an indispensable asset for addressing the unique challenges of remote operations. (49; 50)

Figure 2.15: Let L-410 Turbolet (51)

Characteristics of this plane are shown in Annex F.

2.6 Certification Requirements

In this section aviation regulations and aircraft certification will be explained. In the United States, aircraft are certified in accordance with regulations called the FAR (Federal Aviation Regulations) which superseded the CAR (Civil Aviation Regulations). In Europe, the regulations are called CS (Certification Specifications) which superseded the JAR (Joint Aviation Regulations) in 2003. The CS are enforced by the EASA (European Aviation Safety Agency), which is an Agency of the European Union.

International harmonization of the certification standards is on-going and will help simplify the compliance process needed from an airplane, to be able to fly in one country and being accepted in others.

Regulations can either be prescriptive or performance based, with prescriptive regulations specifying what is required to meet a standard, while performance based regulations allow some flexibility that accommodates nonstandard design solutions.

The FAA (Federal Aviation Administration) defines General Aviation as aircraft other than airliners and military aircraft, and in the US, GA (General Aviation). (1)(p.10)

For each aircraft category there are different certification requirements and codes, in this particular case, the certification specifications of small aircraft category are FAR-23 and CS-23. FAR-23 (52) and CS-23 (53) certification values can be found in their respective references.

Part II

Core of the Dissertation

Chapter 3

Aircraft Finite Element Model

In this chapter the choice of the reference aircraft used for the several studies will be justified, as well as providing an explanation of the procedure for the finite element model development along with the braces choices itself. The steps made for mass and drag concerning braces will be addressed. The different load cases considered, the constrain methods used and all pre-processing information are also part of this chapter.

3.1 CESSNA Sky Courier - Reference Aircraft

From the several aircraft previously described, it was decided to use CESSNA Sky Courier as a reference model for the study of braced wings, since it was one of the aircraft with more data available. It offers a wealth of technical information and data as shown in Annex A, that will be useful for both reference and validation, being an aircraft from the CS-23 category. It was also developed by a reputable manufacturer, Cessna (a subsidiary of Textron Aviation) which means that it has also recognition from the aviation industry which can be useful for this study, being one of the most recent developments in the aircraft exhibiting braces. It has undergone rigorous design, engineering, and testing processes to meet regulatory standards, choosing it as a reference provides a solid foundation for studying braced wing models.

From an application point of view The Skycourier is designed with a modern braced wing configuration, for similar purposes of those of CEiiA and thus it can provide a good base study for further development.

3.2 Operating Conditions

Before starting to model the aircraft, several operating conditions were defined. This conditions will determine the respective structural behavior, loads and overall performance of the aircraft, so it is of utmost importance to correctly define them for what it is intended to be studied.

As mentioned before the intention is to compare the performance of wings with and without braces. Considering SkyCourier baseline geometry and operating conditions.

An operation speed of $108m/s$ ($388.8km/h$) was defined, which is very close to its maximum cruise speed $389km/h$ (36). This option was taken since the speed influences the magnitude of the loads acting on the aircraft's structure, being that the highest values of loads on the wings, fuselage, and other components, occur at higher values of speed.

Regarding altitude, the value chosen was $5000ft$ ($1524m$) instead of the $7620m$ maximum operating altitude. This is due to the fact that at lower altitudes such as the value chosen, the forces on the structure are generally higher due to higher air density and dynamic pressure being higher, which will result in increased drag resistance. Flying at sea level, would be the most demanding scenario for the aircraft's structure, however due to the velocity chosen this situation is incompatible with sea level flight since it is known that flying at sea level only happens during takeoff and landing phases, being unrealistic to fly at maximum speed at this altitude. It was then defined this $5000ft$ as the minimal altitude at which the airplane could fly at its highest cruising speed.

Regarding aircraft weight it was defined as $6500kg$. This value is lower than the MTOW which is $8618kg$ for this aircraft. Although it's common practice to analyze structures under worst-case scenarios (such as MTOW), a more typical operating condition value was chosen, since using the highest value would lead to excessively high force values that the model could not withstand, since although the entire aircraft is modeled, it is not fully correctly sized, this would lead to an overestimation of the structural forces and stresses applied on the wings, and consequently an overestimation of it's design, ultimately making the analysis less accurate and the results obtained unrealistic.

By choosing these conditions it is guaranteed that if the aircraft wings can withstand these conditions anything below these values are safe.

3.3 Load Cases

Regarding the load cases used, a positive load case was defined in line with the flight envelope of a typical aircraft of this category Fig.(3.1). For this aircraft CS-23 was used. (54)

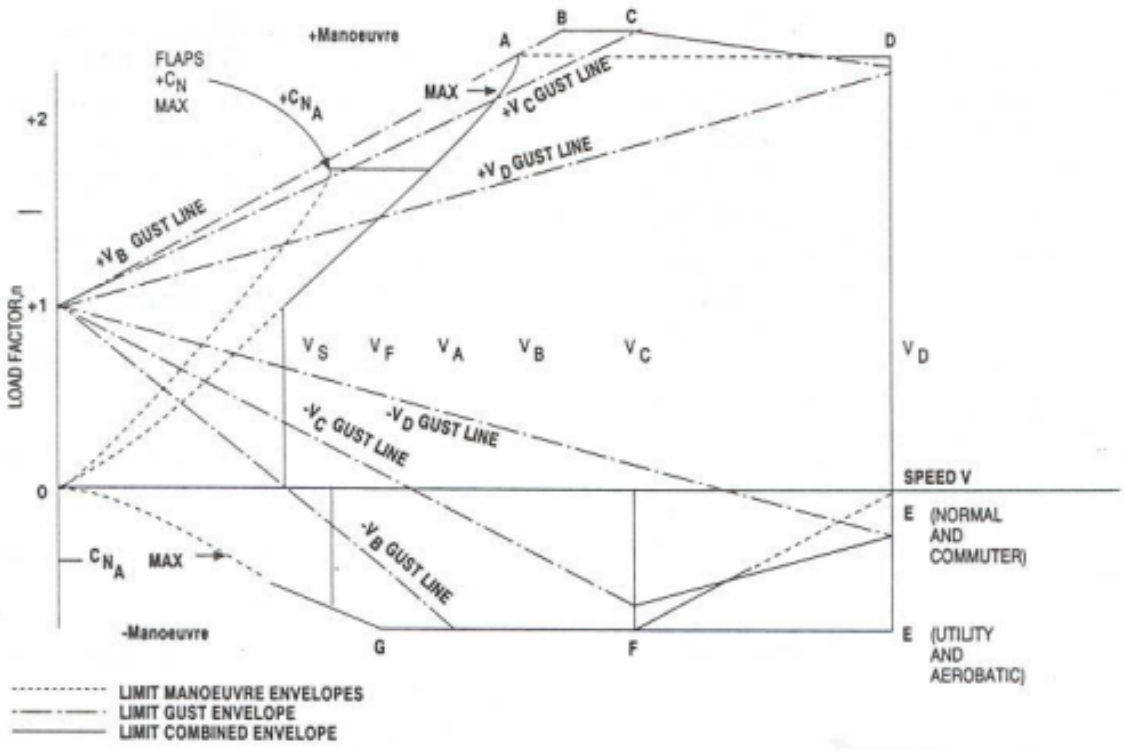

Figure 3.1: Flight envelope for CS-23 category aircraft (55)

Although the limit positive load factor is 4.4, for utility category aeroplanes, as it is stated in CS 23.337 Limit manoeuvring load factors (56)(p.33), it was considered a positive load factor of 3.5 for the simulations, since the aircraft isn't fully sized and thus the aircraft wings would not be able to withstand such values.

For the sake of brace sizing, it was used a representative load case with a negative load factor, so that the brace can be sized for both tension and compression. To avoid running extra simulations for that load case, it was thought of factoring the existing positive case. It was ran the baseline wing with that negative load factor to understand what a realistic factoring would be, and then that same factoring was applied to the other wings.

According to CS23-337, line b) the limit negative maneuvering load factor should be 0.4 times the positive load factor. For normal, utility or commuter categories.

This results in a real negative load factor of $3.5 \times 0.4 = 1.4$, being this the value considered for the compression cases.

3.3.1 Aerodynamic Load

To determine the aerodynamic loads in a first stage it was defined single point actuating forces on the tip of the wings in *Hypermesh*[1]. Then using the CFD software AcuSolve[2], several simulations were run, from which resulted documents written in *NASTRAN*[3], which were imported into Hypermesh, including the grid points of the actuating forces, as well as the force value in the three Cartesian axes.

It is important to note that the section that has no dihedral, which is above the fuselage in both cases, were not simulated, since in that region, the load will be the same on wings with and without braces, and so it won't matter for marking differences between the models. Removing this section was beneficial since it made the analysis quicker in numerical calculation and easier for post-processing.

In addition, since only the wings of the aircraft were used in the CFD simulations it would introduce the error of not having the fuselage affecting the flow in that region, so the validity of the simulation in that area would be already compromised since the beginning, being pointless running it.

3.4 Finite Element Model Development

For the finite element model the used software was *Hypermesh* but in order to do so, first a geometry was needed. For that purpose and since this software isn't the best for geometry modelation *Fusion360*[4] was used.

3.4.1 Fuselage and Overall Dimensions

In a first stage, the dimensions of the airplane were taken from screenshots from the aircraft website (36), then using *Adobe Acrobat Reader* and it's measuring functionalities, a scale using the cramming measures of the airplane in the figure it was possible to determine approximate dimensions of the different components of the aircraft. However it is important to note that due to the view angles, there can be some visual distortion of the sizes in the plane, and thus some measurements might be more prone to higher errors in comparison with others. In Annex J the measurements of Cessna Skycourier are present.

[1] Altair's 3D modeling and simulation pre-processing software for engineering and finite element analysis.

[2] A computational fluid dynamics (CFD) solver developed by Altair, utilized for simulating and analyzing fluid flow, heat transfer, and related phenomena.

[3] Part of NASTRAN software, it handles finite element analysis (FEA) for structural and thermal simulations in engineering.

[4] Fusion 360 is Autodesk's cloud-based software for 3D design, CAD, CAM, and CAE applications.

3.4.2 Airfoil Measuring

The challenging part regarding this phase was deducing the type of airfoil used in the aircraft since this is usually not revealed by the companies. However trough some investigation of NACA (National Advisory Committee for Aeronautics) codes it was possible to roughly identify which kind of airfoil it was being dealt with.

In order to understand which NACA airfoil was used first it is important to understand what does the code stand for. Most common NACA airfoils have a code of four numbers (57), where the first digit denotes the maximum chamber as a percentage of the chord. Based on the measurements made the camber maximum distance from the chord is $0.05m$ while the chord length is $1.6m$, by calculating the respective ratio $0.05/1.6 = 0.03125 = 3\%$ was obtained. Regarding second digit, it relates the position (distance) of the maximum camber from the leading edge in tenths of the chord, in this case the maximum camber is located at $0.48m$ from the leading edge of the airfoil by solving the ratio its obtained $0.48/1.6 = 0.3 = 30\%$. Finally the last two numbers refer to the maximum thickness of the airfoil as a percent of the chord, in this study the airfoil thickness is $0.18m$ dividing by its chord $1.6m$ and solving the ratio $0.18/1.6 = 11\%$. And thus the first estimate concludes that this wing would be a NACA3311. By consulting a database (58) it was concluded that this standard wing doesn't exist being the closest one the NACA4412. This was the airfoil chosen since the values of the maximum chord were over dimensioned and in comparison with a Cessna 172 wich possess a NACA 2412 airfoil, the difference in maximum camber was noticeable by comparing the two wings.

3.4.3 Aircraft Modelling

Several modelling considerations were taken during the development process of the aircraft, that will affect the overall results of the simulations and consequently its reliability.

First of all the accuracy of the finite element model will depend on the quality of the input geometry. Due to software limitations, simplifications had to be made to reduce computer processing time and this resulted in a simplified geometry. Some elements such as the turbines or the landing gear weren't modelled, parts which would account for the total weight.

After making the respective drawing in Fusion 360, the file was exported in IGES and STEP to prepare the geometry before its meshing. Below a picture of the geometry that was previously developed in Fusion and its corresponding imported file in Hypermesh Fig.(3.2).

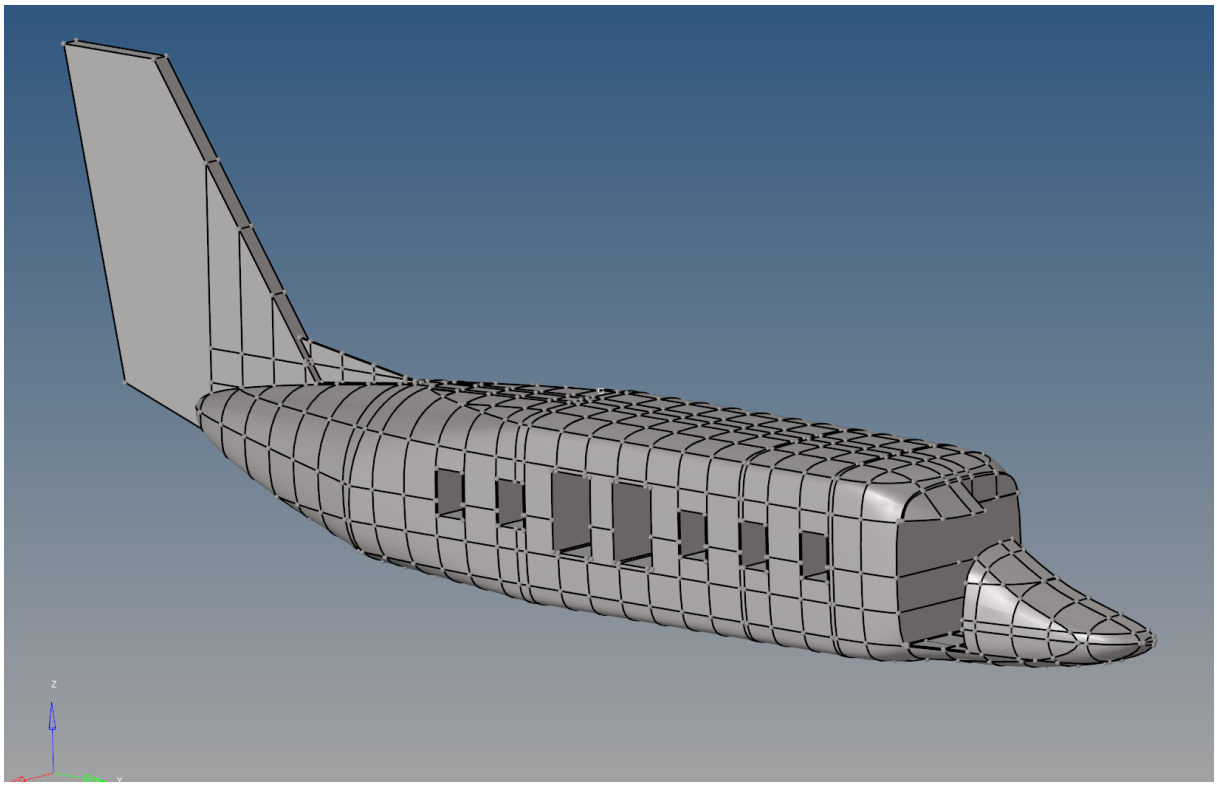

Figure 3.2: Baseline for the Fuselage Geometry of Cessna Skycourier

After having the geometry defined, some of the most relevant variables are the kind of elements to be used for the meshing process and size or density of the mesh. It was stipulated that for element type shell CQUAD would be the favoured choice. Since shell elements provide an accurate representation of thin structures, being able to capture bending and buckling behaviors while reducing computational costs.

By choosing quadrilateral 2D elements (CQUAD) over triangular 2D elements (CTRIA), it is possible to create an overall more structured and regular mesh compared to CTRIA, and simultaneously providing a better representation of the stiffness properties in certain directions due to their rectangular shape and adapting better to other 1D elements used such as CBEAMS, improving the numeric quality of the results Fig.(3.3).

For mesh density, an overall density of 25mm would be a fine enough mesh to obtain reliable results while keeping computational time low enough to run several simulations.

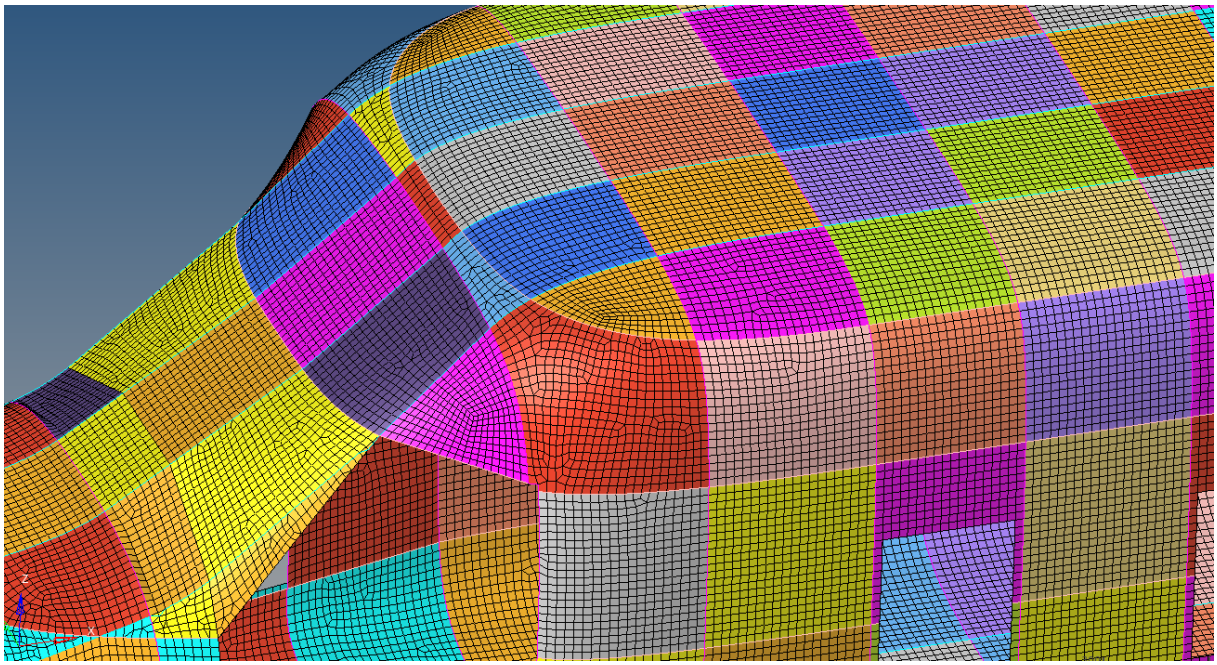

Figure 3.3: Detail of generated mesh with shell elements in Cessna Skycourier

Regarding the wing modeling, this was done recurring to a software developed by André Pereira named WinG3N (59), which through a series of inputs allows to generate several wing cases in an easy way, being the user able to control aspects such as the number of structural elements as well its spacing, such as ribs, spars, leading and trailing edge caps, and wing dimensions and angles (such as diedral across different segments). Also several extra inputs such as loads can be directly added to each case.

It is important to note that in this model the doors were considered "non structural" meaning that these structures do not resist loads. Since the windows are never a structural component they were not represented in a curved way, but either in an approximated rectangle way which made the mesh more squared formed.

The baseline wing was divided into several sections as seen in Fig.(3.5). Those parts were divided according to the existence of diedral and taper. The first zone consists of the segment of the wing above the fuselage, which consists in a non-diedral and non-tapered zone, followed by a wing root with a diedral zone of 2°but with no tapper. It is also in this section where the engine would be mounted. The third and last division consists in a zone with the same diedral as the previous one but exhibits a taper angle.

Below a scheme in Fig.(3.4) of this division with some dimensions for the baseline wing.

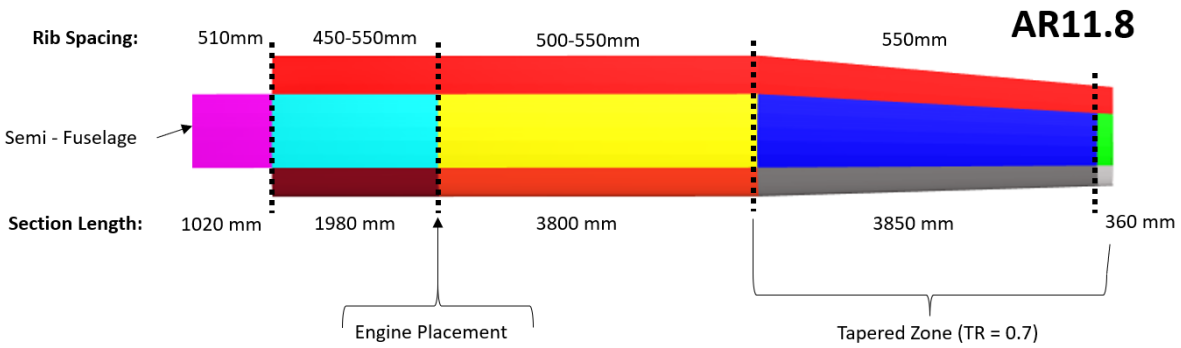

Figure 3.4: Baseline wing section dimensions for cantilever wing and defined rib spacing

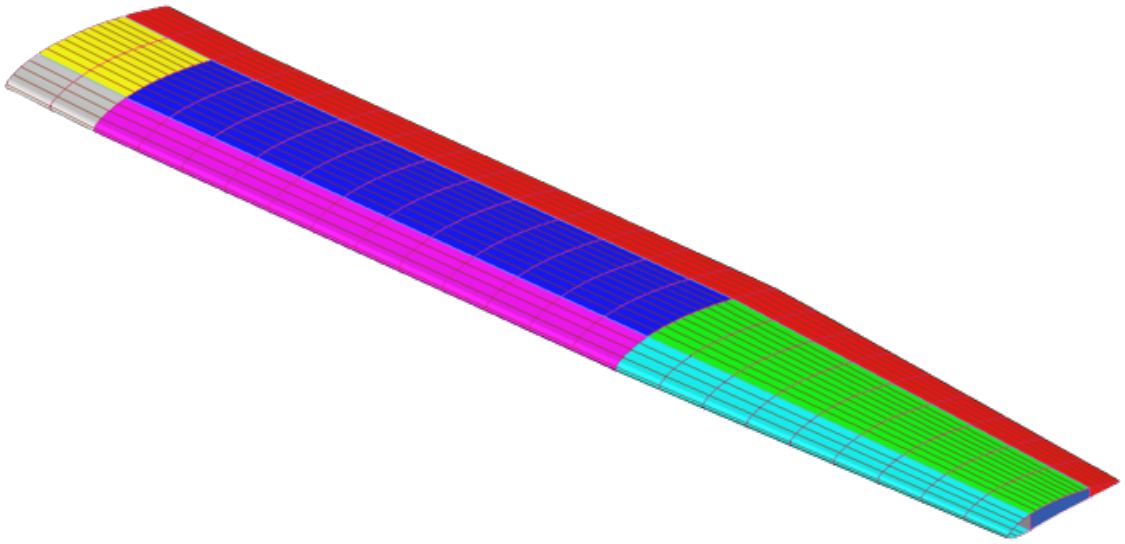

Figure 3.5: Different Wing Sections: In gray the denominated base part placed above the fuselage, in purple the non tapered part of the wing and in light blue the tapered zone of the wing

3.5 Wing Brace Modelling

In the next subsections the procedure regarding mass and drag estimates will be shown using as reference model the baseline model, from which all the other results were calculated. Also a fuel consumption estimate will be made.

3.5.1 Mass and Drag Estimates

In relation to the mass estimate, the structure was sized in order to hold compressive loads of -0.4 of the force applied as well a maximum of 400MPa of tension since the considered material was the same as the rest of the model, an aluminium alloy.

In order to size the wing braces the resultant file from the simulation was analyzed, in particular the *GRID POINT FORCE BALANCE*, where there it is possible to obtain the respective forces in the three axes of the two extreme points of the brace, then this values were applied in a force vector in a simulation where the wing brace was isolated, similar to the principle of a fixed beam, so it would be possible to understand if it was correctly sized to compression load. In Annex G these forces are shown in a table with all the relevant data used for the brace dimensions.

In a first stage, before any sizing process, an *I* beam was assumed both for the brace as well for the component which was named as *Landing Gear Backup Structure* since it directly connects to the landing gear. These two components can be seen below in Fig.(3.6):

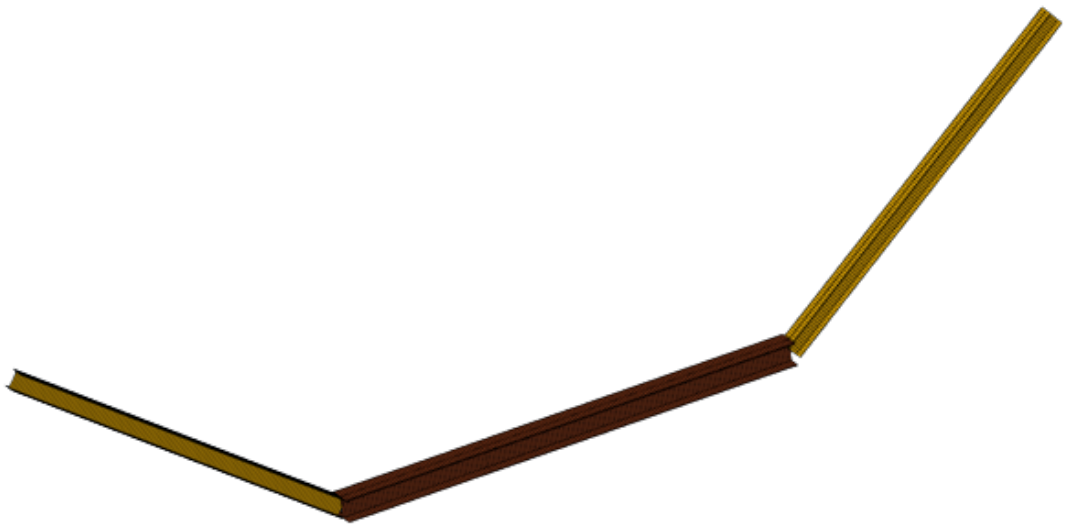

Figure 3.6: Brace (yellow) and Landing gear backup structure (brown) components modeled

Initially this components would weight in total $104.22kg$ a value significantly bigger than the $76.133kg$ of the removed central mass of the Cantilevered Wing model. This meant that the addition of the brace components alone, even with the removal of the central mass of the Cantilevered Wing model above the fuselage would prove insufficient to provide any benefit in terms of weight savings to the structure. Of

course this happened because both wing thicknesses were now way oversized for the stresses that were being obtained. This was due to a much better distribution of these loads across the wing sections instead of the stress peaks that were being obtained in the Cantilevered Wing model.

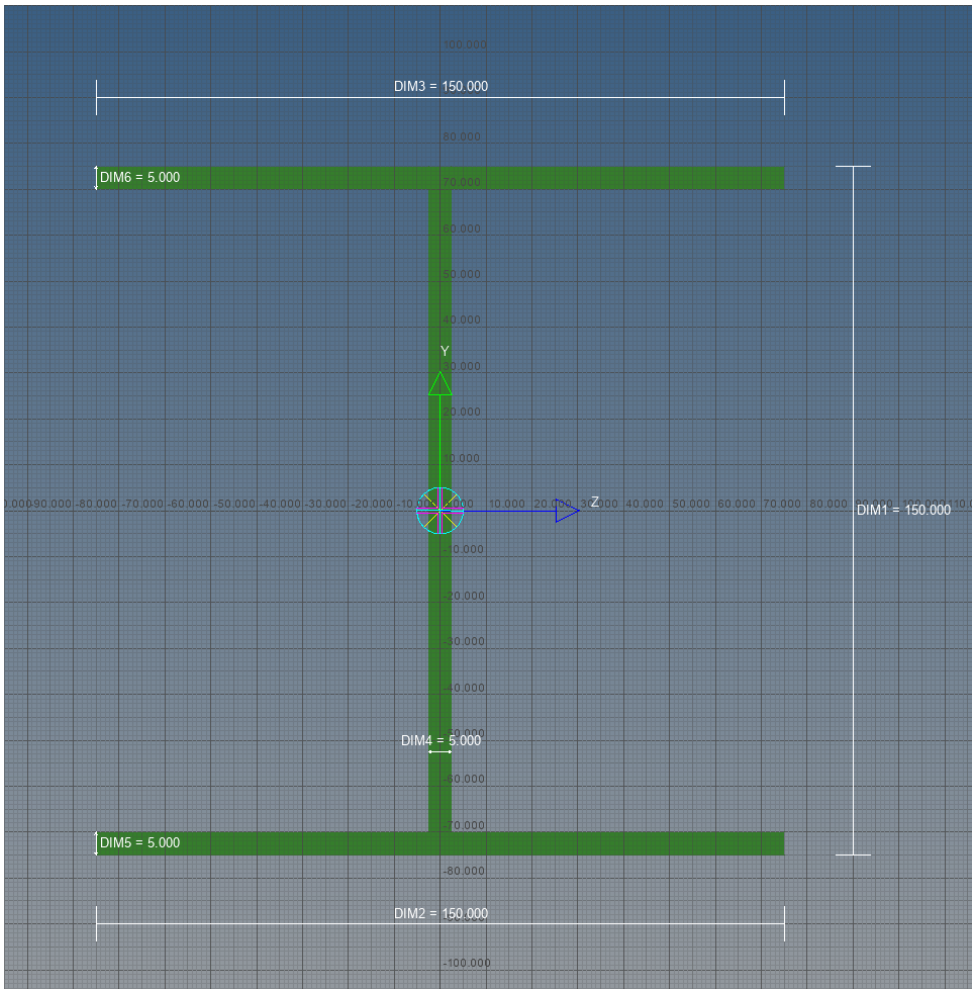

Figure 3.7: Brace initial cross section

The brace thickness is $5mm$ and its cross-section length and width reduced from an initial value of $150mm$ to $110mm$. This would lead to a total weight of the structure (including Trem) of $63.9kg$, which meant a reduction of 40.73% in comparison with the initial mass of this same structure of $107.847kg$. In order to visualize how big of an impact this made on the braces, it is worth noting that the Trem itself initially weighted $66.3kg$ this means that the brace alone initially accounted for $41.5kg$ of this value and went down to only $28.7kg$ after the trial and error sizing process. This meant a reduction of 30.8% in brace mass.

The Landing gear backup structure structure wasn't fully sized, although it is expected an improvement of the results obtained, since it would benefit of extra rigidity due to the possibility of connecting the main landing gear to this structure. It was defined that the Trem beam overall thickness would be $7.5mm$, and

it's cross section dimensions which had to be $150mm$ in order to withstand the tension force coming from the braces without deforming the fuselage skin, in comparison with the initial values of $210mm$ of cross section dimensions and $10mm$ thickness, which it was clearly oversized, after realizing the respective analysis. The trem finished with a mass of $35.2kg$ which represents a reduction of 46.96% regarding its initial value of $66.3kg$.

Since each model will have different brace lengths, it is expectable for its weight contribution to change. The same procedure was then done for each wing brace, where the relevant variables of each brace are shown in Table (3.1):

Table 3.1: Relevant Measures of the Wing Braces

Wing Aspect Ratio	**9.837**	**10.837**	**11.837**	**12.837**	**13.837**
Wing Brace Length [mm]	3052.0	3187.0	3325.0	3289.3	3407.3
Wing Brace Square Cross-Section [mm]	97	102	110	107	112
Wing Brace Mass [kg]	23.7	26.1	28.7	28.3	30.7

Although the wingspan increases, it should be noted that in the model for the wing aspect ratio of 12.837 the wing brace length reduces, this is due to the fact that the criteria used to fix the wing brace was the 3rd rib counting from the engine. The rib spacing between the different models are different, in this case since the model produced by WinGen surpassed the defined threshold, the rib spacing for this model was reduced resulting in more ribs as well as its stringers spacing. This resulted in a shorter brace and sturdier wing in comparison with its homologous models.

The physical weight alone of the structure is not representative of the downside of using braces, which is intimately connected to aerodynamics. The drag produced by a wing brace alone is usually high considering that from a structural point of view it will be designed in a "H" or "I" shape, that's why it's of utmost importance to design an aerodynamic fairing to cover this structural component and reduce the overall drag produced.

To estimate this value, the drag formula was used, applied to the braces:

$$D_{Strut} = \frac{1}{2}\rho V^2 S \Delta C_{D_{Strut}} \tag{3.1}$$

Where:

$D_{Strut} \rightarrow Drag\ for\ the\ strut\ in\ N$

$\rho \rightarrow Air\ Density\ in\ kg/m^3$

$V \rightarrow Speed\ in\ km/h$

$S \rightarrow Surface\ Area\ in\ m^2$

$C_{D_{Strut}} \rightarrow Drag\ coefficient\ for\ the\ strut$

All of the above values are known with exception of the drag coefficient of the strut, for that reason it was used the following empirical equation which was obtained through experimental results (1) to obtain an estimate of that value:

$$\Delta C_{D_{Strut}} = [2\bar{C}_f[1 + (t/c)] + (t/c)^2](\frac{lc}{S}) \tag{3.2}$$

Where:

$C_{D_{Strut}} \rightarrow Drag\ coefficient\ for\ the\ strut$

$C_f \rightarrow Skin\ friction\ coefficient$

$t \rightarrow Thickness$

$c \rightarrow Chord$

$l \rightarrow Length$

$S \rightarrow Surface\ Area$

Taking into account that aerodynamic factors often determine the shape and dimensions of the aviation components, it is necessary to design a wing strut fairing in order to minimize this induced drag component. It's clear that the thickness to chord ratio (t/c) plays a fundamental role and thus should be optimized. In order to do so, the following empirical equation was used:

$$FF = 4 + \frac{2}{(t/c)} + 120(t/c)^3 \tag{3.3}$$

Where:

$FF \rightarrow Form\ Factor$

By determining the derivative, setting it equal to zero, and solve for the optimum t/c, as shown below:

$$\Rightarrow \frac{dFF}{d(t/c)} = 360(t/c)^2 - \frac{2}{(t/c)^2} = 0$$
$$\Rightarrow (t/c)_{opt} = \sqrt[4]{\frac{1}{180}} = 0.273$$

It was determined that the optimum thickness-to-chord ratio is 0.273. This means that the fineness ratio for this optimal value is ≈3.663, since $Fineness\ Ratio = \frac{Chord\ Length}{Thickness}$.

Taking these values as references, we can now dimension the rest of our strut fairing to be aerodynamically enhanced. In Fig.(3.8) it is possible to see several standard cross sections of wing struts fairings:

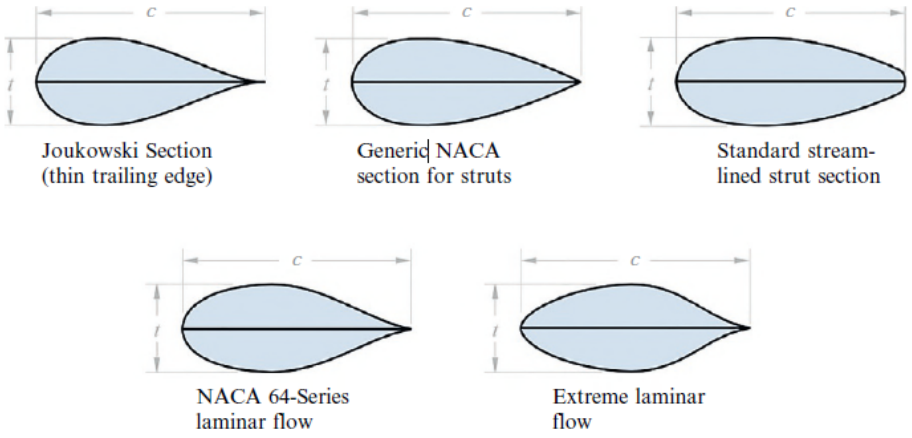

Figure 3.8: Different Strut Fairing Sections (1)(p.716)

Depending on the flight conditions, such as speed, altitude and consequently the kind of flow characteristics, we can choose optimal section for this case. In order to determine whether the air flow is laminar or turbulent around the wing braces Reynolds Number should be calculated, following the equation:

$$Re = \frac{\rho V D}{\mu} \tag{3.4}$$

Where:

$Re \rightarrow Reynolds\ Number$

$\rho \rightarrow Air\ Density$

$V \rightarrow Velocity$

$D \rightarrow Charateristic\ Length$

$\mu \rightarrow Fluid\ Dynamic\ Viscosity$

Considering $108m/s$ as cruise speed at $5000ft$ altitude, assuming U.S. Standard Atmosphere Air Properties in SI Units (60), air density at this conditions is $0.7364kg/m^3$ at $-17.47°C$ and its dynamic viscosity $1.628 \times 10^{-5} N.s/m^2$. Assuming that the brace is similar to a circular pipe, its characteristic length would be its diameter, which in this case is the structure thickness, which consists of the brace thickness $118mm$ plus a small thickness of the brace covering it, it can be estimated to be $125mm$ wide. With all the variables determined, it is now possible to determine:

$$Re = \frac{0.7364 \times 108 \times 0.125}{1.628 \times 10^{-5}} = 610651 \tag{3.5}$$

Since it is known that the flow is turbulent when $Re > 4000$, it can be assured we are in turbulent regime.

Given this turbulent flow regime, laminar strut section such as the "NACA 64-Series laminar flow" or the "Extreme laminar flow" can be excluded since they would be better suited for lower speeds. A thicker leading edge can perform better in this condition, and thus a good example would be the Joukowski Section which resembles a streamlined teardrop shape, since it has a smooth, streamlined profile that minimizes the impact on the overall drag, however it is simultaneously impossibly to manufacture, and that's why a "Generic NACA section for struts" is the viable option since it conciliates both price of manufacture and the shape properties of Joukowski Section.

Considering the wing strut thickness of $125mm$ and the ideal Form Factor determined in equation (3.3). The chord of the cross section should be $125 \times 3.663 = 457.9mm \approx 460mm$. Having defined the strut covering thickness and chord in order to accommodate the brace dimensions, it is now possible to determine the drag coefficient in equation (3.2) and how much parasite drag will be generated by the brace (3.1).

To calculate the skin friction coefficient (C_f), it would be needed detailed data about the respective material and knowledge about the skin treatments done to the strut fairing, so it was assumed a value of $C_F = 0.008$ as seen in example of (1)(pp.717). The length of the strut was obtained through *Hypermesh software* which resulted in $l = 3325.026mm$. Regarding the reference area it was determined using *Fusion360 software* $S = 3380900mm^2$ as seen in the following picture:

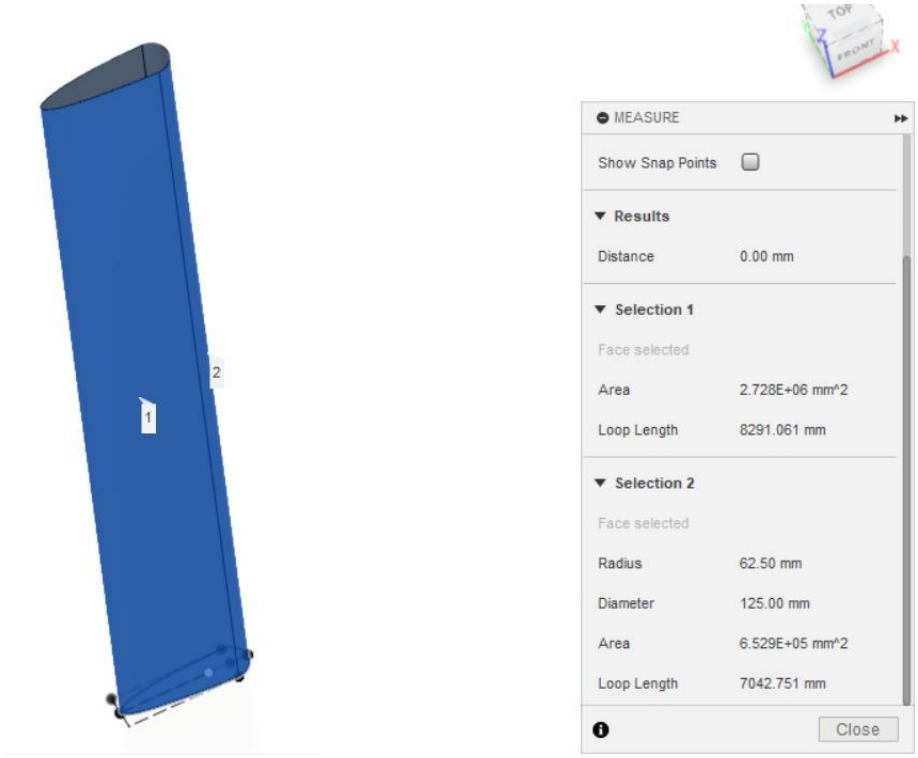

Figure 3.9: Modeled Strut in Fusion360 with area calculation

We can now proceed to calculate the drag coefficient as shown below:

$$\Delta C_{D_{Strut}} = [2 \times 0.008[1 + (125/460)] + (125/460)^2](\frac{3325.025 \times 460}{3380900}) = 0.042611334$$

And finally the additive drag:

$$D_{Strut} = \frac{1}{2} \times 0.7364 \times 108^2 \times 3380900 \times 10^{(-6)} \times 0.042611334 = 618.7123024N$$

3.5.2 Fuel Consumption Estimation

Having determined the drag force generated by the brace it is now possible to determine the fuel consumption following some basic equations.

It is known that power (P) is force (F) times speed (V). In this case, by multiplying the drag force by the air speed the following power is obtained:

$$P = F \times V \tag{3.6}$$

$$\Rightarrow 618.71 \times 108 = 66820.93W$$

With the power calculated it is now possible to convert it to extra energy needed to carry this structure since:

$$P = \frac{E}{\Delta t} \tag{3.7}$$
$$\Rightarrow E = P \times \Delta t$$

In this case, assuming the typical mission range of $1000km$, and considering the $108m/s$ airspeed, it would take $9259.26s$ or $2.57h$ to realize this mission. This will result in an extra energy needed of:

$$E = 66820.9 \times 2.57 = 171864.53Wh.$$

Assuming the specific energy of JET A-1 which is commonly used in aviation of $11990Wh/kg$ (61), it is possible to determine how many fuel kilograms would be needed:

$$Fuel\ Consumption = \frac{E}{Specific\ Energy} \tag{3.8}$$
$$Fuel\ Consumption = \frac{171864.53}{11990} = 14.3kg.$$

This accounts for the extra weight of adding this structure for only one brace to account for the two it would represent $28.7kg$ of fuel.

This procedure was then repeated for each brace, in Table (3.2) it is possible to know each brace corresponding fuel mass.

Table 3.2: Relevant Variable of the Wing Braces and Faring

Wing Aspect Ratio	**9.837**	**10.837**	**11.837**	**12.837**	**13.837**
Faring Cross-section Chord [mm]	405.6	426.6	460.0	447.5	468.4
Faring Cross-section Thickness [mm]	110.2	115.9	125.0	121.6	127.3
Faring Surface Area [mm^2]	2736800	3004800	3380900	3253400	3527900
Wing Brace Drag [N]	500.62	549.90	618.71	595.4	645.74
Equivalent Power Consumption [W]	54066.9	59389.5	66820.9	64303.6	69740.1
Equivalent Energy [Wh]	139061.0	152750.8	171864.5	165390.0	179372.8
Equivalent Fuel Consumption [kg]	23.2	25.5	28.7	27.6	29.9

For the differences in width and length of fairing it was kept the same proportional distances, considering the baseline fairing in relation to the baseline cross-section dimensions of the wing brace.

To sum up, comparing the weight of the different braced wing models, these additional masses resulted from the structure itself which is dependant on the brace length and cross-section, an extra fuel mass that

will be needed to overcome the drag generated by this brace and trem surface as well as the fairing which will cover it. Below a visualization of these different components in the several aspect ratio wings.

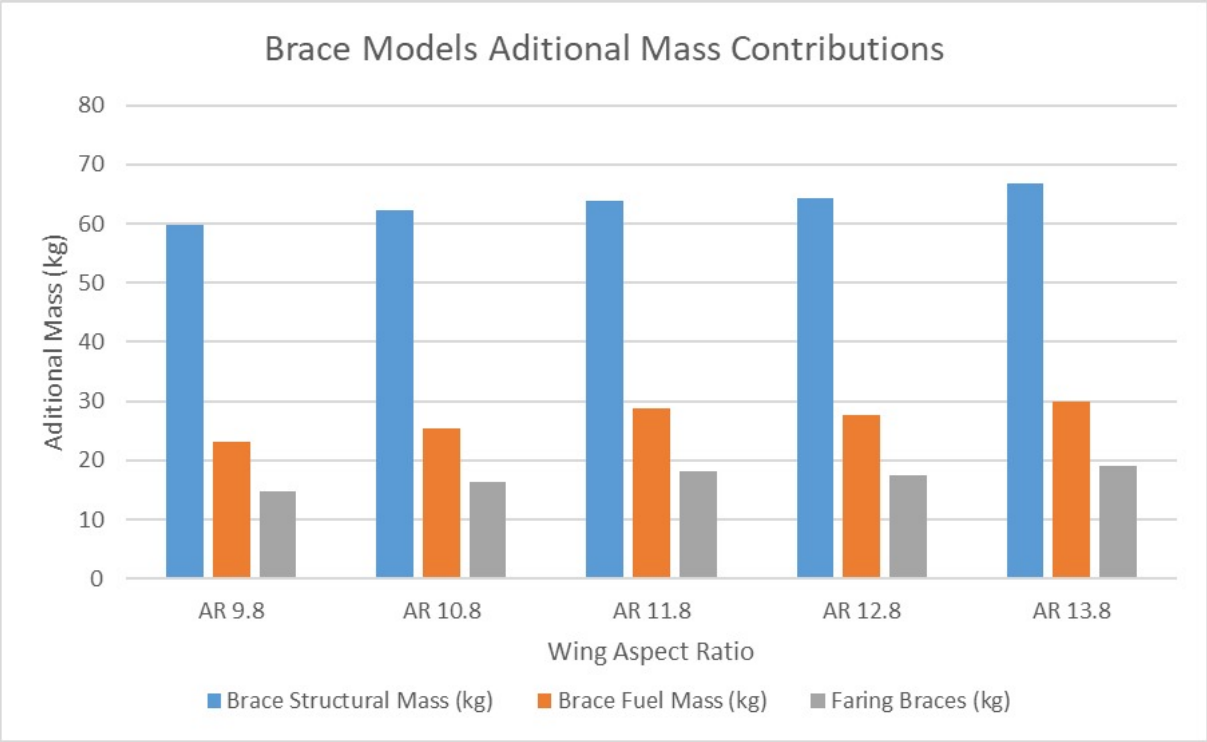

Figure 3.10: Additional Masses from Braced Wing models

3.6 Model Constraint - Inertia Relief

In this section the method used for constraining the developed model will be discussed. An objective view of its advantages and limitations, as well as how it should be applied will be the focus in this next sub chapters.

3.6.1 Definition of Inertia Relief

Inertia relief studies the equilibrium of free bodies under constant loading. In this analysis, inertial loads balance other applied loads to maintain a state of equilibrium without inducing motion. This type of analysis is performed on parts or components which are not fixed in any point in space, such as ships, automobile suspension systems or satellites, for example an use case could be re-establishing the degraded orbit of a satellite; burning an impulse rocket applies a load to the structure resulting in acceleration, but since it's out in space, the satellite is not fixed to anything so there are no fixed boundary conditions (SPC). In this particular case since an airplane in cruise flight is being studied, the same kind of problem is being dealt

with. It is also assumed that any transient effects due to the applied loading have long died out.

The reason why inertia relief is employed in this cases is to account for the rigid body motions caused by the inertia forces of the structure. It allows the system to be subjected to a quasi-static analysis while still considering the influence of these rigid body inertia forces.

By applying inertia relief, the inertial forces due to the mass distribution of the structure are included in the analysis as additional loads or adjustments to the system matrices. This enables the consideration of rigid body movements without the need to explicitly model constraints or stress-free conditions.

To apply inertia relief in a structural analysis, the acceleration field within the structure is typically determined by solving the dynamic equations of motion without considering the external loads. This acceleration field is then used to generate "inertia loads" that act in the opposite direction to the inertial forces, effectively canceling them out. The analysis is then performed using the inertia loads along with the externally applied loads, resulting in a balanced equilibrium state. (62)

3.6.2 Inertia Relief using NASTRAN

In NASTRAN there are two ways to define inertia relief. Both were using during the development of this thesis, and are explained below:

- INREL= -2: By setting this control card parameter to the value -2, inertia relief will be defined using automatic support constraints, it does not need a reference frame (DOF) to be defined by the user so no SUPPORT entry (which is another parameter), needs to be defined. This option was used for all static analysis (SOL101), however it is important to note that for buckling analysis (SOL105), using parameter -2 isn't supported by the used version of NASTRAN in this thesis, NASTRAN 2008 version. The frame of reference is computed from the mass weighted average of all DOF where mass is defined; for the general case, this ends up being very close to the CG of the structure whether there is a GRID point there or not. Studying the displacements of the structure due to small changes resulting in a different mass distribution becomes problematic because the frame of reference changes.

- INREL = -1: This method allows fewer, but no more than 6 singular modes. It is an elimination method which requires a statically determinate set of DOF for the reference frame. These DOF are defined on the SUPORT1 entry, and should be chosen where the structure has stiff behaviour to avoid poorly conditioned shapes. It is vitally important that the choice of SUPORT1 DOF does not over-constrain the structure. (63)

In both methods, the displaced shapes of the singular mode shapes are generated from geometry. A consequence of this is the mass and constrained displacements of SPOINTs and any independent DOF of MPC or RBE3 connections that are fixed (SPC) are not handled correctly leading to wrong answers.

Neither method is able to study (correctly) a structure with more than 6 singular modes. For the same model and correct choice of SUPORT1 DOF for INREL=-1, while staying withing the limitations of INREL=-2, the 2 solutions will yield the same stress field while the displaced shape will be different as the frame of reference in the 2 cases is not the same.

It is important to note that initially Optistruct[5] solver was the prefered option for buckling analysis, due to the possibility of choosing a parameter called EXCLUDE, which would allow to select a set of elements and only analyze the instabilities on the wing, reducing the processing time needed. In NASTRAN 2008 this option isn't available, although recent versions have added this possibility. However when trying to run buckling analysis in Optistruct with INREL parameter it was discovered that it doesn't support the parameter INREL.

3.7 Model Loads - Application

Since applying a direct force on each wing element would be unfeasible due to the fact that the mesh used in AcuSolve is different from the one used in Hypermesh, the proposed solution for each model was that the corresponding forces were applied using a discretization on a mesh that although it doesn't match both softwares previously mentioned, can still be used as an input for WinGen. Four hundred discretized forces were created in four hundred nodes with their respective coordinates, then they were united to all the nearby surface element nodes by RBE3 elements, which is a kind of rigid body element that will transmit this force to the wing, directly connecting this grid point to the two nearest ribs from each wing, excluding the zone from the wing with no dihedral.

Below a visualization of this discretized forces as well as its surface distribution are shown in Fig.(3.11,3.12):

[5] A solver within the Altair HyperWorks suite, primarily used for structural analysis and optimization tasks.

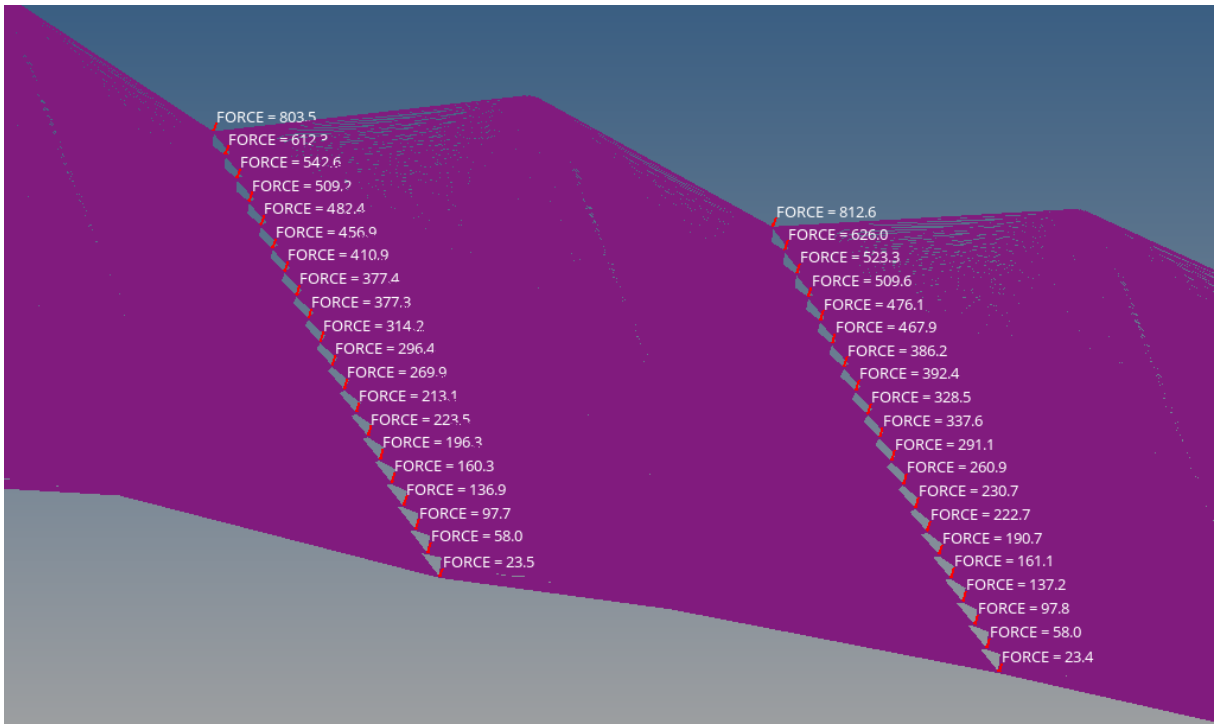

Figure 3.11: Leading edge detail of discretized Forces, being distributed across wing elements connected to the ribs

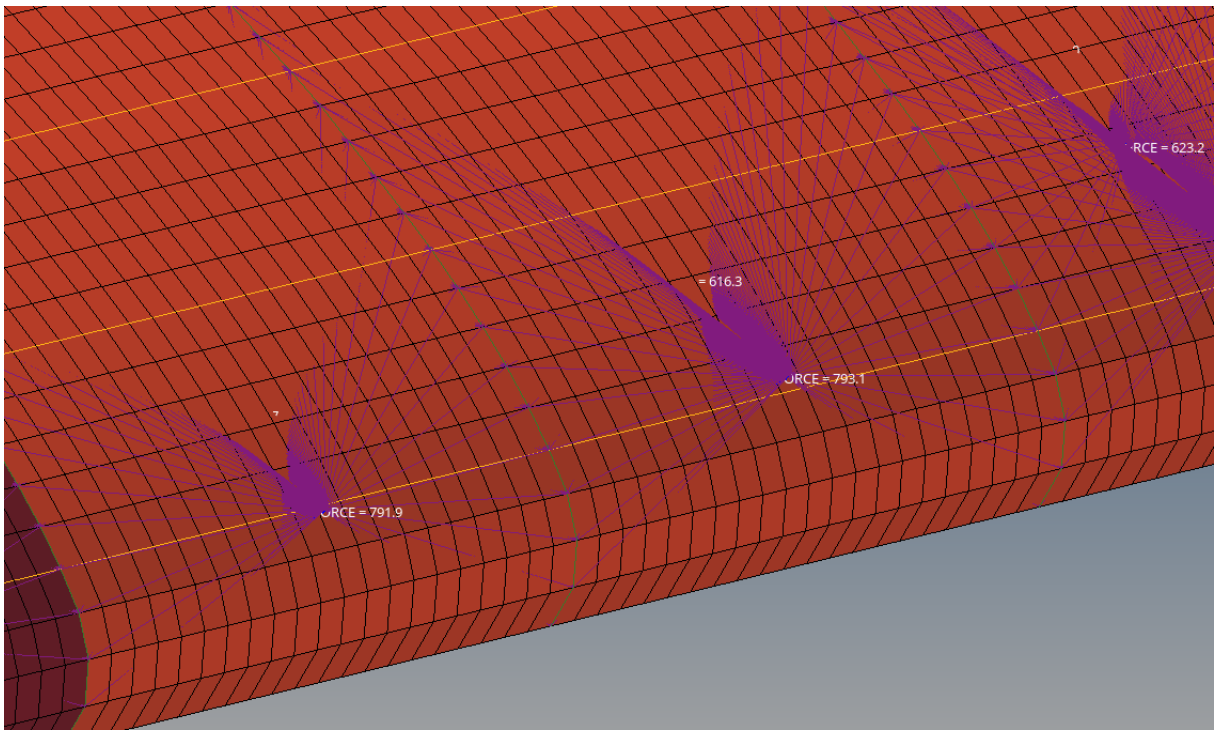

Figure 3.12: Distributed forces across wing ribs, close up

Chapter 4

Results Analysis

4.1 Disclaimer:

Aircraft sizing is an inherently multidisciplinary task and while the aircraft loft is mostly dictated by aerodynamics, performance and operational & certification requirements, its internal structural layout is mostly dictated by operational and certification requirements, acting loads and structural strength. Both the aircraft loft and the internal operational and performance requirements will set the boundaries which will limit the room for structural optimization.

In a complete aircraft development program, the structural design process will be iterative and include analysis of a wide range of failure modes, which, altogether, will size the aircraft. These include:

- Static Analysis
- Joints Analysis:
  - Fasteners Failure modes: shear, tension and combined shear/tension;
  - Sheet Failure modes: bearing, shear-out and pull-through.
- Buckling Analysis (Sheet and Columns):
  - Global Buckling;
  - Local Buckling;
  - Crippling.
- Normal Modes
- Fatigue
- Damage Tolerance

Most of these analyzes are obviously out of the current thesis' scope and it would be unfeasible for them to be inside the scope of a master thesis. The results presented in the current master thesis should neither be regarded as optimized solutions nor even sized wing structures. They aim to provide guidelines on the use of braces worthiness with respect to the wing aspect ratio. In addition, the impact of brace

inclination is evaluated.

In this chapter the main results of the studies done on the several aircraft will be presented. Comparisons, changing variables between different wing configurations, wing brace angles or even thicknesses will be done. In the aspect ratio and wingspan subsection the procedure used for the Baseline Wing (SkyCourier) aspect ratio modeled will be done and then an overview of the dimensions of the different wings is presented.

4.2 Baseline with and without Braces

For the baseline model the Cessna Skycourier 408, Cantilevered Wing equivalent was used. This choice was made since Textron choosed to use braces on their final design, so it is plausible to assume that there may have some benefits to its use in comparison with a cantilever design, and thus every model will be based on this initial Cantilevered Wing version.

4.3 Design Variables

There are several variables to take into account when performing these comparisons between models. The ones chosen were the aspect ratio of the wings, its wingspan and brace inclination, since all of this will have direct huge impacts on the brace performance and overall wing weight.

4.3.1 Aspect Ratio

In the initial model we took as reference the aspect ratio indirectly provided by Textron on their Cessna Sky Courier 408. With the wing span and respective wing area it is possible to determine its aspect ratio according to the following formula (64):

$$AR = \frac{b^2}{S} \tag{4.1}$$

Where:

$AR \rightarrow Wing\ Aspect\ Ratio$

$b \rightarrow Wing\ Span$

$S \rightarrow Wing\ Area$

With the known wing-span of 22.02m and the total wing area of 40.97m^2 we obtain an aspect ratio of 11.837.

One of the parameters of study for the recommendation of braces is deeply connected with the aspect ratio of the wing. Intuitively, from a structural point of view, it seems more advantageous to use struts, the higher the value of the aspect ratio of the wing, since the stress produced by the lift force will be concentrated in a thinner area with the increase of the wingspan above the fuselage, considering an aircraft wing with the same wing area, but this should be corroborated with the next analysis.

In this study five different wing geometries will be considered. By keeping the same wing area and changing the aspect ratio with increments or decrements of 1 unit, we can determine the new wing span and it will be possible to analyze the impact of this parameter in the use of braces.

Using the previous equation, for an aspect ratio of 12.837 we have:

$$\Rightarrow b^2 = AR \times S$$
$$b^2 = 12.837 \times 40.97$$
$$b = \sqrt{12.837 \times 40.97}$$
$$b \approx 22.933\text{m}$$

With a wing span of 22.933m, we have each individual wing with 11.467m.

It is possible now to model the new wings following the next steps. Considering that the baseline length of the several aircraft sections were 1.02m for the base, 5.78m for the non tapered part of the wing and the 4.21m for the tapered part of the wing Fig.(4.1). It's easy to conclude that in order to keep the same wing area the chord of this sections should reduce while keeping the same proportions.

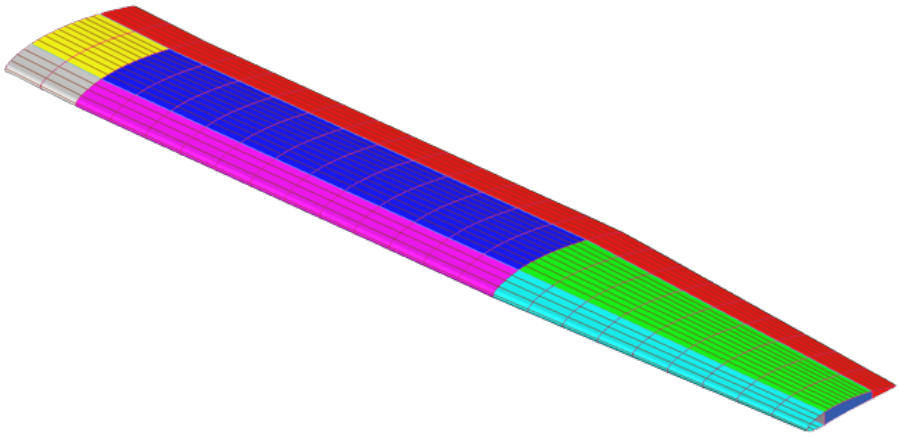

Figure 4.1: Different Wing Sections: In grey the denominated base part with no diedral and no taper, which is placed above the fuselage, making the respective connection with it, in purple the non tapered part of the wing and in light blue the tapered zone of the wing

Taking the increment of each individual wing span of 0.456m and distributing it proportionally to the non tapered and tapered part of the wing we conclude that this amount to 57.86% and 42.14% respectively or $0.264m$ and $0.192m$

Knowing the total area of one wing is 20.485m^2, and having defined the increments, the chord of the sections of the wing is given by:

$$1.02x + (5.78 + 0.264)x + \frac{(4.21+0.192)(x+y)}{2} = 20.485$$

Where:

$x \rightarrow Width\ non\ tapered\ sections\ in\ m$

$y \rightarrow Width\ of\ tapered\ section\ in\ m$

The first term is the area of the wing above the fuselage which has 0 dihedral angle;

The second term is the area of the wing without taper;

The last term is- the area of the wing tip or the area of the tapered zone.

In Fig.(4.2), the different area terms are schematized, using the baseline wing model dimensions in meters.

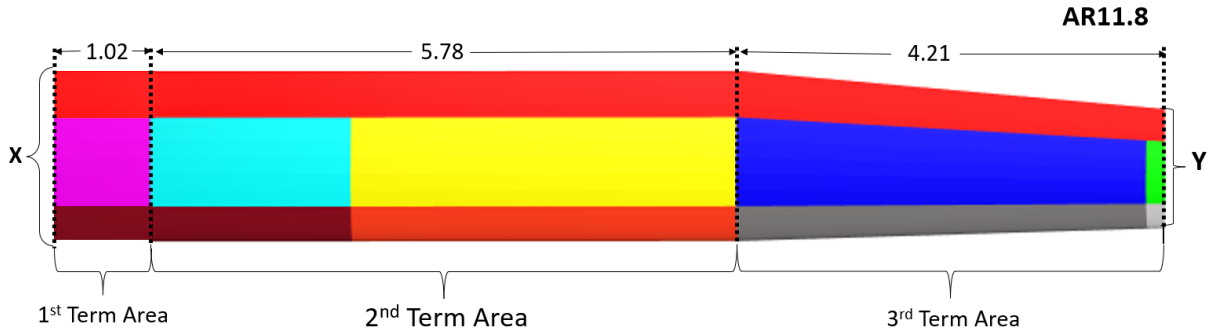

Figure 4.2: Different Wing Sections Length in meters, featuring the three different area components

From the model baseline and the measurements taken from the Cessna Skycourier 408 it was estimated that the taper ratio is around 0.7, assuming that value we can solve the previous equation since $y = 0.7x$. We can then simplify the previous equation to:

$$7.064x + 3.7417x = 20.485 \Leftrightarrow x = 1.896\text{m}$$
$$y = 0.7 \times 1.896 = 1.327\text{m}$$

It is important to note that although the chord of the base section gets reduced, it makes no sense increasing the length of this section since the fuselage keeps the same dimensions and thus the length increments were made only on the part of the wing where dihedral exists.

This means that from the original values of 1.975m for the non tapered part and the 1.374m for the tapered part we obtained new values of 1.896m and 1.327m which corresponds to a decrease in chord of 4% and 3.42% respectively.

The same procedure was used for the other three modeled aspect ratios, so for the sake of simplicity the relevant measurements were organized in the Table (4.1):

Table 4.1: Relevant Measures of the Modeled Wings

Wing Aspect Ratio	**9.837**	**10.837**	**11.837**	**12.837**	**13.837**
Wing Fuselage Span [m]	1.020	1.020	1.020	1.020	1.020
Wing Span Non-Tapered Region [m]	5.218	5.506	5.780	6.044	6.297
Wing Span Tapered Region [m]	3.800	4.010	4.210	4.402	4.587
Total Wing Span of one Wing [m]	10.038	10.536	11.010	11.466	11.904
Wing Root Chord [m]	2.164	2.062	1.975	1.896	1.826
Wing Chord Non-Tapered Region [m]	2.164	2.062	1.975	1.896	1.826
Wing Chord Tapered Region [m]	1.515	1.443	1.374	1.327	1.278

With these geometries defined, the modeled wing still needs to be placed correctly in the fuselage model and in order to minimize the differences between the different fuselage models, it was defined that the connection elements which are CBEAM should be the same length Fig.(4.3), which will also provide the same rigidity to the model, however in order to do so, extra measurements need to be done.

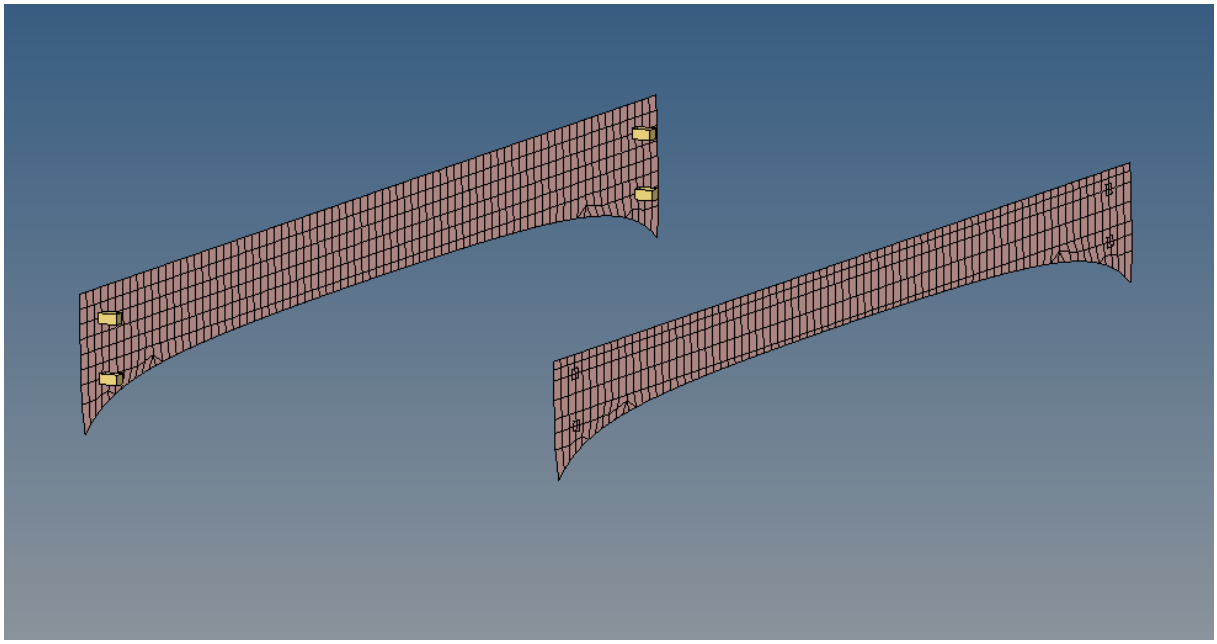

Figure 4.3: Connection modeled zone with CBEAM elements for the Cantilevered Wing baseline model

The distance between the baseline model and the frames can be obtained by subtracting the known distance between two frames, which is $1024.81mm$, from the baseline wing box width of $948mm$. This calculation yields a total distance of $76.81mm$, which will be divided equally between the two sides where the connection zones are made. Consequently, each connection element will have a length of $38.405mm$, as depicted in Fig.(4.4).

To ensure that the connection zone's distance remains consistent across different models with varying aspect ratios, adjustments were made to the front spar and rear spar widths by different percentages. The objective was to maintain a similar length for the connection elements. The specific adjustments for various models are provided in Table (4.2):

Table 4.2: Measures of the distance between the Modeled Wings and Connection Zones

Wing Aspect Ratio	**9.837**	**10.837**	**11.837**	**12.837**	**13.837**
Wing Box Width [mm]	952.158	948.5	948	948	949.52
Total distance to connection zone [mm]	72.652	76.291	76.81	76.81	75.29
Connection element length [mm]	36.326	38,1455	38,405	38,405	37,645
Front Spar [Chord %]	23	24	23	22	21
Rear Spar [Chord %]	69	70	71	72	73

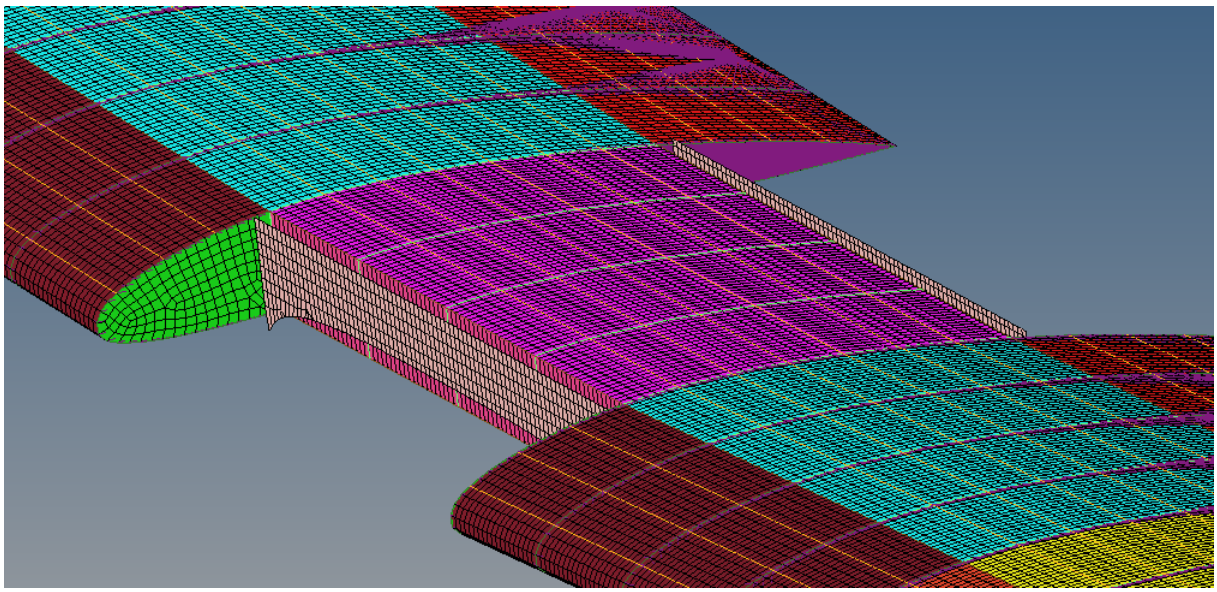

Figure 4.4: Cantilevered Wing baseline model placed and connected to the respective fuselage model

With these models, linear static analysis was performed on them to understand the stress variation, across the models below in Fig.(4.5,4.6) a comparison of the effect of Cantilevered Wing vs. braced wing.

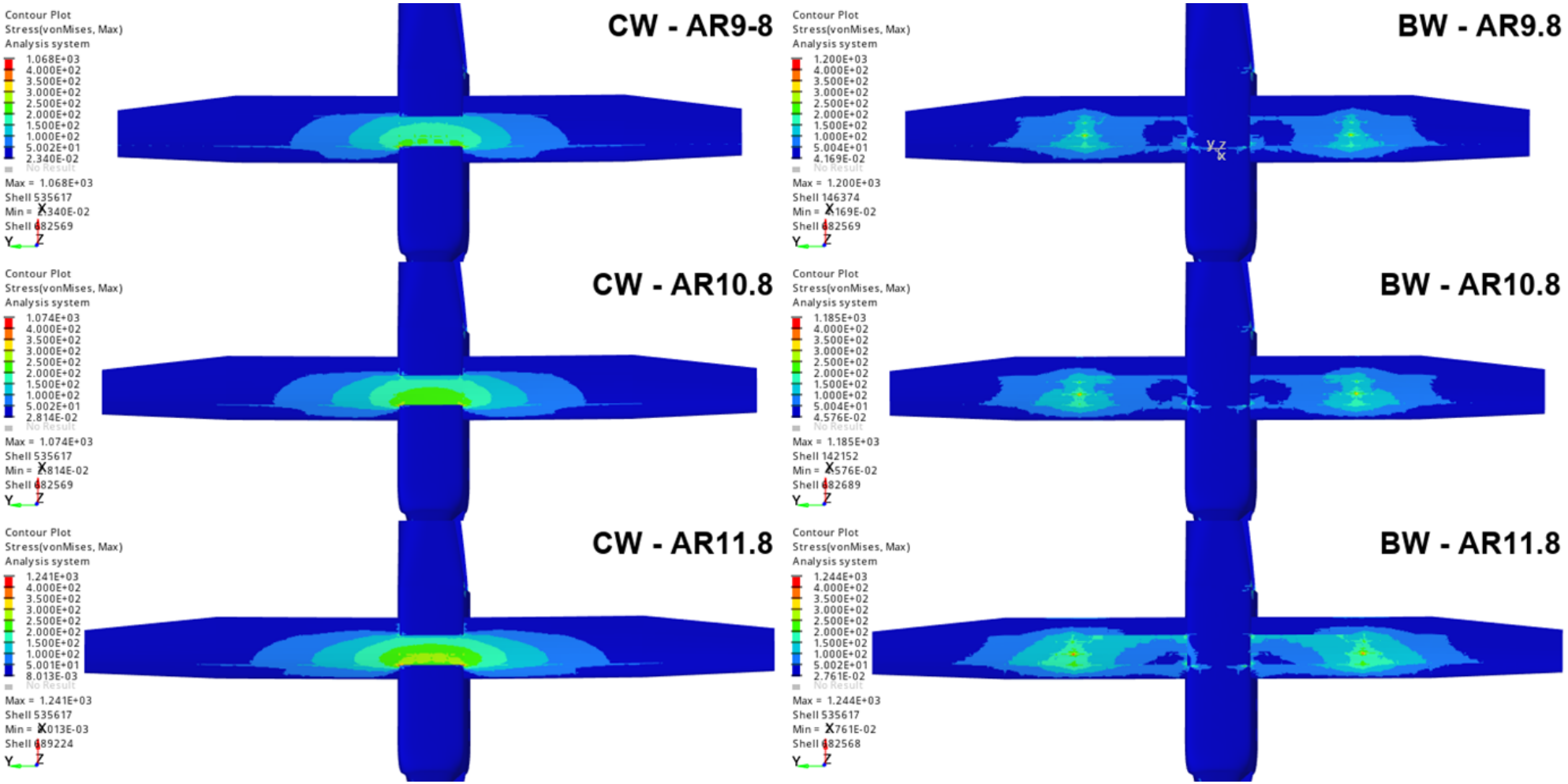

Figure 4.5: Average Stress between Cantilevered Wing (Left) and Braced Wing models (Right) - Part 1

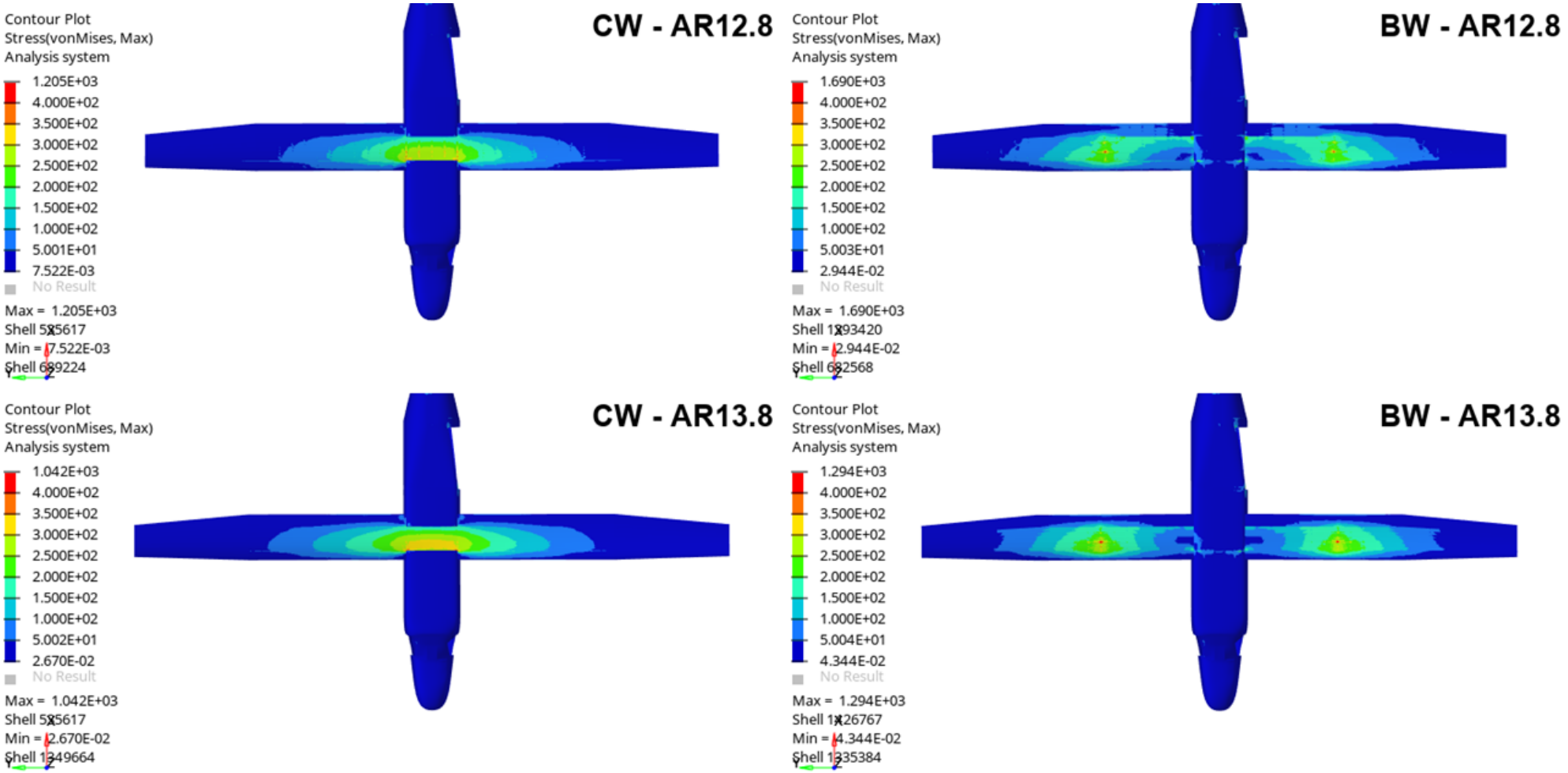

Figure 4.6: Average Stress between Cantilevered Wing (Left) and Braced Wing models (Right) - Part 2

As seen in the above figures, the critical zones in the CW model are related to the panels in the wing root, while for the Braced Wing model the highest stresses are near the brace connection to the wing. The information these models convey will be further explored in the Results section of this thesis.

By dividing the VonMises stress results between both models for each AR, taking as reference the CW model, it is possible to define a stress ratio for each element as seen in Fig.(4.7,4.8) to identify the areas where this stress reduction will be more noticeable.

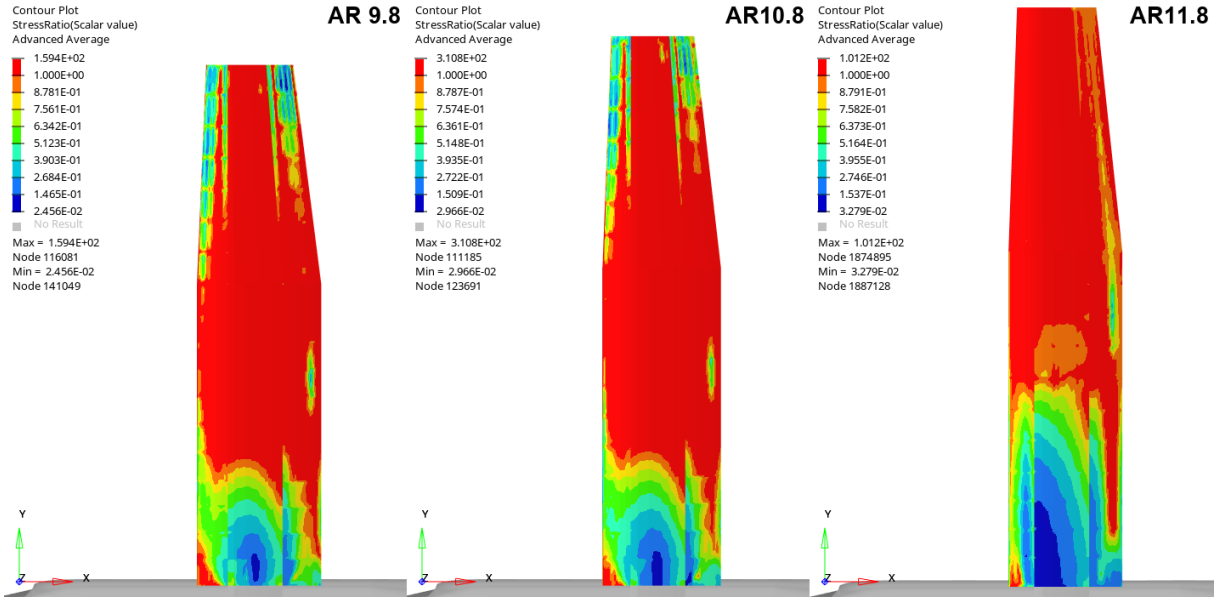

Figure 4.7: Stress Ratio between Cantilevered Wing and Braced Wing models (BW/CW) - Part 1

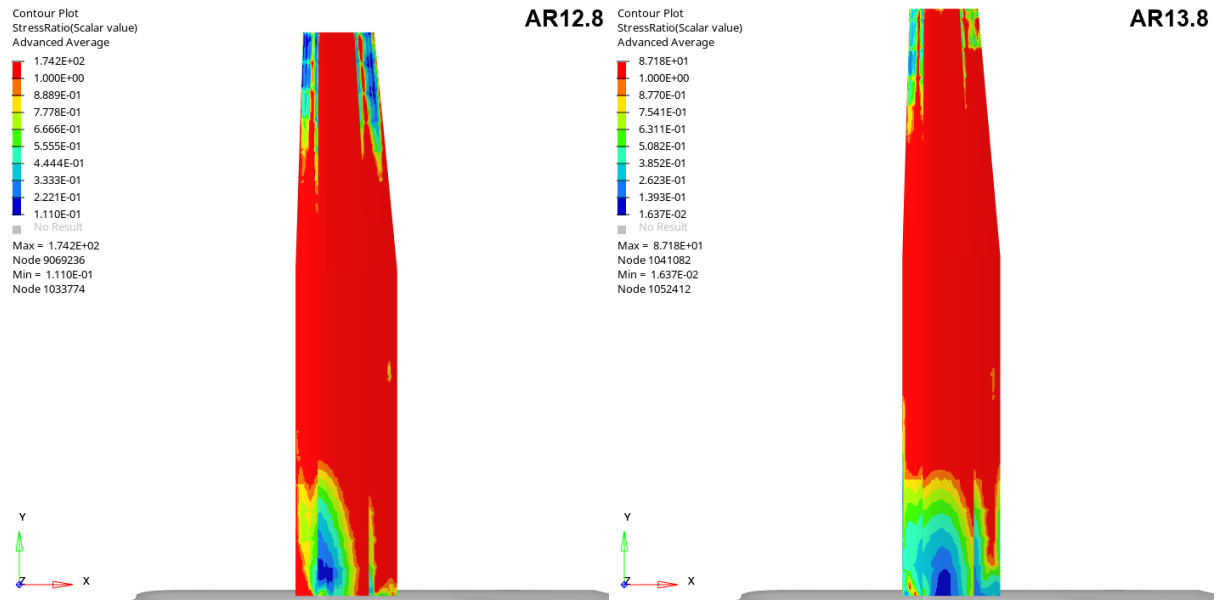

Figure 4.8: Stress Ratio between Cantilevered Wing and Braced Wing models (BW/CW) - Part 2

Although there was some variation in the size of the relieved zone by the incorporation of braces in the different models, the same critical wing root zone had significant stress reductions.

4.3.2 Brace Inclination

Regarding the wing brace location, its initial position was defined in relation to the distance from the engine placement, which in the baseline model corresponded roughly three ribs from the engine placement or 1.629m from the engine in the model. This distance varied roughly according to the spacing between ribs in that zone in the other models, so it was always assumed to place the connection zone three ribs away from the engine placement to keep the same proportions.

To investigate the influence of wing brace angles, two additional simulations were made while maintaining the baseline model, in which the brace to the wing angle was altered. The cross-section dimensions of the brace remained unchanged in both scenarios. These simulations were designed to assess the impact of altering the angle of connection between the brace and the adjacent ribs. In Table (4.3) the respective data collected is shown, while in Fig.(4.9) a graphical representation with the expected tendency for the brace angle vs. its tensile stress is shown. In Fig.(4.10) the brace angle is plotted vs. the appearance of the first buckling mode:

Table 4.3: Braces Measurements Comparison - Baseline Model

Wing Brace Location	**Inboard Rib**	**Baseline Rib**	**Outboard Rib**
Brace Length [mm]	2901.1	3325.0	3779.7
Distance From Engine [mm]	1086	1629	2172
Angle Between Brace and Wing Plane [°]	44.0	37.7	32.9
Brace Applied Force X [N]	337.8	267.7	231.8
Brace Applied Force Y [N]	43205.9	48200.4	46737.5
Brace Applied Force Z [N]	38398.4	35447.7	29232.2
Total Applied Force Transmitted [N]	57804.0	59832.2	55126.9
Maximum Tension Stress [MPa]	337.7	279.8	238.0
First Instability [Force Applied %]	157.2	115.6	97.42

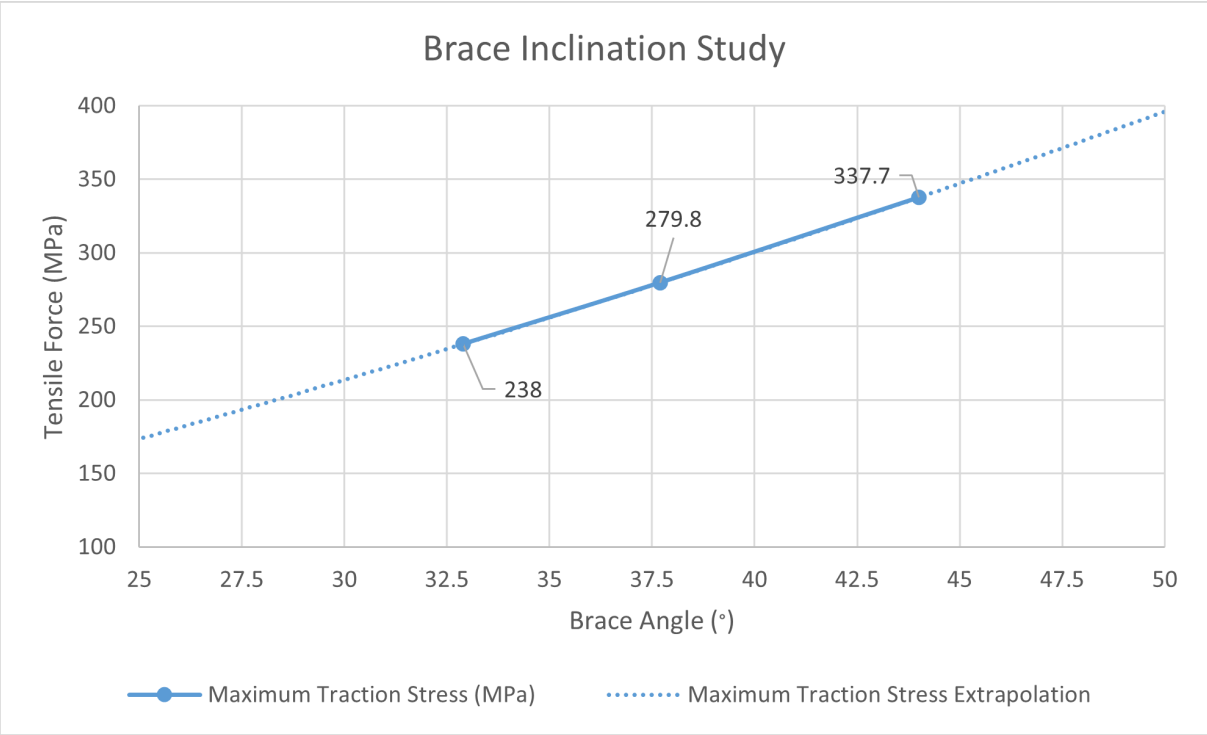

Figure 4.9: Braces Study - Angle Comparison vs. Tensile Stress for a Cross-Section of 110mm

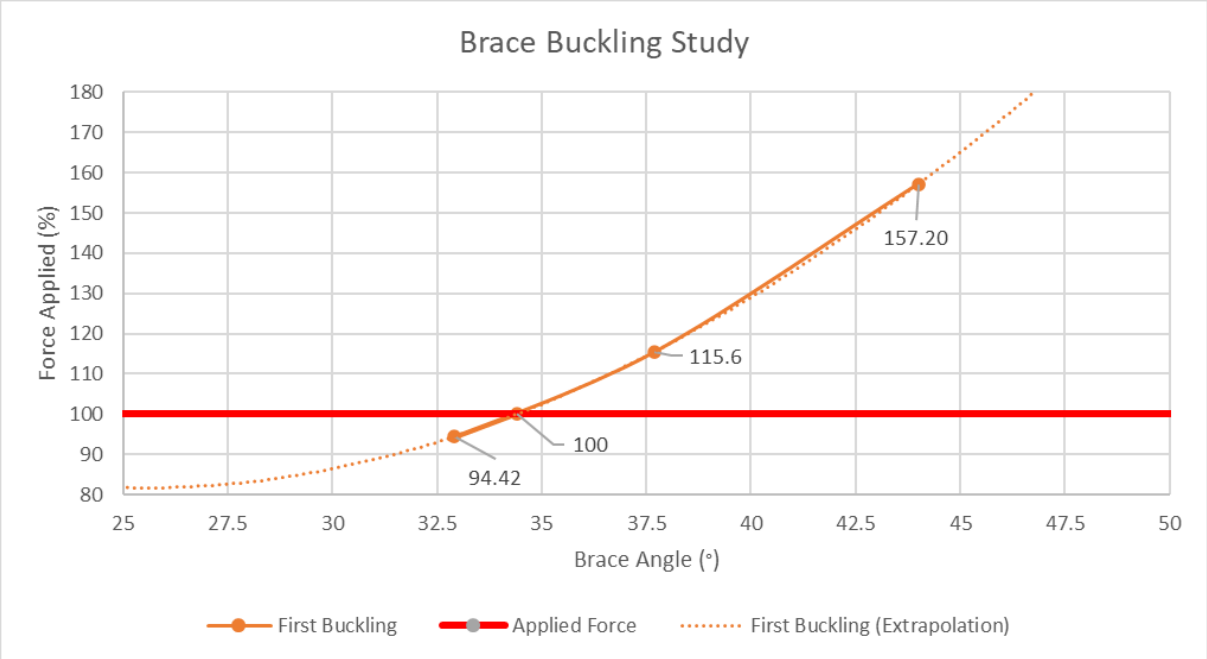

Figure 4.10: Braces Study - Buckling vs. Brace Angle for a Cross-Section of 110mm

By changing the dimensions of the cross section of the brace, it is possible to increase the moment of inertia which will allow for the delay of the appearance of the first buckling mode. The aim of this study is to demonstrate the limiting factor in the sizing of the braces.

The optimal solution exclusively from a stress point-of-view, would be a brace that would connect directly to the wing tip of the aircraft, as it can be seen according to the above graph, as the angle between the the wing and the brace decreases Fig.(4.11), this reduces the tensile stress, however this increases its length and thus it is more susceptible to buckling.

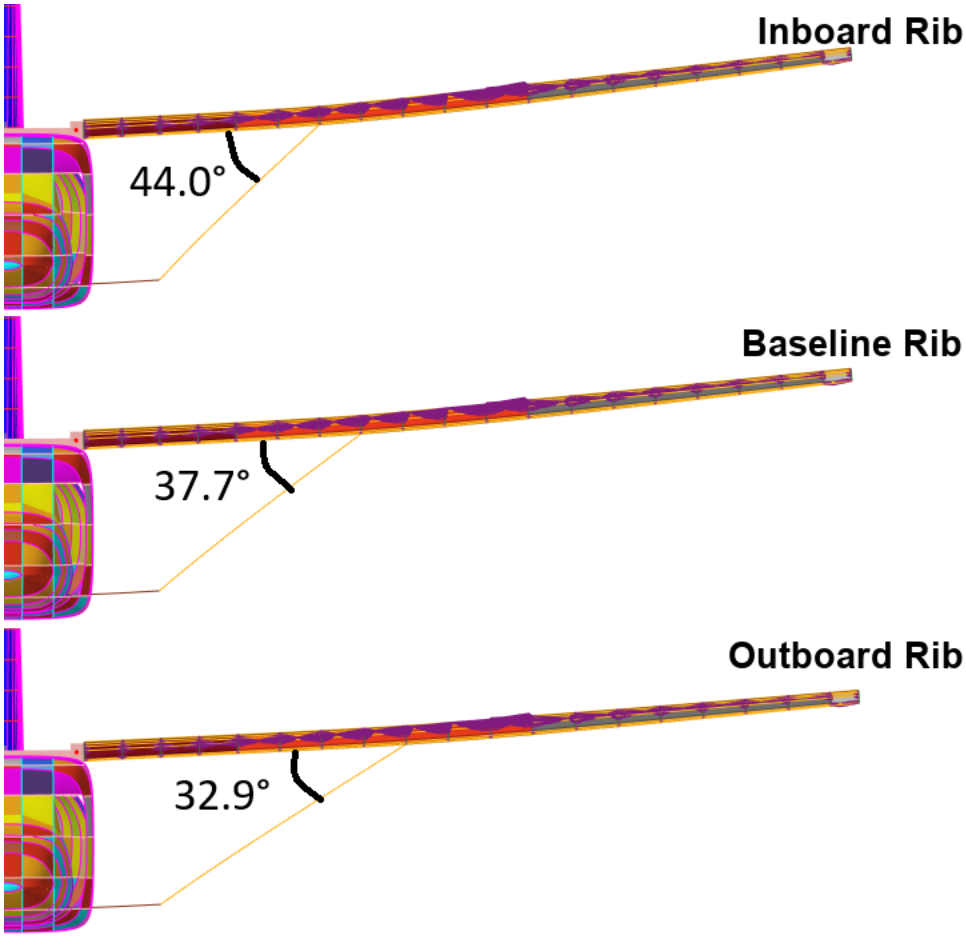

Figure 4.11: Braces angle visualization

Braces are thus sized in compression by buckling and in tension by the yield strength. While for a maximum value this should not surpass 50° since it is expectable to reach the yield stress of this material, according to the extrapolated tendency blue line that can be seen in Fig.(4.9). Assuming 400MPa as the yield strength for a typical aluminium alloy, which is the defined material for this study, it can be seen in Fig.(4.10) that the minimum angle possible for this current cross-section would be 34.4°, since it is the minimum value for which the brace can withstand buckling produced by the applied force.

Approaching the brace to the wing root, and therefore increasing its angle, will lead to an increased wing deflection and tensile force. This is due to the fact the earlier the connection from the brace to the wing is made the greater load it will have to support, as seen in Fig.(4.12).

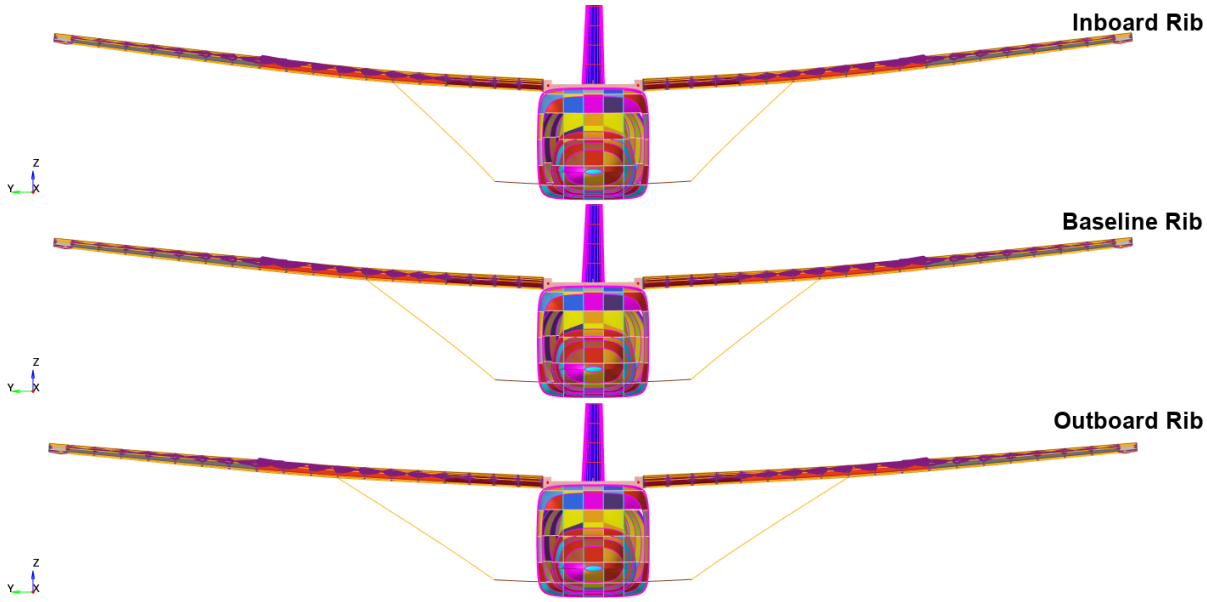

Figure 4.12: Wing deflection visualization for different braces angle

By reducing the brace's connection angle and increasing its length, there is an improvement from a structural point-of-view in the tensile force throughout the pre-brace region as it can be seen in Fig.(4.14), however it will buckle sooner, which will demand a bigger cross section, and consequently result in additional weight and drag created by the covering structure as well as the brace beam itself. These results were obtained by overlapping the baseline rib stresses in Fig.(4.13) with the Inboard and Outboard rib models. It is important to note that the inflexion point of this trade-off, will be highly dependent on each case, between an increase in weight and drag produced by the brace structure and the savings made by the reduction in wing weight due to the reduced wing thickness needed.

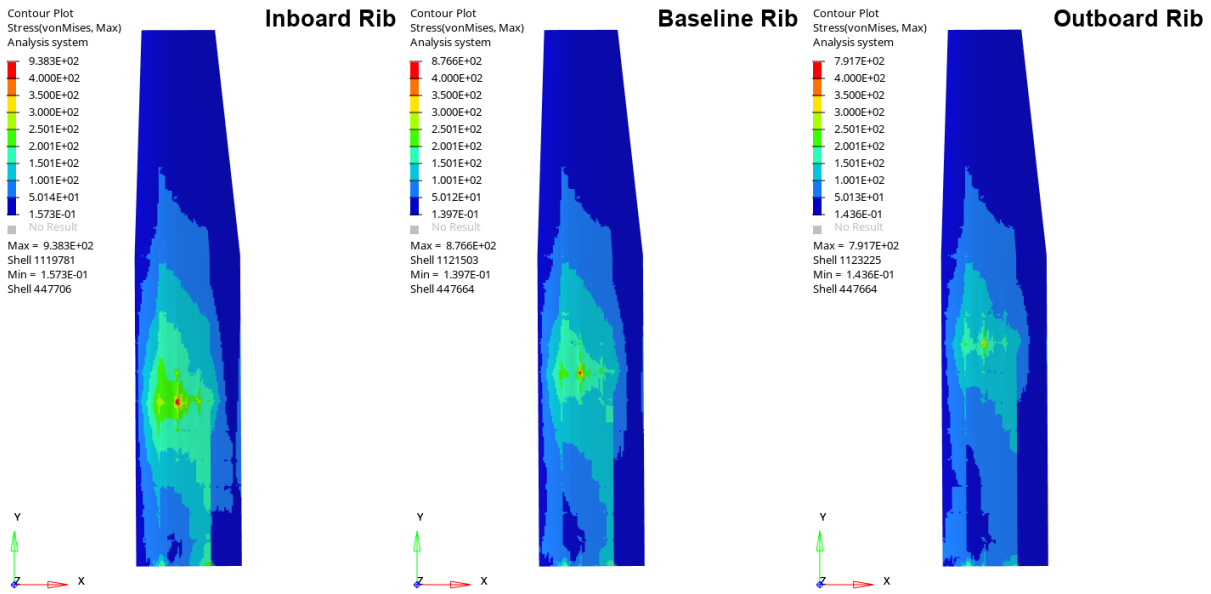

Figure 4.13: Braces Stress Angle Comparison

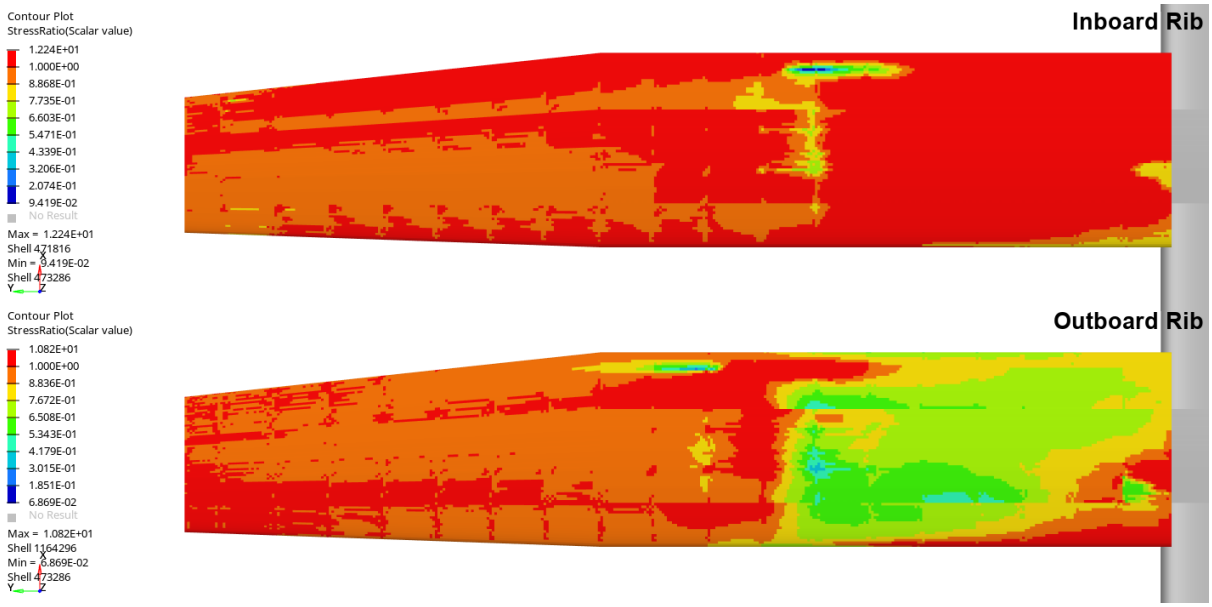

Figure 4.14: Stress Ratio using Baseline Rib for Comparison

4.4 Wing Weight

The resulting wing weight will depend on all the previously mentioned design variables (wing aspect ratio, wingspan and brace inclination). For the procedure of weight comparison between the different models, Cessna 11.837 with CW will be taken as example, being the following method replicated for the other aspect ratio wings. Hypermesh can compute the mass as well as volume and area of each element,

however the results obtained depend on the selected data. It was decided that one interesting analysis to be done would be determining the overall mass needed for the Braced Wing model in order to achieve the same level of stress, which, as seen before, was lower for its Cantilever equivalent model, and therefore it is expected an increase in weight regarding the assumed initial element thicknesses.

The procedure for the individual element weight measurement was the following:

- Opening an *HyperView* and uploading the respective model; then an *HyperMesh* window in order for the Tools and *Matrix Broswer* option appear.

- By clicking *HV Data* in *Data Source* and the option *elements* in *Entities*, and *Query*, a selection tool appears, then half of the wing was selected, considering all common elements (not including the 1D elements such as stringers), having selected this data, it was possible to list all existing elements in the model for the half wing. The *HV data* was selected again but this time the option *Results* and then *Shell Thickness*, in order to obtain one of the variables for the calculation of each element individual mass.

- Since all selected elements are close to QUAD elements, the calculation of the area was considered as side times side for later use in the volume formula. In order to obtain the length of each side of each element it was first, selected the element column of the queried data, and *HV Data* and *elements* selected once again but this time *Datanames* and *connectivity* option appears; this will allow to determine the four nodes that constitute the respective element.

- Then by selecting each node column and repeating the same procedure an option will be available that makes it possible to determine each node coordinates. It can be visualized in Fig.(G.1) an excerpt of the produced sheet.

- With this data collected an Excel sheet can be exported that will contain all this information where simple calculations can be made to determine the Volume and mass of each element.

- It was calculated the distance between node 1 and 2 and node 2 and 3 to obtain the values of the length and width of each rectangle, using the distance between points formula:

$$D = \sqrt{(x_2 - x_1)^2 + (y_2 - y_1)^2 + (z_2 - z_1)^2} \tag{4.2}$$

Where:

$D \longrightarrow Distance$

$x_n, y_n, z_n \longrightarrow Cartesian\ Coordinates\ in\ Space$

- Element area was obtained through the multiplication of this two lengths and then the volume was obtained trough the multiplication of the area by the thickness of the respective element.

- By summing all values of each individual element the total volume was determined and then an arbitrary value of density was attributed to Aluminium (which was the material considered for this study) with a density of $2.77 \times 10^{-6} kg/mm^3$, knowing $V = \frac{m}{\rho}$, where V stands for Volume, and m for mass, and ρ is the material density, it was possible to determine the respective common mass of the models. This data can be visualized in Fig.(G.2).

Below, in table (4.4), all the values for the mass comparison between Aircraft 11.837 CW and its BW version are shown.

Table 4.4: Variables analyzed for the mass comparison between Aircraft 11.837 CW and BW model

Variable	**CW (AR=11.837)**	**BW (AR=11.837)**
Total Volume [mm^3]	119170990	55524161
Total Volume [m^3]	0.11917099	0.055524161
Aluminium Density [kg/mm^3]	2.77E-06	2.77E-06
Half Wing Shell Mass [kg]	329.87	153.69
Half Wing Stringers, Frames, Rib Caps [kg]	233.39	158.91
Central Mass [kg]	76.13	-
Connection Zone [kg]	11.05	1.79
Brace Fuel Mass [kg]	-	28.67
Total Brace Mass [kg]	-	63.92
Fairing Braces [kg]	-	18.26
Fairing Landing Gears [kg]	-	6.13
Half Wing Mass [kg]	606.84	371.99
Total Wing Mass [kg]	1213.68	743.97
Mass Ratio [%]	100.00	**61.30**
Average Stress [MPa]	39.98	51.86
Average Stress Ratio (BW/CW) [%]	**129.72**	
Maximum (Excluding Top 1%) [MPa]	199.65	185.23
Maximum (Excluding Top 5%) [MPa]	140.49	138.70

To note that although the average stress is $\approx$ **30%** higher it is better distributed, allowing for a wing weight reduction of almost $\approx$ **40%**.

A result verification test was conducted to clarify if the obtained result of $329.9kg$ for half of the

wing shell mass would be close to the estimate of the software. By conducting the same study with the *Hypermesh* the value of $319.8kg$ was obtained as seen in Table (G.2). This value is approximately 3% lower than the value obtained analytically. This difference can be justified by the fact that for the area calculation formula it was assumed that all elements were CQUAD, and thus either square or rectangular in nature. It is known that most of this elements have a trapezoidal shape and thus its formulation would be different. Assuming the elements were squared, saves time and effort, because the trapezoidal area formula, involves two base lengths and this would require an extra length calculation in comparison to the formula used, including information from the fourth node. Additionally, it is a conservative approach due to the increased weight in comparison with the software exact value.

The weight in Table (G.2) is only for the common 2D elements in the CW and BW versions of the airplane, for the first, half of the wingspan above fuselage should be considered named as Central Mass, while for the Braced version, the additional mass from the brace itself needs to be considered, as well as the extra equivalent fuel mass needed for this structure.

With this total mass determined for both models, it was calculated the exact mass increment per element needed to achieve the same stress level for the CW model, which corresponds to the Same Stress column in the Table below (4.5).

Another study was done considering a 50MPa threshold. This was done in order to keep the same thicknesses at low stress zones, to study their influence in the overall skin mass. All comparisons were made with the CW model, which as seen before has its lowest stress zones located at the wing tip Fig.(4.5), since a small increase in the absolute value of small stress zones may represent a relative big percentage increment that would result in reinforced zones with low stresses, something unwanted.

Table 4.5: Results obtained for the Aircraft 11.837 BW model in order to obtain the same stress level and considering a threshold of 50MPa

Variable	BW Same Stress (AR=11.837)	BW Same Stress 50MPa Threshold (AR=11.837)
Total Volume [mm^3]	120978698.9	130948828.4
Total Volume [m^3]	0.120978699	0.130948828
Aluminium Density [kg/mm^3]	2.77E-06	
Half Wing Shell Mass [kg]	334.87	362.47
Half Wing Stringers, Frames, Rib Caps [kg]	158.91	
Connection Zone [kg]	1.79	
Brace Fuel Mass [kg]	28.67	
Total Brace Mass [kg]	63.92	
Faring Braces [kg]	18.26	
Faring Trem [kg]	6.13	
Half Wing Mass [kg]	553.16	580.76
Total Wing Mass [kg]	1106.33	1161.52
Mass Ratio [%]	**91.15**	**95.70**

The visible increase in mass ratio is due to the fact, that in order to obtain the same average stress in the braced wing with the comparable cantilevered wing model, most of the wing will have to be reinforced.

In order to obtain the new thicknesses, the stress ratio obtained between the CW and BW models was determined for each element, then if it proved to be higher than the Cantilevered Wing baseline model it would result in an adjustment of its element thickness assuming a linear relationship, as seen in Fig.(G.3)

It is important to note that a minimum thickness threshold was defined of 1mm, so in cases where the stress ratio were lower than the baseline model but its thickness were already at this minimum value imposed, it wouldn't go below that value. This is because thicknesses lower than 1mm are virtually nonexistent in conventional aircraft wings. Considerations like accidental damage, aerodynamic smoothness and elastic buckling/post-buckling criteria and alike often limit the minimum possible thicknesses.

This is an important minimum value to define since due to manufacturing limitations, certification requirements, higher possibility of instabilities and also maintenance issues could arise even if, from a purely structural point of view, it could theoretically withstand those loads with lower thicknesses.

Since this study conducted resulted in positive results, and still managed to obtain a lower mass ratio even for the same stress level, it was conducted a theoretical study to know if the imposed limit of 1mm would affect drastically the mass savings for the same stress level. The relevant tables are shown in

Appendix H. The result conducted proved to lower the mass ratio to 89.47% in comparison with the 91.15% that would be obtained by keeping the 1mm rule.

It is important to note that Mass Ratio for the Same Stress was actually higher than the previously defined thicknesses for the wing sections. It is possible to conclude that due to the average stress ratio in the wing with braces is actually higher than the Aircraft with Cantilevered Wing. It resulted in a reinforced structure, however since the stresses were more evenly distributed across the wing, it made it possible to reduce its overall thicknesses.

The same procedure and study was conducted for the different five wing aspect ratios.

In Table (4.6,4.7) a comparison between all CW and its braced Wing versions overall weight is presented.

Table 4.6: CW Weight for different wing aspect ratios

CW - Wing Aspect Ratio	**9.837**	**10.837**	**11.837**	**12.837**	**13.837**
Wing Structural Mass [kg]	1207.1	1217.3	1213.7	1215.6	1203.4
Remaining Component Masses [kg]	1323.3	1373.3	1303.2	1323.2	1322.9
Aircraft Structural Mass [kg]	2530.4	2590.6	2516.9	2538.8	2526.3
Wing/Total Structural Mass Ratio [%]	47.7	47.0	48.2	47.9	47.6

Table 4.7: BW Weight for different wing aspect ratios

BW - Wing Aspect Ratio	**9.837**	**10.837**	**11.837**	**12.837**	**13.837**
Wing Structural Mass [kg]	755.6	767.0	744.0	753.2	758.1
Remaining Structural Masses [kg]	1252.2	1248.2	1204.3	1245.1	1241.3
Aircraft Structural Mass [kg]	2007.8	2015.2	1948.3	1998.3	1999.4
Wing/Total Structural Mass Ratio [%]	37.6	38.1	38.2	37.7	37.9

Typically, an aircraft wing should account for 30% of the aircraft total mass (1)(p.160). The fact that in the baseline model it accounts for 48.2% of its total weight, is due to the fact that the wing has not been completely sized, and thus this resulted in some discrepancies, which may be due to several reasons such as the fuselage and other component masses being underestimated.

Some variations regarding the remaining component masses are due to different thicknesses in the modelled vertical and horizontal stabilizer.

In Table (4.8) several mass and stress results are summarized, which will be used for a graphical overview. The presented BW ratios take as reference the corresponding CW model.

Table 4.8: Results from different Wing Span Comparison

Wing Aspect Ratio	**9.837**	**10.837**	**11.837**	**12.837**	**13.837**
BW Mass Ratio [%]	62.60	63.01	61.30	61.96	62.99
BW Average Stress Ratio [%]	113.71	111.65	129.72	149.73	127.85
BW Mass Ratio Adjusted for Same Stress [%]	87.96	89.35	91.15	94.60	94.25
CW - Maximum Stress, Excluding Top 1% [MPa]	151.84	175.29	199.65	220.42	248.25
BW- Maximum Stress, Excluding Top 1% [MPa]	139.58	154.03	185.23	218.73	249.22
1% Maximum Stress Reduction [%]	8.07	12.13	7.22	0.77	-0.39
CW - Maximum Stress, Excluding Top 5% [MPa]	107.13	123.59	140.49	150.12	175.91
BW - Maximum Stress, Excluding Top 5% [MPa]	97.21	109.59	138.70	172.11	184.89
5% Maximum Stress Reduction [%]	9.26	11.33	1.27	-14.65	-5.10

In order to determine the maximum stress, it was defined two excluding groups, one comprising the top 1% elements and another one on the top 5%. This was made to exclude stress concentrations or high peaks of stress which are not representative of the real highest stress in the model.

4.5 Buckling Analysis

During the execution of linear buckling analysis, certain challenges in running the simulations were encountered. Notably, one significant challenge arose from the limitation of the NASTRAN 2008 solver in restricting the global Finite Element Model (FEM) to the specific region of interest, namely the wings. This limitation led to an increased number of instabilities that were not useful for this study, increasing the processing time for each attempt.

In an effort to address this challenge, multiple iterations were performed using the Altair Optistruct solver, which provides an EXCLUDE option for limitting the study zone. However, Altair Optistruct solver proved incompatible with the Inertial Relief method that was employed to restrain the model. Consequently, this solver option was found to be unviable for this particular study requirements.

For each AR model several buckling analysis were made, however obtaining comparable results between the two configurations for the different aircraft proved challenging, especially due to the amount of buckling modes obtained outside of the study zone. This was due to the low thicknesses and model errors in zones such as the vertical stabilizer or the fuselage of the aircraft as it is possible to see in the following example in Fig.(4.15).

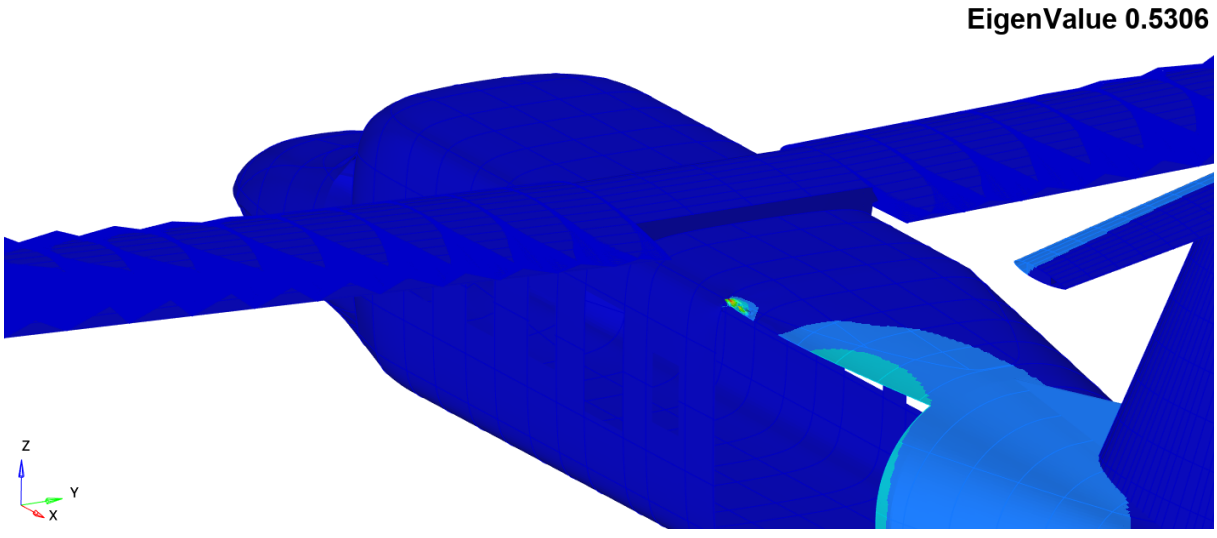

Figure 4.15: Aircraft 11.837 CW - Buckling mode example near door zone

The long processing time for each run (up to 6 hours), due to the fact that the whole model had to be run in order to obtain results, limited this analysis.

Although the wings of the aircraft were object of study, in the version of NASTRAN used, the 2008 version, it was proved to be unable to isolate this zone. Later versions of the software feature new param-

eters such as "EXCLUDE" which enable the exclusion of pre-defined element sets and focus on the study zone.

In order to reduce the amount of buckling modes outside the study zone, it was assumed that all the components outside of the analysis scope would have a thickness of 5mm Fig(4.16).

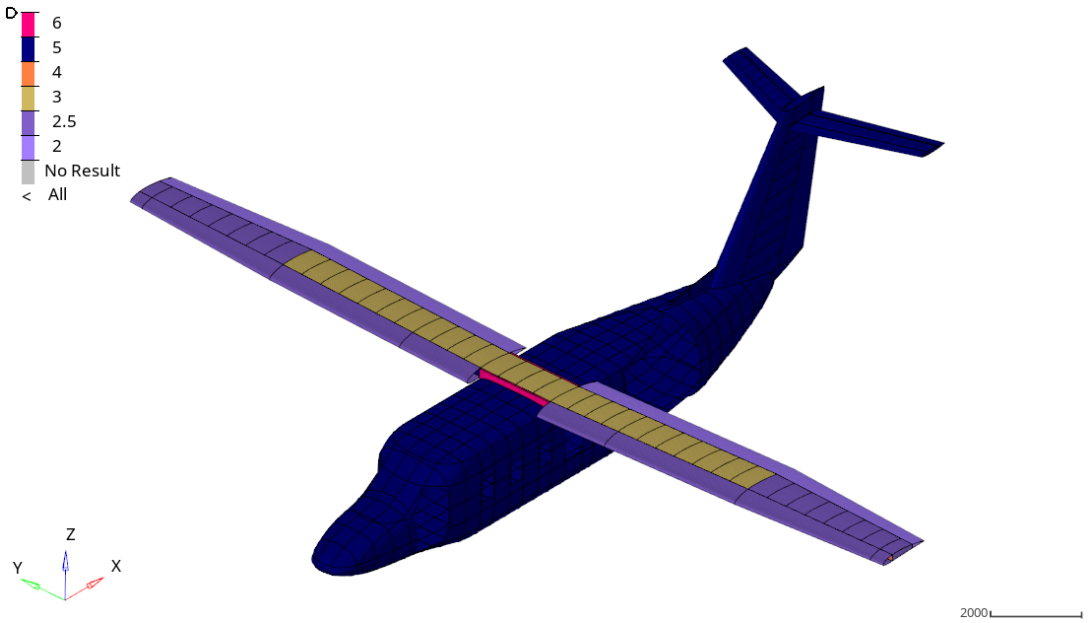

Figure 4.16: Aircraft 11.837 CW featuring the following thicknesses: dark blue (5mm), dark yellow (3mm), dark purple (2.5mm), light purple (2mm)

With this assumption it was possible to find the first buckling mode happening in the baseline CW model to occur at a load factor of 0.5367 or 53.67% of the load applied, as seen in Fig.(4.17) this is located in the critical panels where most of the stress is found as seen in the previous studies presented.

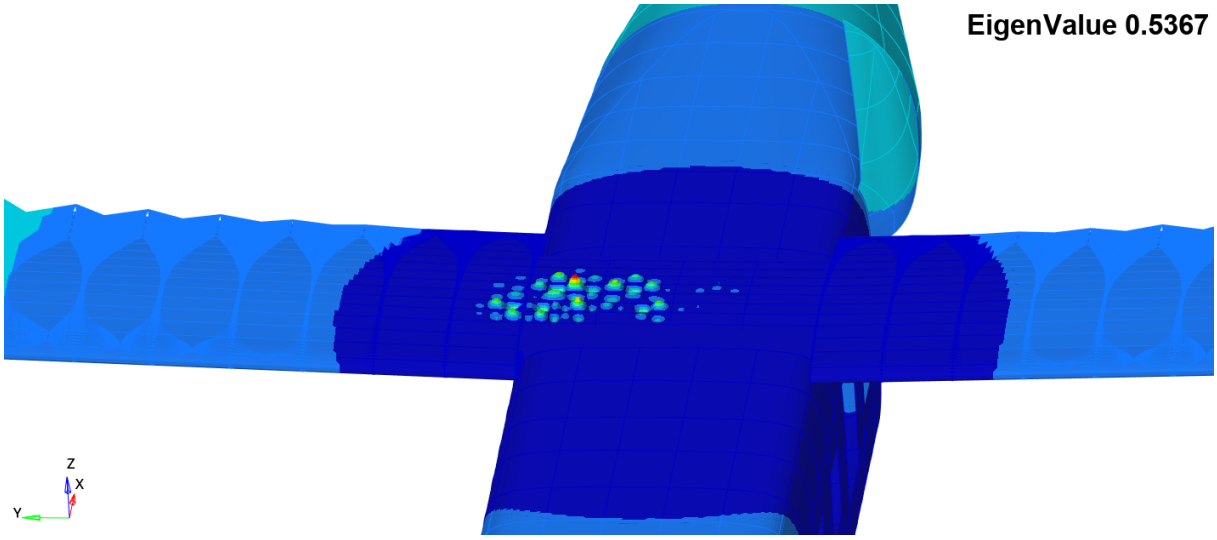

Figure 4.17: Aircraft 11.837 CW - 1st Buckling Mode in Wing Central Panel

Regarding the corresponding BW baseline model the same procedure was done to the fuselage to reinforce the structure and reduce the appearance of buckling modes, since the skin thicknesses of the BW baseline model were reduced in comparison with CW model, as seen in Fig.(4.19). New buckling modes appeared in the connection zone of the brace to the wing and fuselage due to the high stress concentration in those zones Fig.(4.18).

One implemented solution was to reinforce this critical connection zone (featured in pink in Fig.(4.19)) in order to obtain comparable results between both aircraft Fig.(4.20), since it is known that this high peak of stress does not exist if the brace connection wasn't directly made to the wing structure.

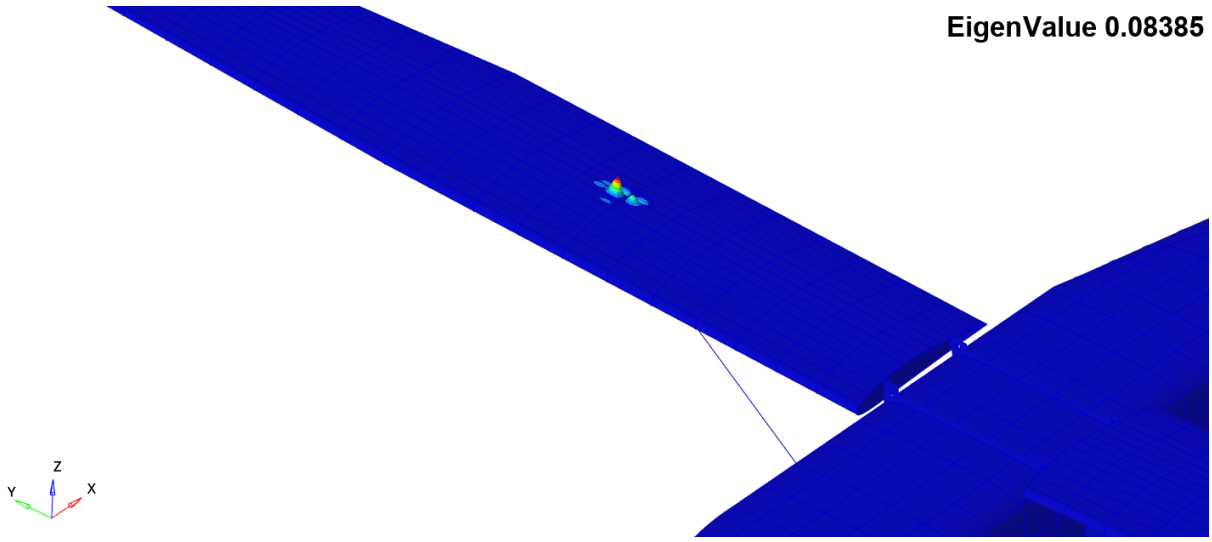

Figure 4.18: Aircraft 11.837 BW - Buckling mode example in brace connection zone

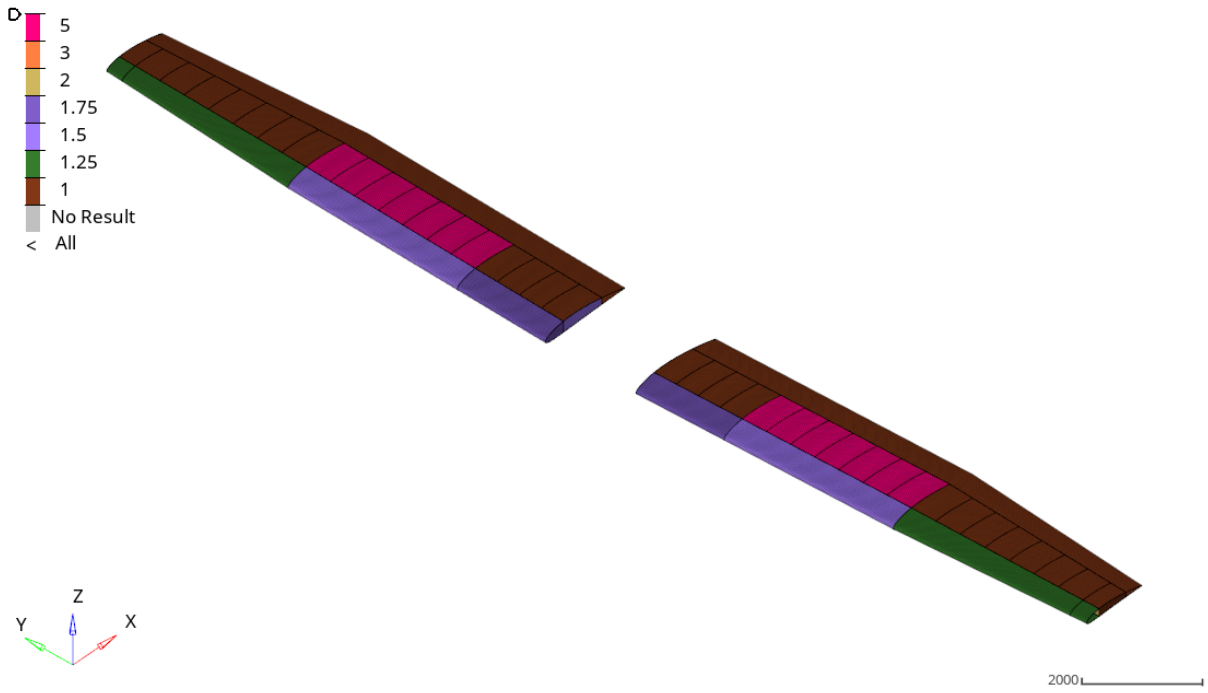

Figure 4.19: Aircraft 11.837 BW - Reinforced panels in aircraft wings in pink with 5mm thickness, brown (1mm), light green (1.25mm), light purple (1.5mm), dark purple (1.75mm)

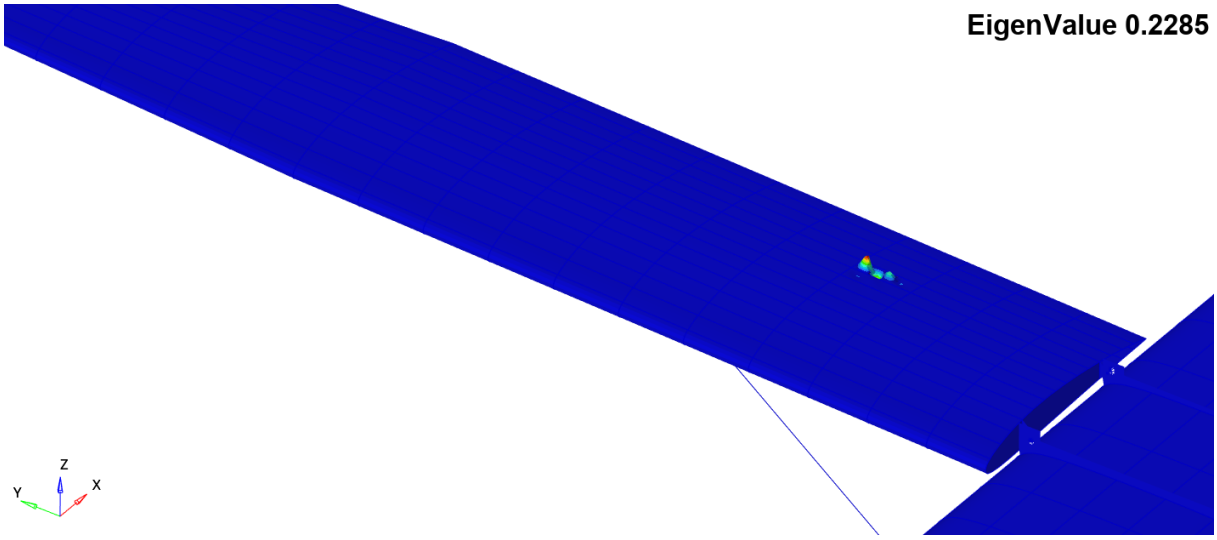

Figure 4.20: Aircraft 11.837 BW - 1st Buckling Mode in Braced Wing

This first mode happening in the brace wing structure, happens at 0.2285 of the load factor or 22.85% of the load applied.

It is possible to conclude that although buckling modes don't occur at the same wing location, there is a reduction of 30.82% in the applied load until the first buckling modes start to appear. It can be said that the modeled brace wing structure is more susceptible to buckling, and it will reach a critical load at a

lower applied load. The reduction in wing skin thickness has significantly impacted the structural stability, since thinner skins are more prone to buckling due to reduced resistance to bending loads, especially if the loads are concentrated. One way to solve this could be the addition of stiffeners or reinforcing the ribs nearby the brace connection to the wing structure, especially in areas where buckling tends to occur.

Due to the poor performance of the braced wing model in this buckling analysis, an additional study was conducted for this model configuration. This time, instead of locally reinforce the wing skin thickness, it was considered the same thicknesses all across the wing as for the cantilevered wing model, as seen in Fig.(4.16). By ensuring that this variable remained unchanged in both models, a direct comparison can be made between the two configurations Fig.(4.21).

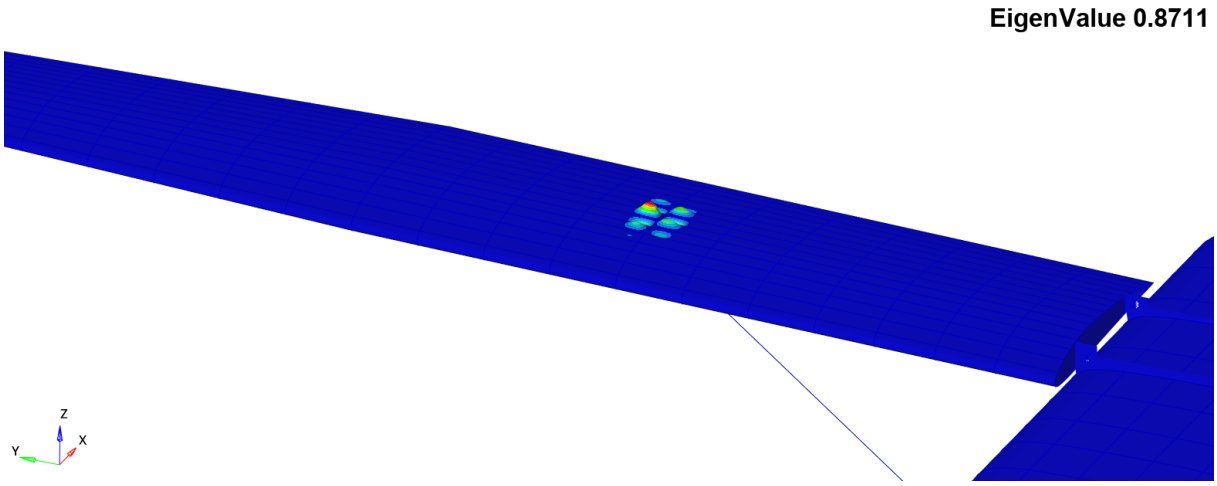

Figure 4.21: Aircraft 11.837 BW - Same Wing Skin Thickness as Cantilevered Wing Configuration - 1st Buckling Mode in Braced Wing

The first mode appeared at 0.8711 or 87.11% of the force applied representing an increase of 33.44% when compared to the cantilevered wing performance of 53.67% for the same wing skin thickness. It is of utmost importance to conclude that when eliminating thickness differences, the braced wing configuration performed better in comparison to its corresponding cantilevered wing model, which can be justified by the better stress distribution and lower critical maximum stress.

This drastic improvement when comparing to the results obtained in the braced wing model with lower skin thickness, can be justified by the reinforced panels in the braced connection zone that went from 1mm in the study of Fig.(4.20) to 3mm. However the thickness in this region is still not enough to withstand the forces applied and so a third study was conducted reinforcing this zone from 3mm to 5mm. The first buckling mode appearance is shown in Fig.(4.22).

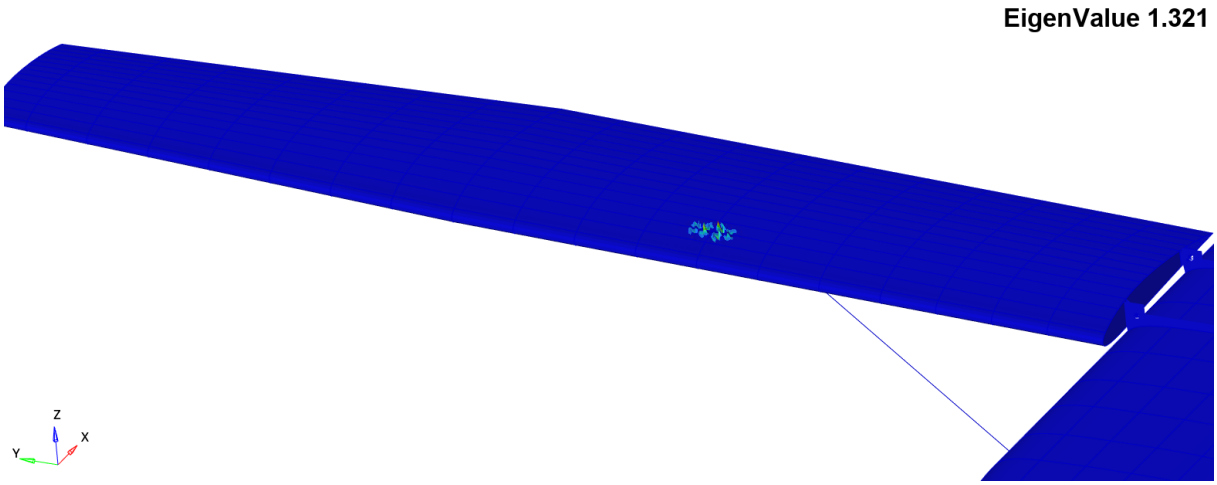

Figure 4.22: Aircraft 11.837 BW - Same Wing Skin Thickness as Cantilevered Wing Configuration with reinforced panel in braced connection zone - 1st Buckling Mode in Braced Wing

As seen in Fig.(4.22), the new first buckling mode appears closer to the leading edge since it's a section subject to more stress and thus more prone to buckling. This first mode happened at 1.321 or 132.1% of the applied load, which represents a considerable safety factor when sizing for buckling.

It is imperative to emphasize that these increases in wing skin thickness have a direct and significant impact on the potential payload savings achievable within the scope of the static analysis performed. This underscores the critical role of the chosen wing skin thickness as a key parameter in wing weight optimization, since it should simultaneously ensure it is thick enough to withstand admissible buckling loads but thin enough to avoid oversizing in response to the applied stresses.

4.6 Benchmark Study: Cantilevered Wings vs. Braced Wings

Due to the large amount of data collected and to clarify the different studies, some plots were made to illustrate the advantages of each model concerning the different aspects studied. Below graphical comparisons are made for the different variables.

In Fig.(4.5), is present a comparison between the different VonMises stress plots for the different AR of the wings. This information was then translated graphically. In Fig.(4.23) a comparison between the average stress across the different models is shown.

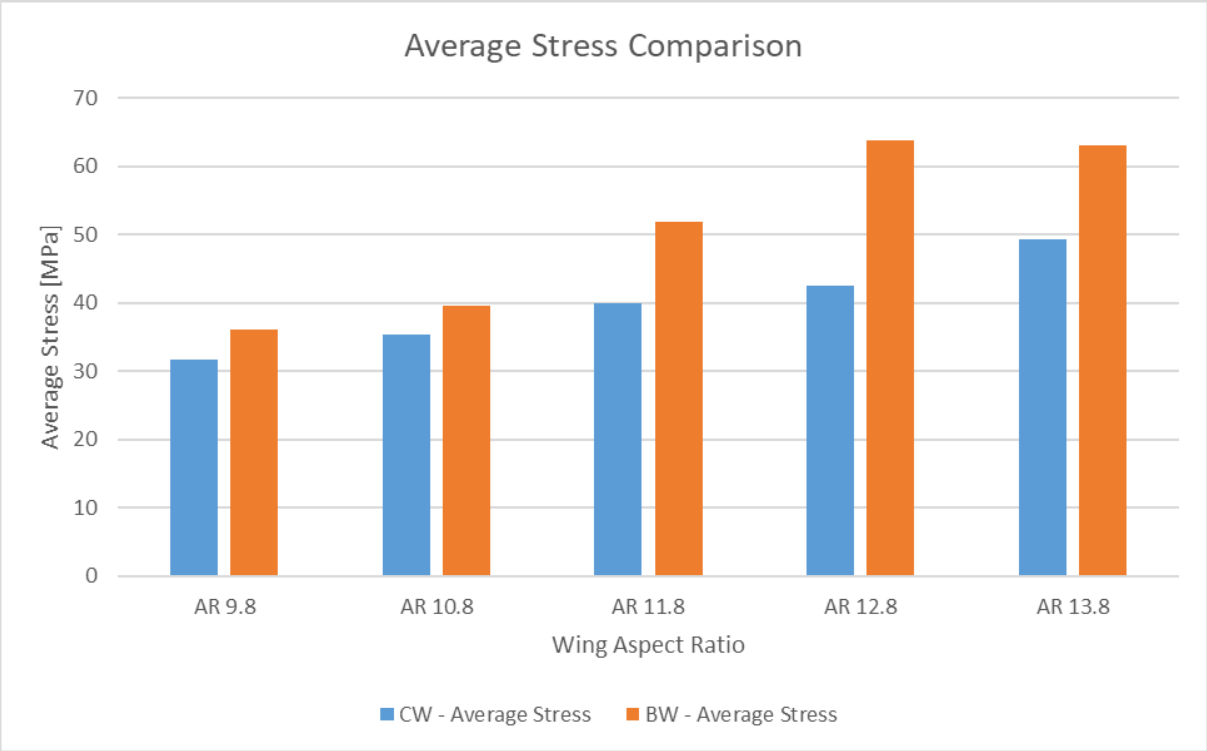

Figure 4.23: Average Stress between Cantilevered Wing and Braced Wing models

The average stress as seen in Fig.(4.23), increases in both configurations with the increase of the aspect ratio, however this increase is not proportional for both configurations, with the braced wing showing a general increase higher than the braced wing with the increase of wing aspect ratio.

The increased stress noticed in the AR12.8 for the braced wing is due to a weaker structure, coming from the distribution of the number of ribs in the structure.

Although average stress can give an overall idea of the forces that are taking place, maximum stress values between Cantilevered and Braced Wing models need to be taken into account. Fig.(4.24) shows a comparison graph with the highest stress values for both models, for each aspect ratio, excluding the highest Top 1% and Top 5% element values, respectively. This was done to remove outliers, and stress

concentration points due to simplifications in the model that wouldn't be representative of the real forces being applied in the respective wings. It is important to note that the highest stress zones aren't located in the same region for CW and BW models. For the CW the highest values are concentrated in the panels near the wing root while for the BW these highest stress zones are in the surroundings of the brace connection zone which is located roughly half of the wing length.

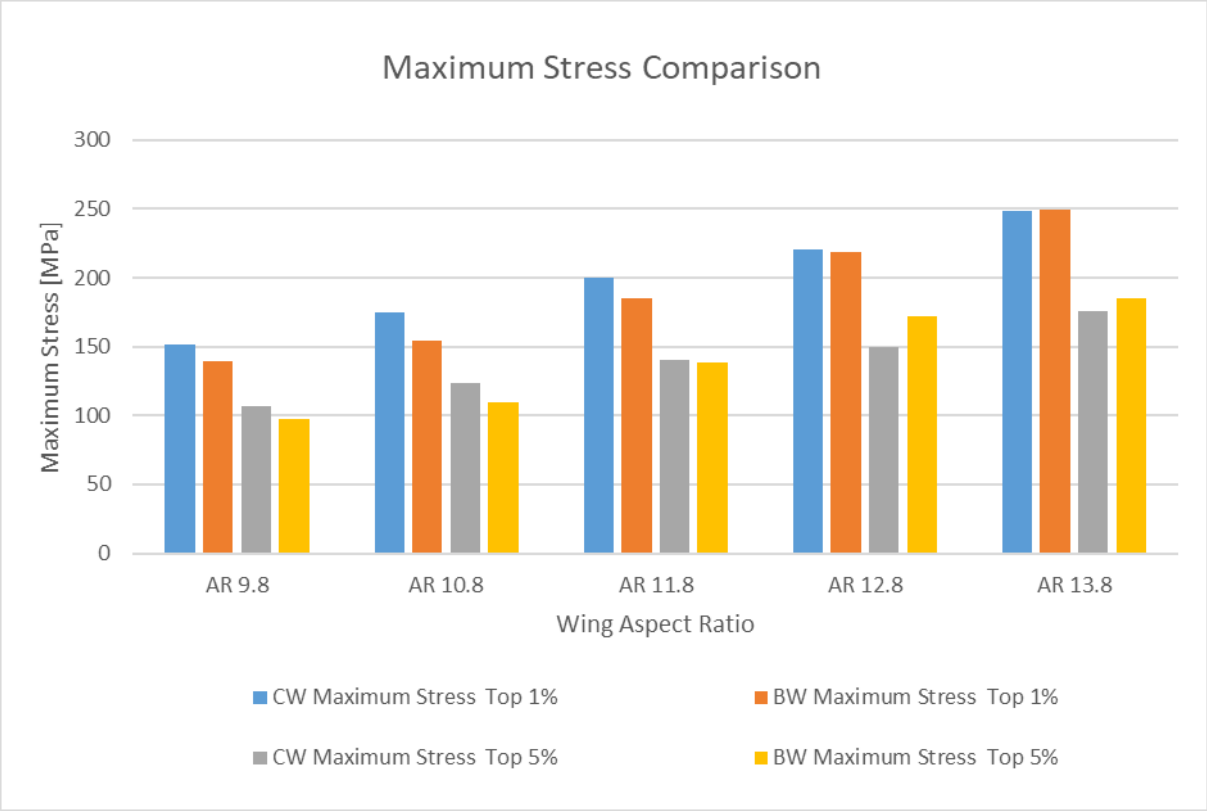

Figure 4.24: Maximum Stress between Cantilevered Wing and Braced Wing models

Regarding maximum stress it is noticeable that an increase in wing span results in a higher maximum load for the structure, however this increase in maximum stress is not the same for both CW and BW versions, since for higher aspect ratio wings the maximum stress increase is superior for the BW model in comparison with its CW homologue model. In this study case the BW surpassed the maximum stress in CW model.

One of the main takeaways from this study is the relative worthiness of each braces for each AR. In order to better visualize the data, a graph was made comparing the braced wing mass savings with respect to its CW model, along with the actual absolute value Fig(4.25). For each aspect ratio two structural mass comparisons were made, in blue the skin thickness reduction assumed as seen in Fig.(4.19). In orange the total mass obtained, reflect the increase in skin thicknesses due to the criteria being used, same stress level. For that purpose, element stresses were compared individually, and since most BW elements

consistently showed a higher average stress, it resulted in a high increase in skin mass to achieve the same average stress.

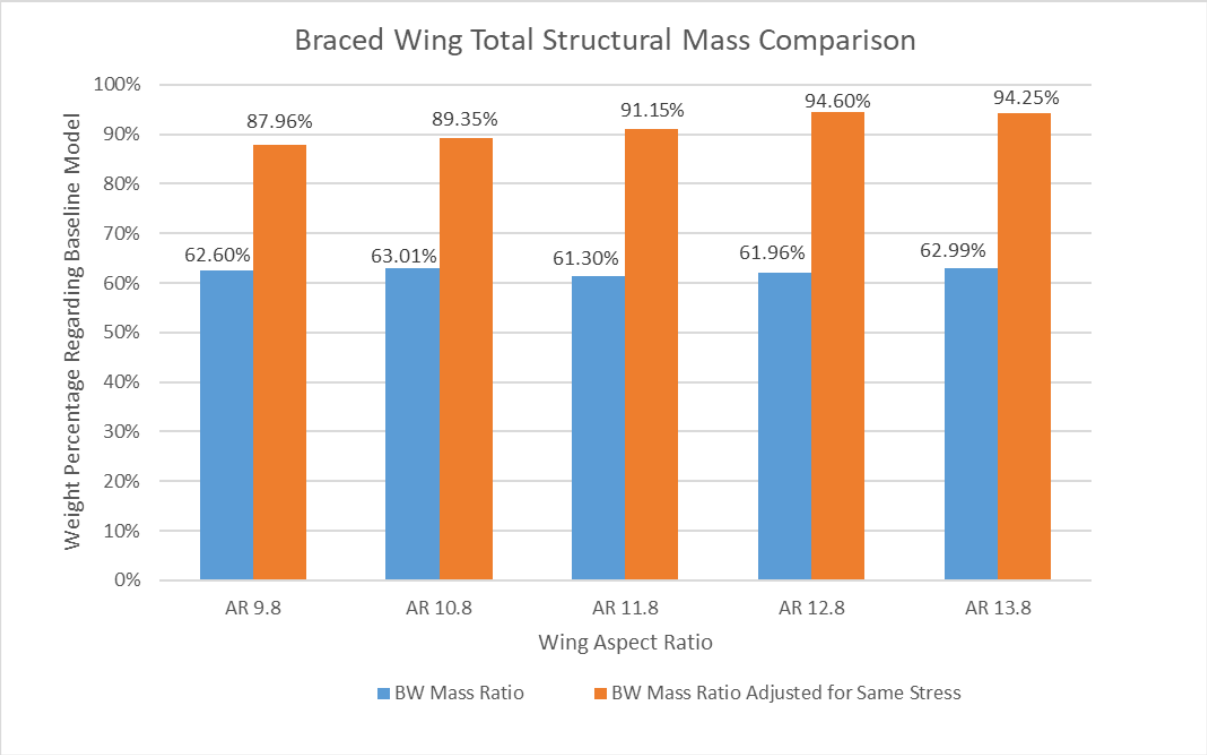

Figure 4.25: Mass Comparison between Braced Wing models

As it is visible in Fig.(4.25), across the different BW aspect ratios the total structural mass varied. In this case this aspect ratio is the one of the baseline model. The increase in aspect ratio leads to a higher structural stress in BW models, which would consequently result in a higher wing brace mass, reducing the potential savings, and thus it's noticeable an increase in total mass for the braced wing. In the opposite direction, the shorter wings would need bigger cross sections, due to the appearance of instabilities, unabling the reduction of the cross section, although tensile stresses were actually lower.

With this mass decrease it is possible now to calculate possible payload increases, fuel or range increases as seen in schematic of Fig.(4.26).

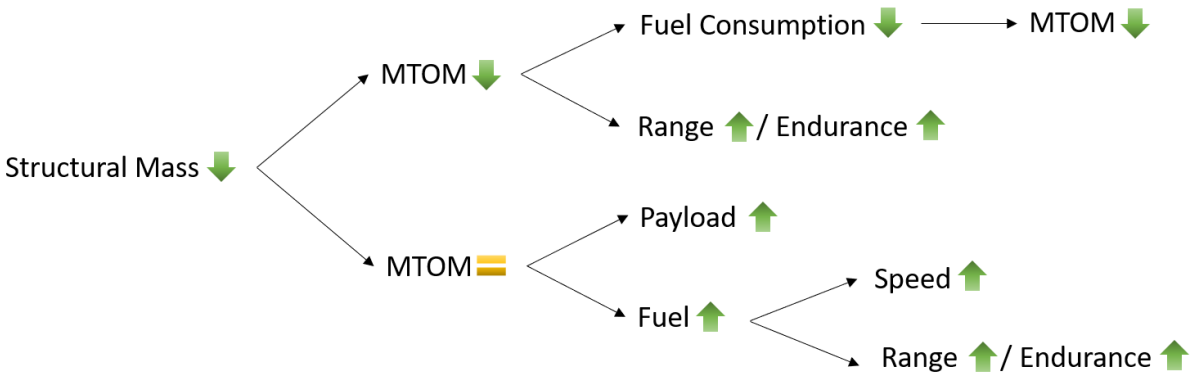

Figure 4.26: Schematic with the possible positive outcomes for the different structural mass reductions

Following the logic of the above graph by reducing the MTOM, the fuel consumption of the aircraft will lower. Knowing that Cessna Skycourier maximum range is 1704km and its maximum usable fuel weight is 2189kg, it is possible to determine for a mission range of 1000km its fuel consumption assuming a linear relationship. The aircraft with the BW base configuration would thus consume 1285kg, which in comparison with its homologue CW model would consume 1782kg or an increased 38.7% of fuel for the same mission length, as seen in Fig.(4.27).

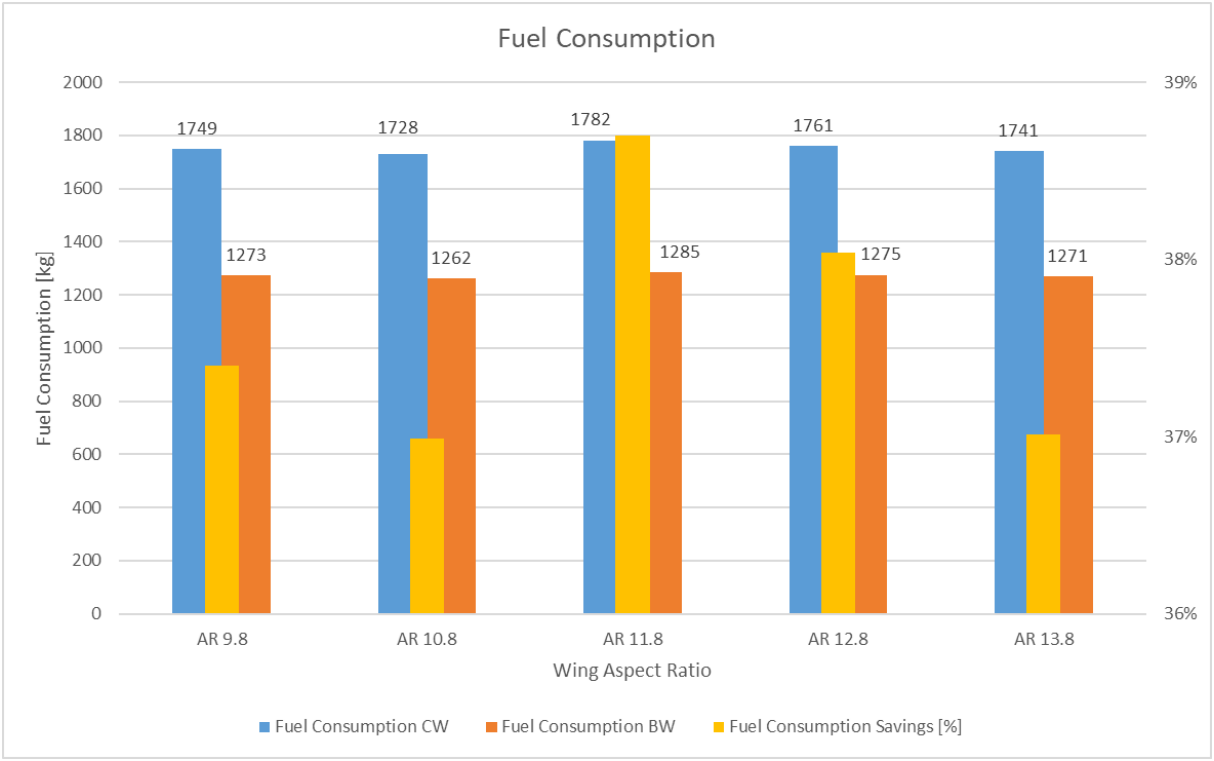

Figure 4.27: Fuel Consumption Comparison for 1000km mission

This reduction in fuel consumption, would mean that for the same mission the aircraft would need

to carry less fuel, which would in turn result in a lower MTOM, which could be calculated in an iterative process.

It would be also possible to keep the original amount of fuel (2189kg) in the aircraft which would translate in higher aircraft ranges due to its lower MTOM as seen in Fig.(4.28).

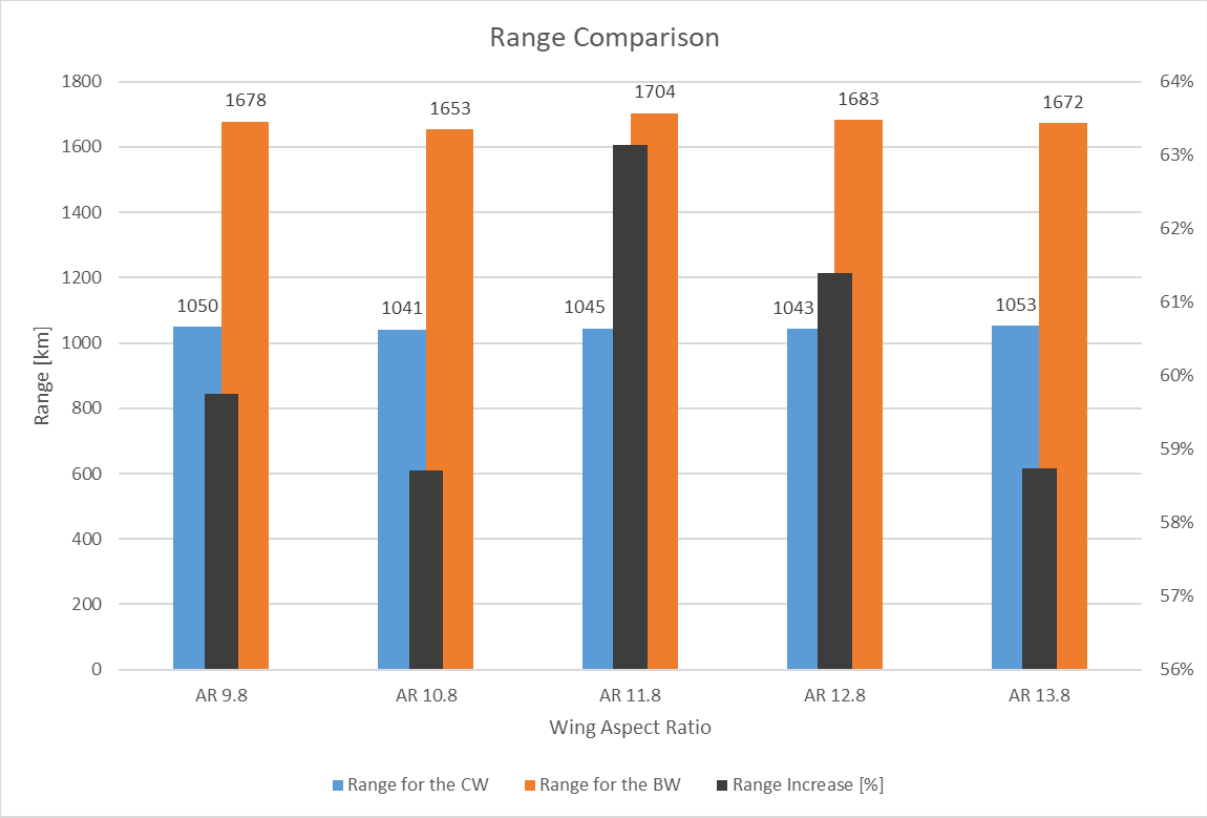

Figure 4.28: Range Comparison for the baseline amount of fuel (2189kg)

Due to the linear relation assumption made between range and weight of the aircraft, CW models mass increase, resulted in huge penalties for range although they would carry the same amount of fuel.

For the cases where MTOM stays unchanged there can be an increase of payload Fig.(4.29) or fuel load Fig.(4.30). The following graphs summarize the impact of these increases for each AR, taking as reference the values of payload, range and fuel consumption of the Cessna Sky Courier 408 present in Annex A.

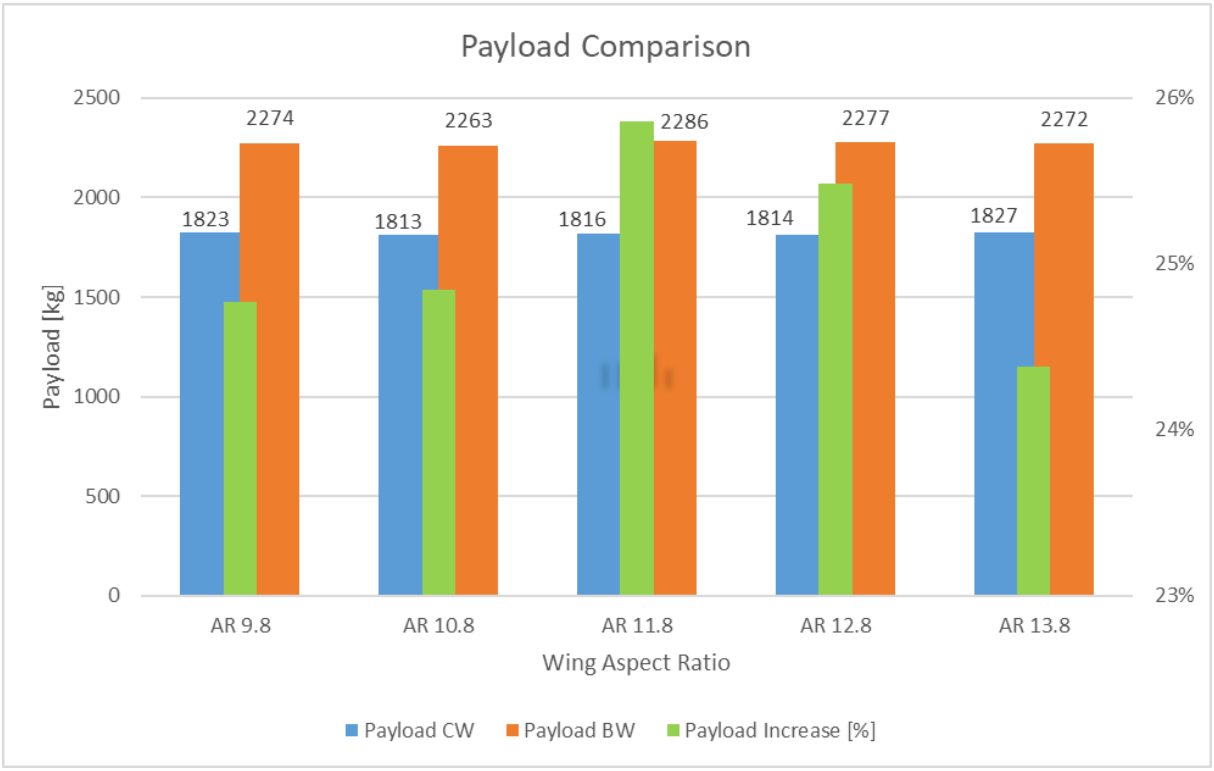

Figure 4.29: Payload Comparison Between CW and BW models

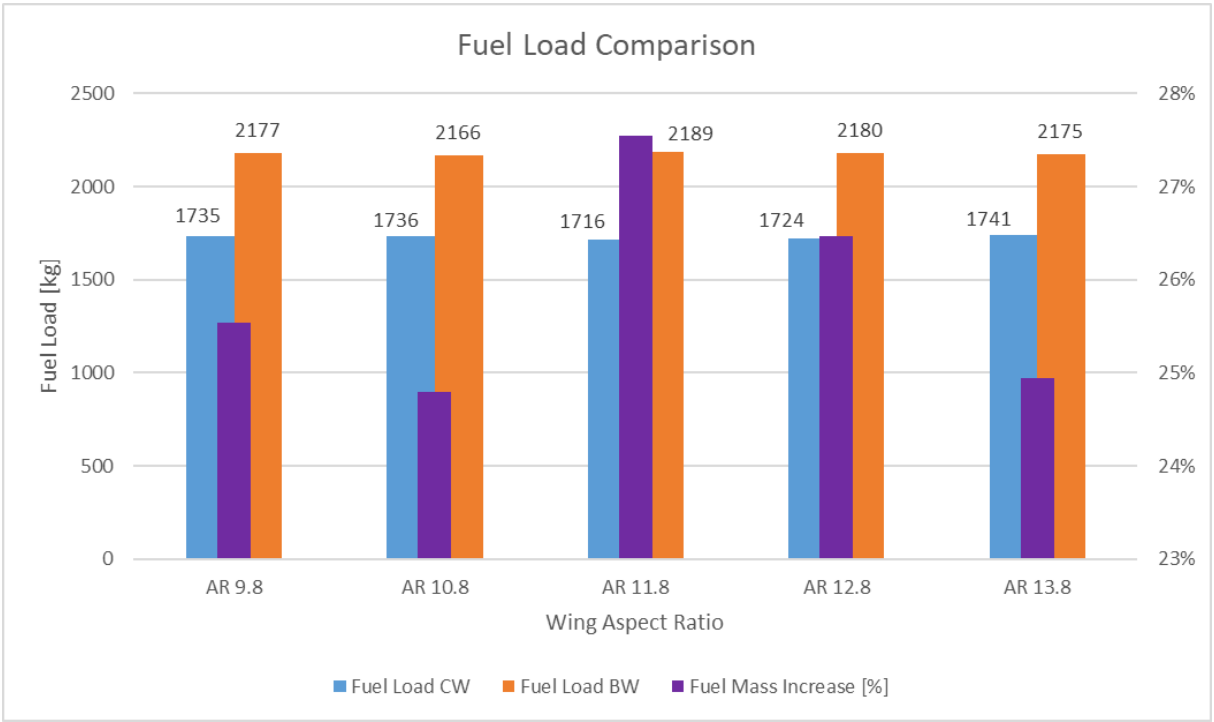

Figure 4.30: Fuel Load Comparison Between CW and BW models

Assuming a linear relationship between the amount of fuel carried by the aircraft and its range, it's possible to determine the different aircraft models predictable range Fig.(4.31). Being the range increase

equal to the fuel increase between models it can be assumed that the percentage increase in fuel mass is equal to the percentage increase of range. The differences in range obtained for the different models in Fig.(4.31) in comparison with the ones obtained in Fig.(4.28), come from the additional fuel added in this later case in comparison with the first one.

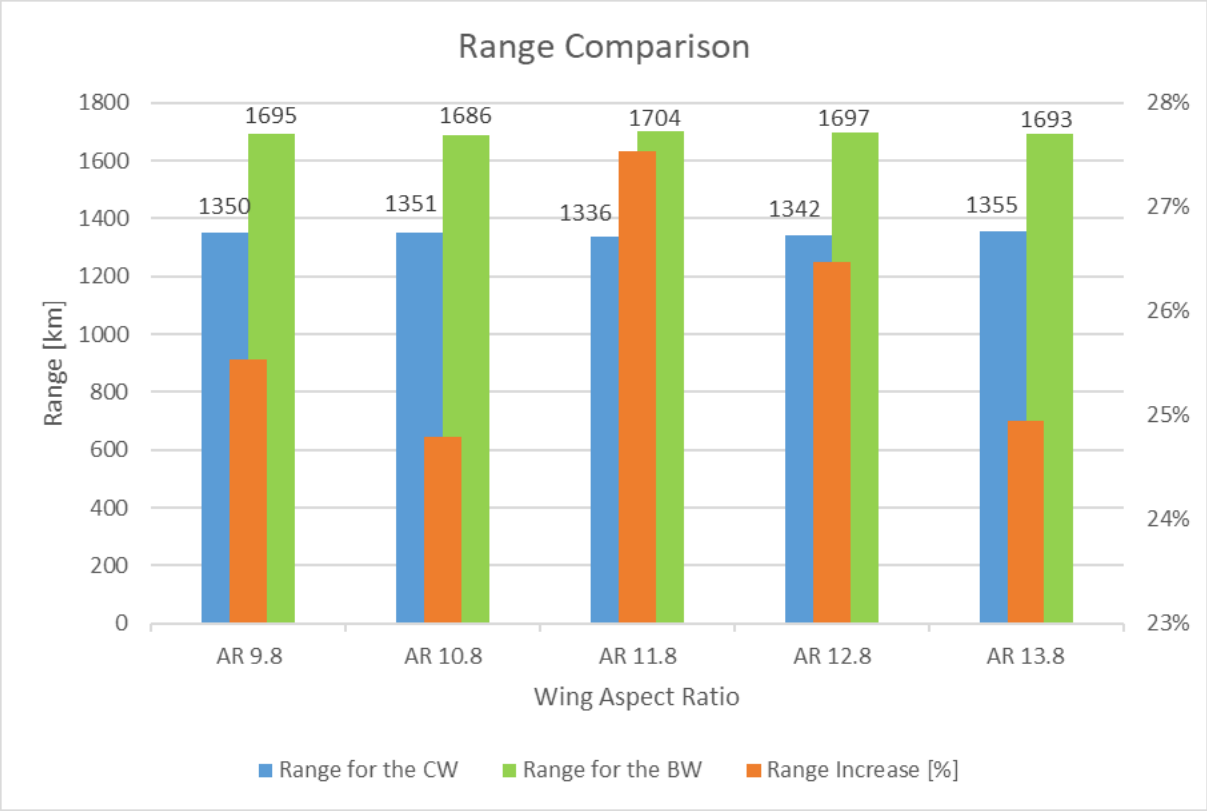

Figure 4.31: Range Comparison Between CW and BW models

To note that a greater amount of fuel could be used to travel the same distance with a higher speed, this would require additional thrust and consequently a less effectively fuel burn rate.

The stress ratios obtained between CW and BW models have been computed to evaluate stress distribution across both models Fig.(4.7,4.8), it was possible to conclude that the wing root in the CW is subject to much higher stresses than in the BW configurations, which provide a better distribution of these forces. The ability of the BW model to distribute loads effectively suggests the potential for a lighter wing structure, which may in turn result in improved fuel efficiency and overall performance.

Buckling analysis was performed on the baseline CW and BW models to compare the stability of the two wing structures under different loading conditions, providing key insights for structural optimization and safety considerations. The improvement in buckling resistance of the BW model in comparison to CW is largely due to its improved load distribution despite its thickness reduction. A small reinforcement was considered, near the connection zone between the brace and the wing in order to obtain relevant results.

Another study performed on the BW baseline model was done, altering the brace inclination angle. Changing inclinations influence the stress distribution across the wing. Lower inclination angles were found to be more effective in reducing the average stress distribution, specially at the pre-brace region. However, it was observed that there was a trade-off between structural efficiency and weight as lower inclination angles often necessitated additional brace length. Achieving an optimal balance between weight and structural performance is critical for overall aircraft efficiency.

Despite the limitations of assumptions of the current wing brace evaluation study, it is interesting to note that the above results obtained corroborate the advantageous use of braces for the modeled braced wing aircraft with an AR of 11.9, validating Cessna Skycourier 408 choice of using this configuration over the cantilevered wing one.

Chapter 5

Conclusions and future work

In this concluding chapter, the key findings and insights garnered throughout this thesis are summarized. A concise overview of this study outcomes is shown along with its limitations, and assumptions. Lastly, potential directions for future research topics are presented, offering a glimpse into the evolution of braces.

5.1 Conclusions

With the studies conducted it was possible to validate the advantageous use of braces in an aircraft such as Cessna 408 Skycourier, which according to the studies made the optimal lowest weight possible in the aircraft.

Considering the load cases and operating conditions (velocity and altitude) the braced wing configuration has shown a relevant advantage with respect to the cantilevered wing configuration for a small aircraft configuration (CS-23). These results have agreed with Roskam prediction (2), which established an overall wing structure mass reduction of the order of 30%.

Taking as reference the publicly available mass distribution data for the Cessna SkyCourier (reference aircraft), and despite the aforementioned analysis limitations and considerations, the results have shown that one could achieve a payload mass increase of about 25% with a braced wing with respect to a cantilevered wing design. Alternatively, one could likewise increase the amount of fuel by roughly 25%, thus increasing the aircraft range, endurance or cruise speed for the same MTOM.

It can be stated that in the small aircraft category (CS-23), the use of braced wings should be studied from the earliest stages of the design process. In order to quantify its worthiness, factors such as wing aspect ratio and wing to brace angle should be considered, evaluating its behaviour in all possible load cases.

It is plausible to argue that, in general, higher ARs will be more prone to higher bending moments in the wings, thus increasing the need for braces as a way to transmit the forces applied, that are concentrated

in the wing root, in cantilever configurations. This is because high AR wings generate less induced drag due to the reduced downwash, making flight more efficient. However, the choice of AR also depends on the purpose of the aircraft. Smaller ARs may be preferable on aircraft that need greater maneuverability and load capacity, but this can increase the need for braces to support the loads during maneuvers.

However it is very important to understand that this study has several limitations as well as modeling assumptions:

- Although variations in wing skin thickness sections were considered, it wasn't thoroughly investigated the accuracy of these values for the cantilevered wing model. Consequently, possible variations on chosen skin wing thickness for the cantilevered wing configuration, in comparison to the braced wing model, will affect the percentage of savings presented.

- A critical limitation of this analysis is the exclusion of the airplane's engines. Engines have weight, and therefore will affect the load distribution and can influence structural reinforcement needs. In addition, the positioning of the braces and its angle will be dependant on the aircraft engines, since its size and placement, may affect the drag penalty due to the increased turbulence in the incoming air flow that will hit the brace fairing.

- Static linear analysis is a simplification of reality, it does not take into account dynamic factors such as vibrations, wing flutter, gust loads and variations in load distribution during flight. These complexities of reality can affect braces requirements in a non-linear way.

- Brace requirements will also vary significantly with flight conditions, such as speed, altitude and payload. The static analysis performed does not fully capture these variations, since only straight level flight was studied.

- The connection of braces to the main landing gear, a critical component in the overall aircraft structure was omitted. Braces play a crucial role in distributing loads and supporting the wings, particularly during landing and ground operations. The absence of this consideration in the analysis may result in an incomplete understanding of how braces affect the structural integrity and performance of the aircraft.

- In this study the connection between the wings and the aircraft was very simplified, while the study has examined the impact of braces on the wing's structural integrity, the method and design of the actual connection between the wings and the aircraft have not been thoroughly explored. The quality and effectiveness of the wing-to-aircraft connection are paramount to ensure the overall safety and stability of the aircraft. Variations in connection design, materials, and attachment methods can significantly influence the distribution of forces and stresses throughout the aircraft structure.

- Aluminium was the only material used for structural analysis, along with the assumption of a fixed

yield strength of 400 MPa. While aluminium is a common material choice for aircraft structures due to its favorable strength-to-weight ratio, this does not account for the full spectrum of materials available for modern aerospace applications. In reality, aircraft design often considers a wide range of materials, including advanced composites, titanium, and high-strength alloys, each with its own unique properties and advantages. Focusing solely on aluminum and a fixed yield strength doesn't capture the potential benefits or challenges associated with alternative materials for the brace, fairings or wing structures.

To sum up the plausibility of having braces on an aircraft geometry depends on many factors, including the chosen AR and the flight conditions. The behavior of the need for braces in relation to the AR may not be linear. This is due to various reasons, such as the variation of aerodynamic loads with speed, angle of attack and atmospheric conditions.

While shorter aspect ratios can reduce the need for braces in theory, the complexities of aerodynamic and structural behavior can lead to a non-linear scenario. It is therefore important to carry out detailed analysis, considering the specific operating conditions of the aircraft and taking into account its limitations. It can also be said that braces can be one design solution to reach a higher aspect ratio wing, which brings several advantages, since the induced drag generated by the wing will be reduced due to its lower width. As shown in the studies, a required wing area can be achieved using different wing aspect ratios. The larger the wing aspect ratio, the less air disturbance is created at the tip. However, for most aircraft, there are both practical limits to maximum wing span for ground operations and structural issues which mean that eventually, the weight penalty by the addition of braces to adequately strengthen a long thin wing becomes excessive. Determining accurately this turning point can be challenging.

5.2 Prospect for future work

For a future analysis, it is recommended to take into account all areas involved, such as aeroelastic effects, in order to achieve a multidisciplinary design optimization of braces regarding all the weight contributions of this structure. There are some research papers that may provide some insights on the braces weight measuring process. (65)

The entire aircraft, including the wings, were not sized, since it would be out of this thesis' scope. The analysis focused on specific aspects or components of the wing, but did not encompass the comprehensive design and sizing of the aircraft as a whole. Consequently, the findings and conclusions drawn from this study may not fully account for the intricate interplay of factors that emerge when considering the complete aircraft design. Future research could benefit from a holistic approach that encompasses the sizing of the

entire aircraft to provide a more comprehensive and realistic assessment of braces performance and characteristics.

The chosen thicknesses for the various wing sections were assumed rather than determined through rigorous analysis or experimentation. These assumed thicknesses were then compared in the several studies presented. These thicknesses' assumptions introduce uncertainty into the findings, as the actual aerodynamic performance and structural behavior of the wings can be highly sensitive to its variations. Aiming to refine the analysis by incorporating precise thickness calculations or conducting experimental tests to validate the chosen wing section thicknesses, will provide more robust and accurate insights into their impact on the overall brace performance among several models.

In a future study it should be incorporated the influence of braces connected to the main landing gear to understand their impact on the aircraft's structural behavior and overall effectiveness.

This study is primarily focused on the structural and aerodynamic aspects of braces, but the implications for fuel storage and stability have not been addressed. Fuel storage is a critical consideration in aircraft design, especially when using the wings for fuel containment. The presence of braces may necessitate adjustments in fuel tank placement, size, or shape, which can impact the overall aircraft weight distribution and performance. The effects of fuel sloshing and its influence on the aircraft's stability and control under various flight conditions should be considered. The interplay between brace design, fuel storage, and overall wing design is a complex and multidisciplinary problem that may require a more in-depth investigation. Next studies should aim to consider their interconnected nature and their impact on the aircraft's performance, safety, and efficiency.

Bibliography

[1] S. Gudmundsson. *General Aviation Aircraft Design Applied Methods and Procedures*. Butterworth-Heinemann, 2nd edition, 2022.

[2] Jan Roskam. *Airplane Design, Part III, Section 4.1.1*. DARcorporation, 1999.

[3] CEiiA. ceiia., (n.d.). URL https://www.ceiia.com/about-us. Accessed 12 May 2023.

[4] Enescoord. Ceiia – centro para excelência e inovação na indústria automóvel, (n.d). URL https://www.enescoord.pt/en/projetos/ceiia-centro-para-excelencia-e-inovacao-na-industria-automovel/. Accessed September 7, 2023.

[5] CEiiA. Embraer kc-390, (n.d.). URL https://www.ceiia.com/aero-embraer. Accessed September 7, 2023.

[6] AviationCult. Conheça o kc-390 da embraer (c390 millenium), 2019. URL https://blog.aviationcult.com/conheca-o-kc-390/. Accessed September 7, 2023.

[7] Museums Victoria Collections. Aeroplane - duigan biplane, mia mia, victoria, 1910, (n.d.). URL https://collections.museumsvictoria.com.au/items/405751. Accessed 13 June 2023.

[8] CEiiA. Embraer kc-390, (n.d.). URL https://www.ceiia.com/aero-embraer. Accessed September 7, 2023.

[9] Wikipedia Contributors. Jet age, 2020. URL https://en.wikipedia.org/wiki/Jet_Age. Accessed 13 June 2023.

[10] CEiiA. Embraer kc-390, (n.d.). URL https://www.ceiia.com/aero-embraer. Accessed September 7, 2023.

[11] Dr. Lakhan Patidar Dhananjay Kumar, Pankaj Pandey. Structural analysis of airplane wing using composite and natural fiber materials: A survey. *IJRASET*, 2023. doi: https://doi.org/10.22214/ijraset.2023.48634.

[12] Sinchai Chinvorarat. Composite wing structure of light amphibious airplane design, optimization, and experimental testing. *Heliyon*, 7(11):e08410, 2021. ISSN 2405-8440. doi: https://doi.org/10.1016/j.heliyon.2021.e08410. URL https://www.sciencedirect.com/science/article/pii/S2405844021025135.

[13] N. Sreenivasaraja, P. Manivannan, R. M. Ragesh, and K. Vinothkumar. Implementation of honeycomb structure in an x-48b supersonic aircraft with blended wing aircraft configuration. *INTERNATIONAL JOURNAL OF ENGINEERING RESEARCH & TECHNOLOGY (IJERT)*, 2015. doi: 10.17577/IJERTCONV3IS26008.

[14] Santosh Malipatil Vishal Musale, Anand C. Mattikalli. Skin instabilities in honeycomb structures of an aircraft wing. *International Research Journal of Engineering and Technology (IRJET)*, 2021. doi: https://www.irjet.net/archives/V8/i8/IRJET-V8I8270.pdf.

[15] Moaz Hussain. Design of 120 seated passenger aircraft, 2019. URL https://www.researchgate.net/publication/340933751_Detailed_Design_of_120_Seater_Passenger_Aircraft_Aircraft_Design_Project-II. Accessed 15 June 2023.

[16] PILOT AHMAD. Aircraft basic aerodynamics (part 1), (n.d.). URL https://pilotahmad.wordpress.com/2020/06/10/aircraft-basic-aerodynamics-part-1/. Accessed 7 September 2023.

[17] Antonio Moran. How effective are winglets in improving an airplane's aerodynamics?, 2023. URL https://www.quora.com/How-effective-are-winglets-in-improving-an-airplanes-aerodynamics. Accessed 7 September 2023.

[18] Simscale. What is lift, drag, and pitch?, 2023. URL https://www.simscale.com/docs/simwiki/lift-drag-pitch/. Accessed 7 September 2023.

[19] SKYbrary. Theory of flight, (n.d.). URL https://skybrary.aero/articles/drag. Accessed September 7, 2023.

[20] Shreyansh Kanshal. Airfoil nomenclature, classification, flow and pressure distribution, (n.d.). URL https://www.aircraftnerds.com/2018/08/airfoil-terminology-and-definitions.html. Accessed September 7, 2023.

[21] Nicolas Shelton. How do flaps work?, 2022. URL https://www.boldmethod.com/learn-to-fly/aircraft-systems/how-do-flaps-work/. Accessed July 4, 2023.

[22] Peter P. Wegener. *What Makes Airplanes Fly?* Springer, 1991. URL https://link.springer.com/book/10.1007/978-1-4684-0403-6. Accessed July 4, 2023.

[23] Glenn Research Center. Determining aircraft weight, (n.d.). URL https://www1.grc.nasa.gov/beginners-guide-to-aeronautics/determining-aircraft-weight/#how-do-engineers-determine-the-weight-of-an-airplane-which-they-are-designing. Accessed July 5, 2023.

[24] Academic Kids. Lift-induced drag, (n.d.). URL https://academickids.com/encyclopedia/index.php/Lift-induced_drag. Accessed September 7, 2023.

[25] statista. Fuel costs of airlines worldwide from 2011 to 2021, with a forecast until 2023, as percentage of expenditure, 2019. URL https://www.statista.com/statistics/591285/aviation-industry-fuel-cost/. Accessed September 4, 2023.

[26] F. W. Pawlowski. Evolution of airplane wing-trussing, 1917. URL https://www.jstor.org/stable/44716165. Accessed June 20, 2023.

[27] aviationfile. What stage of a flight consumes the most fuel ?, 2022. URL https://www.aviationfile.com/what-stage-of-a-flight-consumes-the-most-fuel/. Accessed September 4, 2023.

[28] New Atlas. Boeing to build braced-wing airliner, shooting for 30% efficiency gain, January 31, 2023. URL https://newatlas.com/aircraft/boeing-nasa-truss-braced/. Accessed June 20, 2023.

[29] Simple Flying. Boeing 777x given special fuel tank conditions by faa, 2019. URL https://simpleflying.com/boeing-777x-fuel-tank/. Accessed September 4, 2023.

[30] Frank Gern, J. Gundlach, A Ko, A Naghshineh-Pour, Erwin Sulaeman, P.-A Tetrault, B Grossman, Rakesh Kapania, William Mason, J Schetz, and Raphael Haftka. Multidisciplinary design optimization

of a transonic commercial transport with a strut-braced wing. *SAE Technical Paper*, 10 1999. doi: 10.4271/1999-01-5621.

[31] AEROIN. Cessna volta ao mercado de bimotores com novo avião feito para fedex, 2017. URL https://aeroin.net/cessna-volta-bimotores-com-novo-aviao-feito-para-fedex/. Accessed June 21, 2023.

[32] Flight Aware. Cessna conquest 2 (n441cc), 2018. URL https://pt.flightaware.com/photos/view/729600-eb9344b7ca79eaf313fb07dbd6ebd3da492eeeec/aircrafttype/C441. Accessed September 4, 2023.

[33] Thiago Vinholes. Cessna caravan, o jipe dos ares, 2015. URL https://www.airway.com.br/cesna-caravan-o-jipe-dos-ares/. Accessed September 4, 2023.

[34] AEROIN. Está entregue o 1º avião 'caravan bimotor' do mundo, a quem ajudou a projetá-lo, 2022. URL https://aeroin.net/esta-entregue-o-1o-aviao-caravan-bimotor-do-mundo-a-quem-ajudou-a-projeta-lo/. Accessed June 21, 2023.

[35] KERRY LYNCH. Textron's skycourier takes shape, 2019. URL https://www.ainonline.com/aviation-news/business-aviation/2019-05-19/textrons-skycourier-takes-shape. Accessed September 4, 2023.

[36] Cessna Aircraft. Cessna skycourier (passenger), (n.d.). URL https://cessna.txtav.com/en/turboprop/skycourier-passenger. Accessed June 22, 2023.

[37] Wikipedia. De havilland canada dhc-6 twin otter, 2023. URL https://en.wikipedia.org/wiki/De_Havilland_Canada_DHC-6_Twin_Otter. Accessed June 22, 2023.

[38] Viking Air Ltd. Dhc-6 twin otter, 2021. URL https://www.vikingair.com/viking-aircraft/dhc-6-twin-otter. Accessed June 22, 2023.

[39] Wikipedia. Pzl m28, 2021. URL https://pt.wikipedia.org/wiki/PZL_M28. Accessed August 1, 2023.

[40] Naval Technology. Pzl mielec m28 skytruck / bryza aircraft, (n.d.). URL https://www.naval-technology.com/projects/pzlmielecm28skytruck/. Accessed August 1, 2023.

[41] Army Technology. Sikorsky/pzl mielec to deliver m28 stol aircraft to ecuador army, 2018. URL https://www.army-technology.com/news/sikorsky-pzl-mielec-deliver-m28-stol-aircraft-ecuador-army/. Accessed August 1, 2023.

[42] Aeronautics Guide. Wings - aircraft structures, (n.d.). URL https://www.aircraftsystemstech.com/p/wings-wing-configurations-wings-are.html?utm_content=cmp-true. Accessed August 2, 2023.

[43] PT. Dirgantara Indonesia, (n.d.). URL https://www.indonesian-aerospace.com/. Accessed August 2, 2023.

[44] Wikipedia. Indonesian aerospace n-219, 2023. URL https://en.wikipedia.org/wiki/Indonesian_Aerospace_N-219. Accessed August 2, 2023.

[45] Jakarta Globe. Indonesia to export locally produced n219 plane to china, mexico, 2017. URL https://jakartaglobe.id/business/indonesia-export-locally-produced-n219-plane-china-mexico. Accessed August 2, 2023.

[46] Wikipedia. Dornier 228, 2023. URL https://en.wikipedia.org/wiki/Dornier_228. Accessed August 2, 2023.

[47] Simple Flying. The story of the rugged dornier 228 turboprop, 2022. URL https://simpleflying.com/dornier-228-story/. Accessed August 2, 2023.

[48] Tecnologia & Defesa. Dornier 228 realiza missão de emergência, 2016. URL https://tecnodefesa.com.br/dornier-228-realiza-missao-de-emergencia/. Accessed August 2, 2023.

[49] Wikipedia. Let l-410 turbolet, 2023. URL https://en.wikipedia.org/wiki/Let_L-410_Turbolet. Accessed August 2, 2023.

[50] LET Aircraft Industries. L 410, 2023. URL http://www.let.cz/en/l410uvp. Accessed August 2, 2023.

[51] Airlines Inform. Let l-410, (n.d.). URL https://www.airlines-inform.com/commercial-aircraft/l-410.html. Accessed August 2, 2023.

[52] Federal Aviation Regulations (FAR). Federal aviation regulations, 2003. URL http://elodieroux.com/ReportFiles/FAR.pdf. Accessed September 4, 2023.

[53] European Aviation Safety Agency (EASA). Easy access rules for normal, utility, aerobatic and commuter category aeroplanes (cs-23) (initial issue), 2018. URL https://www.easa.europa.eu/sites/default/files/dfu/CS-23%20Initial%20issue.pdf. Accessed September 4, 2023.

[54] EASA. Cs-23 normal, utility, aerobatic and commuter aeroplanes, (n.d.). URL https://www.easa.europa.eu/en/document-library/certification-specifications/group/cs-23-normal-utility-aerobatic-and-commuter-aeroplanes#cs-23-normal-utility-aerobatic-and-commuter-aeroplanes. Accessed August 7, 2023.

[55] EASA. Certification specifications for normal, utility, aerobatic, and commuter category aeroplanes contents (general layout), 2012. URL https://www.easa.europa.eu/sites/default/files/dfu/agency-measures-docs-certification-specifications-CS-23-CS-23-Amdt-3.pdf. Accessed August 7, 2023.

[56] European Aviation Safety Agency (EASA). Certification specifications and acceptable means of compliance for normal, utility, aerobatic, and commuter category aeroplanes cs-23, 2015. URL https://www.easa.europa.eu/en/downloads/18858/en. Accessed September 5, 2023.

[57] Vanshika. Naca airfoils – nomenclature, 2021. URL https://garudauniverse.com/naca-airfoils-nomenclature/. Accessed August 3, 2023.

[58] UIUC Applied Aerodynamics Group. Uiuc airfoil data site, 2010. URL https://m-selig.ae.illinois.edu/ads/coord_database.html. Accessed August 3, 2023.

[59] P. André. *Airplane Wing Skeleton Structural Efficiency Optimisation*. Repositório Institucional da Universidade de Aveiro, 2023.

[60] Engineering ToolBox. U.s. standard atmosphere, 2003. URL https://www.engineeringtoolbox.com/standard-atmosphere-d_604.html. Accessed July 25, 2023.

[61] Wikipedia. Jet fuel, 2023. URL https://en.wikipedia.org/wiki/Jet_fuel. Accessed August 7, 2023.

[62] Jesper Christensen and Christophe Bastien. Chapter | five - applications of linear optimization to concept vehicle safety structures. In Jesper Christensen and Christophe Bastien, editors, *Nonlinear Optimization of Vehicle Safety Structures*, pages 209–252. Butterworth-Heinemann, Oxford, 2016. ISBN 978-0-12-804424-7. doi: https://doi.org/10.1016/B978-0-12-417297-5.00005-5. URL https://www.sciencedirect.com/science/article/pii/B9780124172975000055.

[63] SIEMENS. Implementation of inertia relief using param,inrel,-1, (n.d.). URL http://www2.me.rochester.edu/courses/ME204/nx_help/index.html#uid:id503211. Accessed August 8, 2023.

[64] Calculator Academy Team. Wing aspect ratio calculator, 2022. URL https://calculator.academy/wing-aspect-ratio-calculator/. Accessed 27 May 2023.

[65] G. P. Chiozzotto. Wing weight estimation in conceptual design: a method for strut-braced wings considering static aeroelastic effects. *CEAS Aeronaut J*, page 499–519, 2016. doi: 10.1007/s13272-016-0204-5.

[66] Flugzeuginfo. de havilland canada dhc-6 twin otter, (n.d.). URL http://www.flugzeuginfo.net/acdata_php/acdata_dhc6_en.php. Accessed August 1, 2023.

[67] Military Factory. Pzl m.28 skytruck (an-28), (n.d.). URL https://www.militaryfactory.com/aircraft/detail.php?aircraft_id=1829. Accessed August 1, 2023.

[68] PT. Dirgantara Indonesia. N219 nurtanio, 2017. URL https://www.indonesian-aerospace.com/aircraft/detail/11_n219+nurtanio. Accessed August 2, 2023.

[69] Airlines Inform. Dornier 228, (n.d.). URL https://www.airlines-inform.com/commercial-aircraft/dornier-228.html. Accessed August 2, 2023.

Part III
Appendices

Appendix A
Cessna Skycourier 408 Measures

LENGTH

55 ft 1 in (16.8 m)

DIMENSIONS	
Length	55 ft 1 in (16.8 m)
Height	20 ft 8 in (6.3 m)
Wingspan	72 ft 3 in (22.02 m)
Wing Area	441 sq ft (40.97 sq m)
Wheelbase	19 ft 11 in (6.07 m)
Tread	12 ft 4 in (3.76 m)

CABIN INTERIOR	
Height	5 ft 11 in (1.8 m)
Width	6 ft 2 in (1.88 m)
Length	23 ft 4 in (7.1 m)
Maximum Occupants	19

BAGGAGE CAPACITY	
Weight	1,500 lb (680 kg)
Volume	186 cu ft (5.27 cu m)

WEIGHTS	
Maximum Ramp Weight	19,070 lb (8,650 kg)
Maximum Takeoff Weight	19,000 lb (8,618 kg)
Maximum Landing Weight	18,600 lb (8,437 kg)
Useable Fuel Weight	4,826 lb (2,189 kg)
Usable Fuel Volume	720 gal (2,725 l)
Basic Empty Weight	12,325 lb (5,591 kg)
Useful Load	6,345 lb (2,878 kg)
Maximum Payload	5,000 lb (2,268 kg)
Full Fuel Payload	1,719 lb (780 kg)

PERFORMANCE	
Maximum Cruise Speed	210 ktas (389 km/h)
Maximum Range	920 nm (1,704 km)
Take-off Field Length	3,660 ft (1,116 m)
Landing Distance	3,010 ft (917 m)
Maximum Operating Altitude	25,000 ft (7,620 m)
Maximum Limit Speed	210 kias (389 km/h)
Stall Speed	74 kcas (137 km/h)

POWERPLANT	
Manufacturer	Pratt & Whitney Canada
Model	PT6A-65SC
Power Rating	1,110 shp (827 kW)
Propeller Manufacturer	McCauley
Description	4 blade aluminum

Figure A.1: Relevant characteristics of Cessna 408 Skycourier

Appendix B
De Havilland Canada Twin Otter Measures

Crew		1-2
Passengers		19-20
Propulsion		2 Turboprop Engines
Engine Model		Pratt & Whitney Canada PT6A-28
Engine Power (each)	507 kW	680 shp
Speed	348 km/h	188 kts *216 mph*
Service Ceiling	8.138 m	26.700 ft
Range	1.296 km	700 NM *806 mi*
Empty Weight	3.363 kg	7.414 lbs
max. Takeoff Weight	5.670 kg	12.500 lbs
Wing Span	19,81 m	64 ft 12 in
Wing Area	39,0 m^2	420 ft^2
Length	15,77 m	51 ft 9 in
Height	5,94 m	19 ft 6 in

Figure B.1: Relevant characteristics of De Havilland Canada Twin Otter (66)

Appendix C
PLZ M28 Skytruck

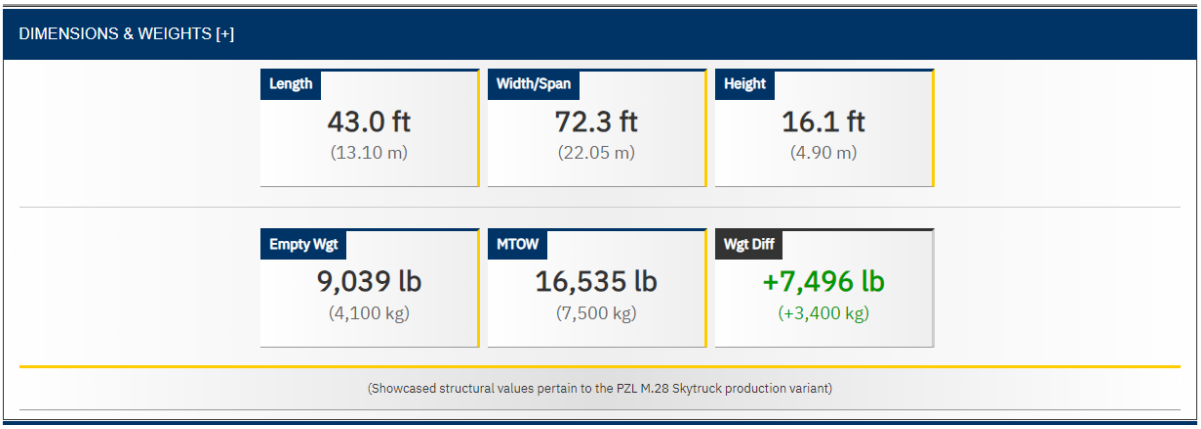

Figure C.1: Relevant characteristics of PZL M28 Skytruck (67)

Appendix D
Indonesian Aerospace N-219 Performance Charateristics

PERFORMANCE

Maximum Take Off Weight (MTOW)	: 7,030 Kg
Max. Landing Weight	: 6,940 Kg
Max. Fuel Capacity	: 1,600 Kg
Maximum Range with Maximum Fuel	: 828 NM
Maximum Payload	: 2,313 Kg
Take Off Distance	: 435 m
Landing Distance	: 509 m
Maximum Cruise Speed	: 210 Kts
Economical Cruise Speed	: 170 Kts
Stall Speed	: 59 Kts
Range with 19 pax	: 480 NM
Range at Max Fuel	: 828 NM
Operating altitude	: 10,000 ft
Ceiling Altitude	: 24,000 ft

Figure D.1: Relevant performance charateristics of Indonesian Aerospace N-219 (68)

Appendix E
Dornier 228 Characteristics

Dornier 228 Specifications

	Do 228-212	Do 228NG
Dimensions		
Length (m)	16.6	16.6
Wingspan (m)	17.0	17.0
Height (m)	4.9	4.9
Wing area (m2)	32.0	32.0
Weight		
Maximum take-off weight (kg)	6 400	6 400
Maximum landing weight (kg)	6 100	6 100
Operating empty weight (kg)	3 740	3 810
Maximum zero fuel weight (kg)	5 940	5 940
Maximum payload (kg)	2 200	2 130
Standard fuel capacity (litres)	2 390	2 390
Performance		
Range with max payload (km)	1100	830
Cruise speed (km/h)	430	430
Maximum speed (km/h)	470	470
Maximum operating altitude (m)	8 500	8 500
Take-off field length (m)	800	800
Landing field length (m)	450	450
Engines	Honeywell TPE331-5A252D, 2 x 780 hp	Garrett TPE331-10, 2 x 776 hp

Figure E.1: Relevant characteristics of Dornier 228 (69)

Appendix F
Let L-410 Turbolet Measurements

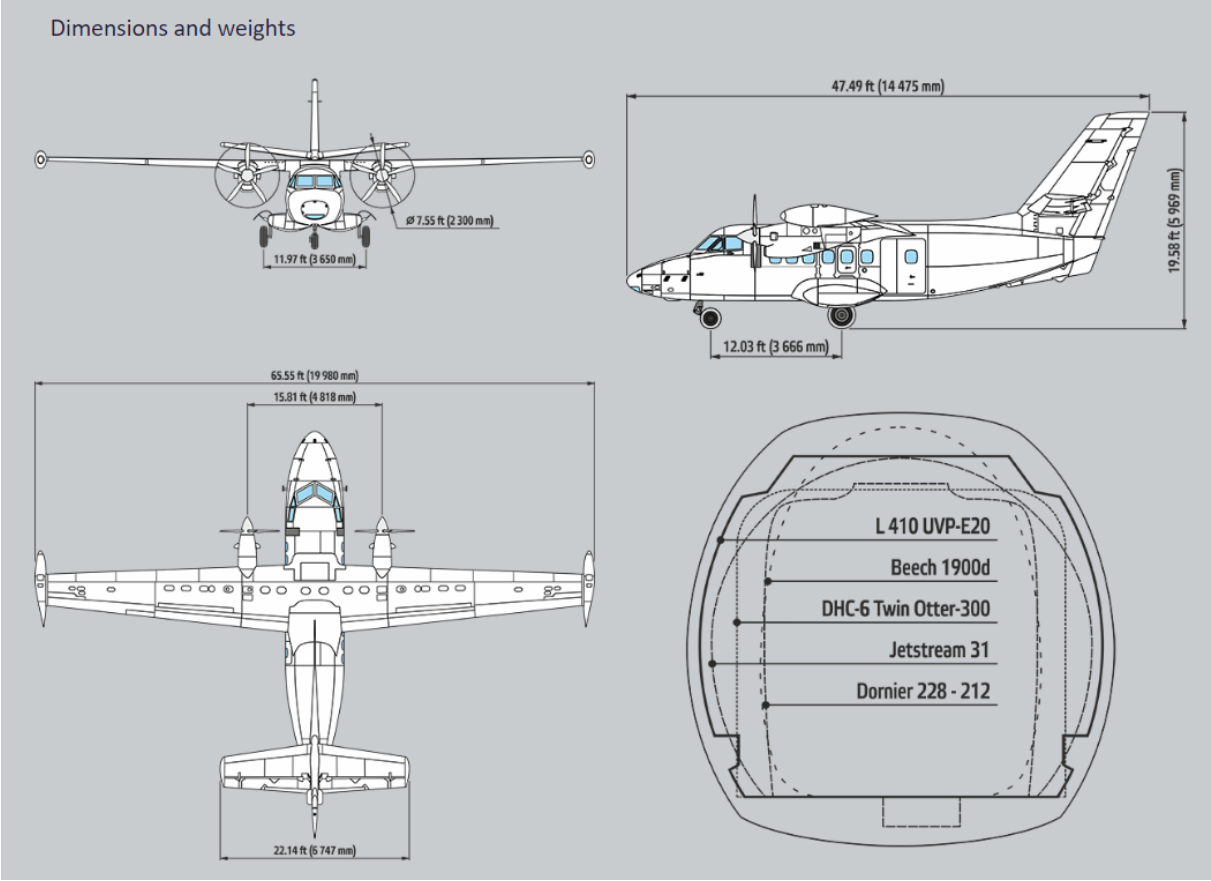

Figure F.1: Relevant measures of Let L-410 Turbolet (50)

Appendix G
Wing Weight Data

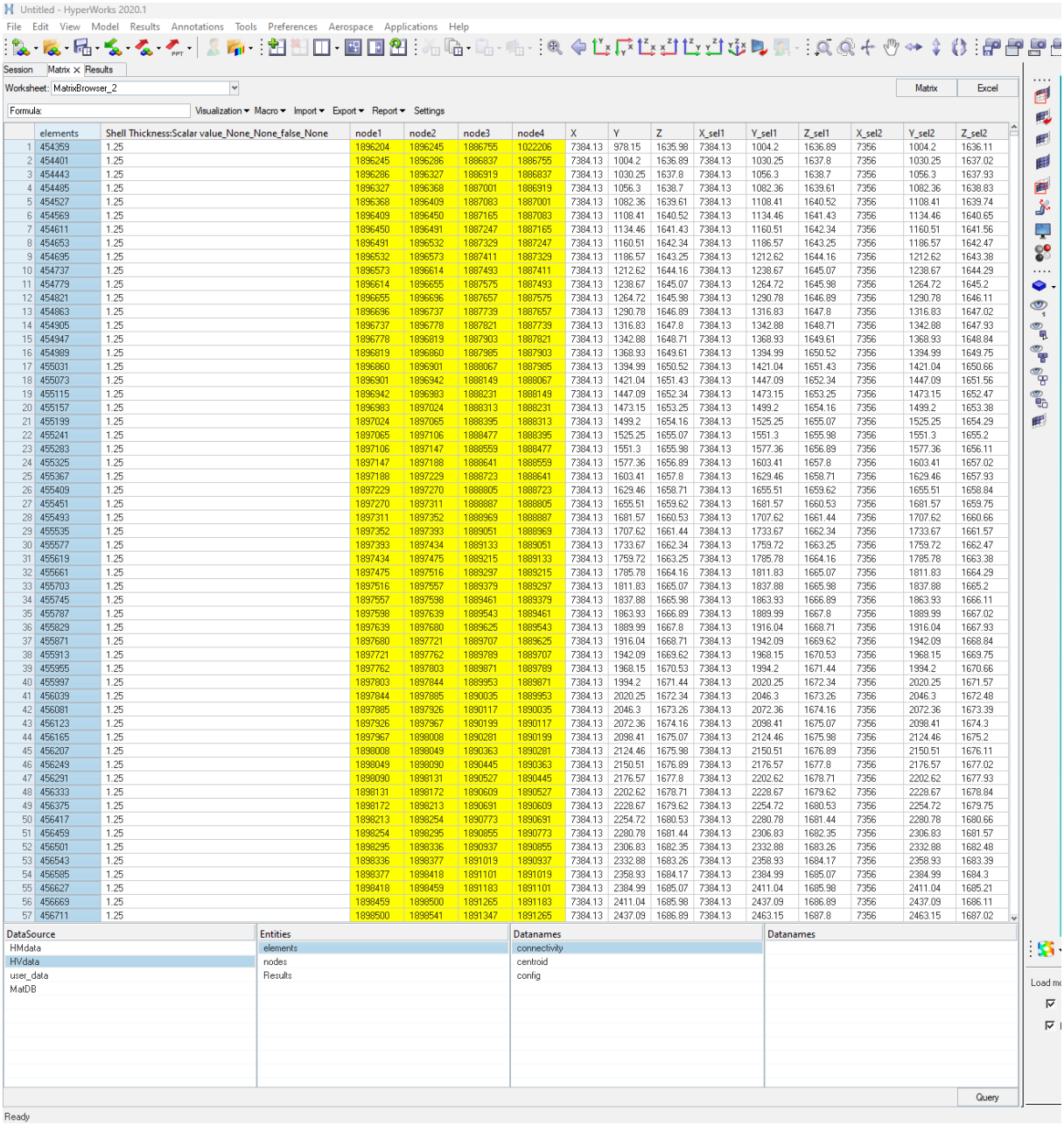

Figure G.1: Illustration of the Hypermesh window with the data collected for the Aircraft 11.837 Cantilevered Wing model

Distance Between Nodes (1-2)	Distance Between Nodes (2-3)	Element Area (mm^2)	Element Volume (Full Wing - mm^3)
25.67487683	20.24774555	519.8583731	1039.716746
25.677938	20.10672524	516.2992442	1032.598488
25.68180874	20.10698635	516.3837777	1032.767555
25.68541999	20.10672524	516.4496825	1032.899365
25.68877187	20.10672524	516.5170777	1033.034155
25.69334933	20.10672524	516.6091156	1033.218231
25.69727028	20.10418116	516.622577	1033.245154
25.70128791	20.10287542	516.6697888	1033.339578
25.70540216	20.10287542	516.7524971	1033.504994
25.70961299	20.10304703	516.8415591	1033.683118
25.71392035	20.10287542	516.9237373	1033.847475
25.71832421	20.10287542	517.0122674	1034.024535
25.72373612	20.10287542	517.1210625	1034.242125
25.72835207	19.3820226	498.6675011	997.3350023
25.73306433	19.38136476	498.7419063	997.4838125
25.73655183	19.39136406	499.0668461	998.1336922
25.74143741	19.38136476	498.9041879	997.8083759
25.74641917	19.38867711	499.1890079	998.3780159
25.75252415	19.3899149	499.3392518	998.6785036
25.75771729	19.3899149	499.4399464	998.8798928

Figure G.2: Excel containing data results for the Aircraft 11.837 Cantilevered Wing model

Wing Aspect Ratio	**9.837**	**10.837**	**11.837**	**12.837**	**13.837**
Wing Brace Upper Force X (N)	271.6	278.0	267.7	1467.8	306.5
Wing Brace Upper Force Y (N)	38395.5	41520.6	48200.4	46821.4	50760.9
Wing Brace Upper Force Z (N)	31914.6	32409.8	35447.7	35618.3	35948.5
Wing Brace Total Force (N)	49928.3	52672.9	59832.2	58847.7	62201.7
Wing Brace 1st Instability Mode (Force Factor)	1.130	1.131	1.156	1.144	1.156

Table G.1: Relevant Forces of the Wing Braces

Area (mm^2)	4.465e+07
Volume (mm^3)	1.185e+08
Total Mass (kg)	319.824

Table G.2: Mass obtained through mass calculator from Hypermesh, for the Aircraft 11.837 Cantilevered Wing model

Thickness Braced Wing	Stress Ratio	Thickness for Same Stress	Equivalent Volume (mm^3)
1	57.00%	1	519.8583731
1	76.38%	1	516.2992442
1	80.00%	1	516.3837777
1	114.74%	1.147435897	592.5929049
1	210.14%	2.101449275	1085.434439
1	329.17%	3.291666667	1700.505006
1	288.89%	2.888888889	1492.465222
1	194.67%	1.946666667	1005.783856
1	137.14%	1.371428571	708.6891388
1	57.75%	1	516.8415591
1	51.77%	1	516.9237373
1	56.73%	1	517.0122674
1	58.82%	1	517.1210625
1	52.25%	1	498.6675011
1	30.92%	1	498.7419063
1	35.66%	1	499.0668461
1	46.58%	1	498.9041879
1	63.64%	1	499.1890079
1	72.08%	1	499.3392518
1	57.85%	1	499.4399464

Figure G.3: Thicknesses obtained for the Aircraft 11.837 Braced Wing model in order to obtain the same stress level

Appendix H
Same Stress for Aircraft Braced Wing without minimum thickness

Thickness Braced Wing	Stress Ratio	Equivalent Thickness for Same Stress	Equivalent Volume (mm^3)
1	57.00%	0.56996587	296.30153
1	76.38%	0.763837638	394.3687954
1	80.00%	0.8	413.1070221
1	114.74%	1.147435897	592.5929049
1	210.14%	2.101449275	1085.434439
1	329.17%	3.291666667	1700.505006
1	288.89%	2.888888889	1492.465222
1	194.67%	1.946666667	1005.783856
1	137.14%	1.371428571	708.6891388
1	57.75%	0.577540107	298.4967293
1	51.77%	0.517699115	267.6109614
1	56.73%	0.567307692	293.3050363
1	58.82%	0.588235294	304.1888603
1	52.25%	0.522522523	260.5650006
1	30.92%	0.309160305	154.1912
1	35.66%	0.356617647	177.9760444
1	46.58%	0.465753425	232.3663341
1	63.64%	0.636363636	317.6657323
1	72.08%	0.720779221	359.9133568
1	57.85%	0.578512397	288.9322004

Figure H.1: Thickness Obtained for Same Stress Braced Wing Without Minimum Thickness

	Aircraft With Braces Same Stress Thickness 11.837
Total Volume (mm^3)	117284021.6
Total Volume (m^3)	0.117284022
Aluminium Density (kg/mm^3)	2.77E-06
Half Wing Shell Mass (kg)	324.64
Half Wing Stringers, Frames, Rib Caps (kg)	158.9125
Central Mass (kg)	N.A
Conection Zone (kg)	1.792
Brace Fuel Mass (kg)	28.66797806
Total Brace Mass (kg)	63.919
Faring Braces (kg)	18.26
Faring Trem (kg)	6.12792
Half Wing Mass (kg)	542.9365508
Total Wing Mass (kg)	1085.873102
Mass Ratio	89.47%

Figure H.2: Results Obtained for Aircraft Braced Wing Without Minimum Thickness

Appendix I
Measurements of Cessna Skycourier

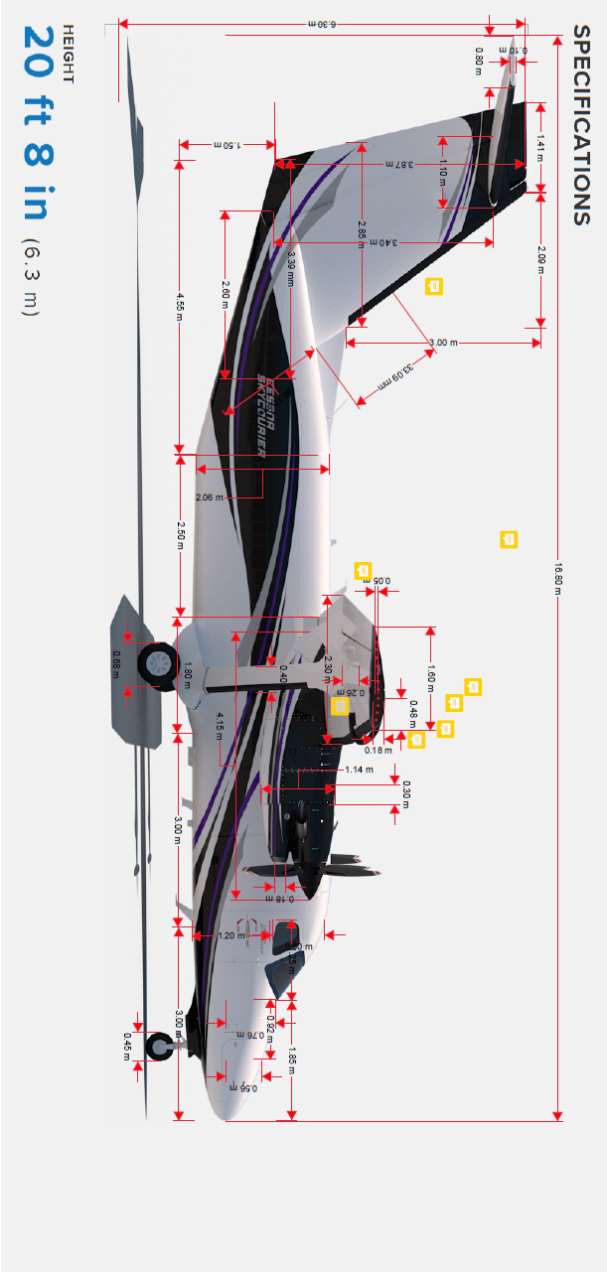

Figure I.1: Measurements of Cessna Skycourier Side View

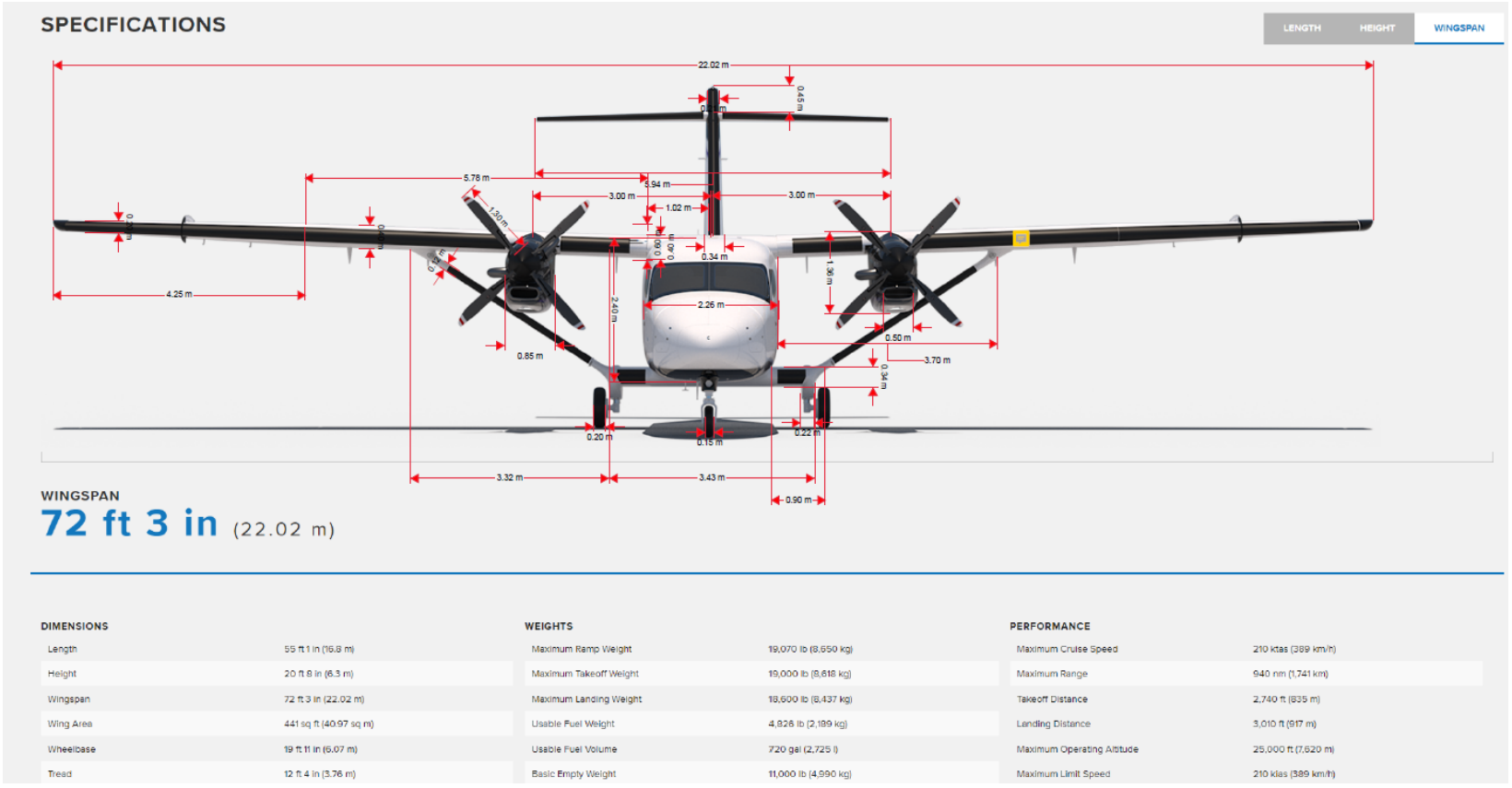

DIMENSIONS		WEIGHTS		PERFORMANCE	
Length	55 ft 1 in (16.8 m)	Maximum Ramp Weight	19,070 lb (8,650 kg)	Maximum Cruise Speed	210 ktas (389 km/h)
Height	20 ft 8 in (6.3 m)	Maximum Takeoff Weight	19,000 lb (8,618 kg)	Maximum Range	940 nm (1,741 km)
Wingspan	72 ft 3 in (22.02 m)	Maximum Landing Weight	18,600 lb (8,437 kg)	Takeoff Distance	2,740 ft (835 m)
Wing Area	441 sq ft (40.97 sq m)	Usable Fuel Weight	4,826 lb (2,189 kg)	Landing Distance	3,010 ft (917 m)
Wheelbase	19 ft 11 in (6.07 m)	Usable Fuel Volume	720 gal (2,725 l)	Maximum Operating Altitude	25,000 ft (7,620 m)
Tread	12 ft 4 in (3.76 m)	Basic Empty Weight	11,000 lb (4,990 kg)	Maximum Limit Speed	210 kias (389 km/h)

Figure I.2: Measurements of Cessna Skycourier Front View